Utrecht University
Institute for Marine and Atmospheric Research

Climate Physics Master Thesis

Modeling the accumulation of floating microplastic in the subtropical ocean gyres

Victor Onink

Supervisor:
Dr. Erik van Sebille
Co-Supervisor:
David Wichmann MSc

July 20, 2018

Abstract

Plastic, in particular microplastic, presents a significant threat to marine ecosystems. Floating microplastic in the oceans tends to accumulate in the subtropical gyres, forming accumulation regions commonly referred to as garbage patches in each ocean basin. The location of the garbage patches is determined by the ocean surface currents. This thesis examines the contributions of the Ekman and geostrophic surface current and Stokes drift components on the accumulation, along with the role of the eddy kinetic energy (EKE), which is seen as a proxy for mesoscale eddy activity, the mixing layer depth, as a proxy for vertical microplastic mixing, and the vertical Ekman pumping velocity, as an indicator of depth integrated current convergence. The microplastic distribution was modeled globally using both linear regression and Lagrangian modeling approaches, with emphasis on the North Pacific and North Atlantic basins.

Global Lagrangian simulations show garbage patch formation in each of the subtropical ocean gyres. The simulated North Pacific garbage patch matches the location from observations. The simulated North Atlantic garbage patch matches the garbage patch latitude from observations, but is too far west. Wind-driven surface Ekman currents account for the location and variability of the garbage patch. On basin-wide scales, the depth integrated Ekman transport is less crucial than the surface Ekman transport. The geostrophic currents are not found to contribute to accumulation, instead counteracting the Ekman current induced accumulation and spreading the microplastic over a larger surface area. The simulations show that Stokes drift has the effect to disperse microplastic from the garbage patch in the North Pacific, while in the North Atlantic it leads to more concentrated accumulation within the garbage patch. Stokes drift also leads with increased microplastic transport to the polar regions. The average position of the garbage patches in the North Atlantic and the North Pacific has seasonal variability. Microplastic tends to accumulate in regions of minimal EKE in the North Pacific, but shows no such behavior in the North Atlantic, indicating a less prominent role for mesoscale eddies in microplastic accumulation in this basin. The mixing layer depth ia not found to be a contributor to microplastic accumulation. Finally, the accumulation pattern of microplastic in the North Atlantic is more sensitive to the temporal resolution of the flow field data used to advect the microplastic than the North Pacific.

The locations of the garbage patches are sensitive to numerous different current components and other processes and this requires them to be consistently incorporated in future modeling efforts. Particularly Stokes drift is currently not always considered for microplastic modeling efforts despite having a significant influence on the global microplastic distribution. Improved microplastic transport modeling can be applied in numerous follow-up studies, including the efficacy of open-ocean plastic clean-up efforts and ecological impacts of plastic pollution in vulnerable ecosystems.

Layman's summary

Plastic is a pollutant that has been found in all the ocean basins. Plastic tends to break down into smaller fragments, referred to as microplastic, which due to its size is easily ingested by wildlife and difficult to remove from natural environments. Floating microplastic forms garbage patches of increased concentrations in subtropical ocean gyres, which are slowly rotating large-scale circulation patterns. Given the difficulty of measuring microplastic concentrations at sea, microplastic distributions are often modeled with computer simulations.

This study evaluates the effects of various physical processes, such as surface currents driven by the wind, waves and surface level gradients, on the location of the garbage patches. While the garbage patches are formed by the wind-driven surface currents, currents due to the waves and surface level gradients determine its final shape. The effects of waves are currently not always included by other microplastic modeling efforts, but this study shows that waves are important for microplastic transport and need to be incorporated in future modeling studies.

Contents

1 Introduction

In the current day and age, there is widespread scientific consent that humans have a profound impact on our planet, with one form of pollution being highly visible: plastic pollution. Plastic is an extremely versatile material that is used to create all sorts of products, from plastic bottles to cell phones to cars [1], and in order to meet the high demand, around 299 million tons of plastic were produced in 2013 alone [2]. A significant amount of the plastic is intended for single use, such as in packaging, and while there are global efforts to recycle plastics, these recover only a fraction of the total amount that is discarded annually [2]. More common ways of processing discarded plastics include incineration and burial in landfills, which bring issues such as the release of toxic fumes and waste of materials. Additionally, it is common for countries to export a portion of their plastic waste to other countries with less stringent environmental regulations, with Europe exporting approximately half of all the plastic that it collects for recycling [2]. A significant amount of waste plastic is thus mismanaged, estimated to have been around 31.9 million tons in 2010 [3].

Mismanaged waste presents a problem in any natural environment, including marine ecosystems. Of the 31.9 million tons of mismanaged waste, 4.8 - 12.7 million tons were estimated to enter the global oceans in 2010 [3] and the plastic spreads to all reaches of the oceans. At the time of writing, plastic has been found in all of the world oceans [4, 5, 6, 7, 8], from the equator [9] to the polar regions [5, 10]. It has also been found within sediments on beaches [11] and ingested by a wide variety of marine wildlife such as fish, birds, and sea turtles [11, 12].

Given the potential harm that plastic can cause to marine life and the longevity of plastic in marine environments [13, 14], technologies are in development [15] to collect and remove the plastic from the oceans. However, we do not currently have a complete understanding of the scale of the waste mismanagement behind the plastic pollution problem. The majority of plastic waste enters the oceans at the coast [3, 16], both from river inputs carrying waste from inland and from direct littering at the coast. Based on population densities and waste mismanagement data, a large fraction of the total pollution appears to originate from Eastern Asia, with the input fluxes varying dependent on factors such as rainfall rates and the presence of artificial barriers such as dams [16]. Globally there a few long-term monitoring stations to monitor plastic fluxes into the oceans, so the input flux estimates have a high degree of uncertainty and are likely an underestimation [16].

Once plastic has entered the ocean, further complications in understanding the final fate of the plastic arise. Plastic comes in a wide variety of types and sizes [4, 8, 17] which can exhibit different behavior. Depending on the buoyancy of the object, plastic can either float at the surface, or sink through the water column until it reaches a zero-buoyancy level or the ocean floor. It is currently not known what fraction of the total input flux ends up directly at the ocean floor or what fraction is advected by the ocean currents. Even if we focus solely on the plastic that remains at the surface, there are still numerous factors that can influence the transport of the plastic. While the surface currents play a dominant role [18], debris items with a significant surface area above the water can experience strong windage effects, where the object will be pushed in the direction of the surface wind [19, 20]. However, modeling such windage effects can be very tricky, for the final trajectory of an object is very sensitive to the strength of the coupling with the wind [19]. Furthermore, the surface currents themselves are a highly complex dynamical system, as the currents vary on multiple time and length scales. Experimental work with drifters released in the Southern Ocean has shown that drifters initially released just 13 m apart can be hundreds

of kilometers apart after just 7 months [21], indicating the sensitivity of drifter trajectories on their initial position. Both observations and modeling have shown plastic accumulation occurs on multiple spatial scales, from meters [22] to hundreds of kilometers [23, 24, 25], but modeling efforts are limited to the spatial resolution of available flow field datasets, which typically do not resolve all small-scale flow structures.

The size of plastic add yet another complication to modeling. Smaller plastic particles tend to have less area exposed at the ocean surface, which means that windage effects for such particles have appeared to be negligible [26, 27]. Also, in studying the processes that lead to the removal of plastic from the ocean surface (e.g. beaching, sinking, ingestion) it is plausible to assume that differently sized particles are removed with different rates. For example, a plastic object in the ocean undergoes biofouling, which means that a biofilm forms on the plastic surface. Over time, this leads to an increase in the density of the object, and the rate of sinking is time-dependent [4, 28]. However, there are still uncertainties in how this ought to be modeled. One also has to consider that the size of a plastic object is not constant, as stresses on the plastic at the surface from waves and UV-radiation can lead to fragmentation[4], with these fragmentation rates also being highly uncertain.

In the literature, numerous different size classifications are used depending on the goal of the study, but generally any plastic fragments smaller than 5 mm is referred to as microplastic. Microplastic specifically poses a great threat to marine ecosystems, since its small size makes it difficult to remove from the marine environment [29] whilst also being very easily ingested by wildlife [12]. As such, numerous studies have focused on modeling the global distribution of microplastic in the ocean [9, 18, 30, 31] with a variety of approaches. While there are some differences in the findings of these studies, overall they agree that microplastic tends to accumulate in the subtropical ocean gyres, forming what are commonly referred to as 'garbage patches'. These regions can have microplastic concentrations orders of magnitude higher than in their surroundings and microplastic measurements taken in the subtropical gyres in every ocean basin confirm that these garbage patches exist [4, 6, 7]. With regard to the amount of microplastic that can be found at the surface, observations and model results estimate the total mass of microplastic is between 7,000 - 236,000 tons made up out of up to 51.2×10^{12} particles [4, 7, 9]. The upper range of this estimate makes up less than 1% of the at least 4.8 million tons that is estimated to have entered the ocean in 2010 [3], which means that most of the plastic is missing. The amount of missing plastic reflects the uncertainties that exist within the field of marine plastic modeling.

For my thesis, I focused on the physical mechanisms behind the transport of microplastic in the ocean basins. The ocean currents can be seen as a sum of different current components, such as geostrophic and Ekman currents and Stokes drift. While there have been some studies that have investigated the contributions of different current components to the location of the garbage patches[32, 33, 34], these focused mainly on the North and South Pacific. Meanwhile, compared to observations previous modeling studies have performed particularly poorly in the North Atlantic [9]. I outline my work to model the position of the floating plastic accumulation regions, henceforth referred to as garbage patches, in the global ocean, with a particular focus on the North Pacific and the North Atlantic basins. The work is based largely on Lagrangian particle simulations using ocean current reanalysis data from the GlobCurrent project [35], as well as regression analysis with time-averaged physical fields, to see how the final position of the garbages patches is dependent on different current components and other physical processes. The Indian Ocean is generally not considered due to the limited microplastic concentration measurements that have been con-

ducted in this region and influence of various mechanisms on the Indian Ocean circulation that go beyond the scope of this research. These include the effects of the Monsoon [36], the El Nino-Southern Oscillation and the Indian Ocean Dipole [37]. The sample data to which the modeled distributions will be compared are solely of floating microplastic, with microplastic referring to all plastic debris that is collected in surface-trawling plankton nets [9]. This definition shall be used in this thesis. In section 2, previous work on modeling the global distribution of marine debris and on the contributions of different surface current components to the accumulation of marine debris is analyzed. Section 3 describes the theory, methods and results for the regression analysis approach, while section 4 describes the theory, methods and results for the Lagrangian modeling approach. Discussion of the results is in Section 5, followed by final conclusions in section 6.

2 Review of literature

Global marine debris modeling

The existence of elevated concentrations of marine debris in the eastern North Pacific has been known since the 1990s [26, 32]. More specific attention was given to the issue of plastic pollution in the eastern North Pacific upon its 'discovery' by Charles Moore in 1997, who reported to have come across plastic "as far as the eye could see" within the North Pacific subtropical gyre [38]. Research since then has confirmed the increased plastic concentrations in the North Pacific gyre [22, 39], and similar elevated concentrations have been found in other subtropical gyres around the world [4, 7, 40]. Given the expense and difficulty in sampling microplastic at sea, there has also been an increased use of modeling to identify regions of microplastic accumulation and to, in combination with samples, give estimates on the amounts of microplastic currently in the ocean.

In 2012, three papers were published independently showing that floating marine debris, which including microplastic, indeed accumulates within the subtropical gyres. Maximenko et al., 2012 [18] used trajectories of buoys from the Global Drifter program to compute the probability that a buoy moves from one $0.5° \times 0.5°$ grid cell to the next over a period of 5 days, with all these probabilities forming a transition matrix. The buoys are drogued with a sea anchor to follow the 15 m depth currents, and this approach yields a probabilistic model of the ocean currents at 15 m depth. Taking an initial globally uniform microplastic distribution, Maximenko et al. [18] advected the debris by multiplying the binned distribution with the transition matrix. Maximenko et al. [18] found that after 10 years, most of the debris had accumulated in the subtropical gyres at around 30° latitude, matching observations of debris. Maximenko et al. [18] attributed this to the convergence of the Ekman currents. However, the garbage patches were not necessarily the end locations of the debris, since over time debris would diffuse out of the gyres again.

While the Maximenko et al. [18] model did lead to a final distribution that matches observations, there are several limitations to the approach. Firstly, the transition matrix was based on trajectories of drifters which are drogued to follow the 15m currents. However, in examining the transport of surface debris the surface currents are most critical, as specifically for microplastic, the concentration drops exponentially with depth [41, 42]. The difference in using 15 m and surface currents can be seen in comparing the trajectories of drogued and undrogued drifters, which show different accumulation patterns [20]. Secondly, the probability calculations for the transition matrix take into account all drifters irregardless of the time of the drifter and so the transition matrix does not include any temporal variations. However, Maximenko et al. [18] notes that temporal variations are important, for otherwise the debris would tend to follow the ensemble mean streamlines.

That particles do not do implies that temporal variations in the currents need to be considered, which is not possible with the Maximenko et al. [18] model. Finally, Maximenko et al. [18] started from uniform initial distribution since the sources of marine debris to the ocean are not well understood and it was hoped that this would not affect the final location of the garbage patches, but it is plausible that the relative sizes of the garbage patches (in terms of number of particles within a garbage patch) are dependent on the distribution of the input sources. Maximenko et al. [18] found the most particles in the eastern South Pacific garbage patch, but attributed this to there being more particles in the southern hemisphere to begin with. However, the largest producers of plastic waste are actually in the Northern hemisphere [3, 16], so it can be expected that the Northern Hemisphere garbage patches contain more plastic.

In contrast to a transition matrix approach which considers debris as a tracer, Lebreton et al. [30] took a Lagrangian simulation approach, in which debris is introduced as a virtual particle which is advected with sea surface currents from the ocean circulation modeling system HYCOM/NCODA [43]. It is thus possible to track the trajectories of individual particles, which is not possible with the tracer approach taken by Maximenko et al. [18]. Additionally, Lebreton et al. [30] took another approach for the input sources of debris. Plastic debris enters the oceans either from land-based sources (such as river input [8], direct littering at the coastline [3], or as runoff from natural disasters like tsunamis [44]) or from marine sources such as shipping and fishing industries [45]. Lebreton et al. [30] scaled the total input of debris with the assumption that most of the land-source plastic enters the oceans at release points corresponding to major rivers and cities while most of the marine-source plastic enters the oceans along major shipping routes. Then various debris-input scenarios were considered where debris was advected for 30 years to obtain the final distribution. In comparison to the results from Maximenko et al. [18] and observations, there is general agreement in the location of the garbage patches within the subtropical gyres, but given the more realistic input distribution that Lebreton used, it was found that the majority of the debris accumulated in the Northern hemisphere (between 25-50% of the total input debris, depending on the input scenario). Similar to Maximenko et al. [18], Lebreton et al. [30] found that debris is able to move between the different garbage patches over time. While some processes are not considered in the model, such as there being no explicit mechanism for beaching nor any form of particle sinking or removal, Lebreton et al. [30] does show the influence of a more realistic debris input distribution on the relative sizes of the garbage patches. However, Lebreton et al. [30] advects the debris using flow fields that are obtained through data assimilation with model output, rather than with direct trajectories like with Maximenko et al. [18] or directly observed ocean currents. Therefore, the debris distribution from Lebreton et al. [30] is heavily dependent on how well the HYCOM/NCODA ocean currents match reality.

Van Sebille et al. [31] took a similar transition matrix approach to Maximenko et al. [18]. However, there are a few key differences in how the transition matrix was computed and applied. While Maximenko et al. [18] used only drogued drifters from the Global Drifter Program, van Sebille et al. [31] used both drogued and undrogued drifters to have a larger drifter dataset for transition matrix and to reflect the fact that debris is spread throughout the upper reaches of the oceans. Several transition matrices were computed by van Sebille et al. [31], each based on drifter trajectories over multiple years for a 2 month period, to capture seasonal variations in the currents. Finally, the debris tracer did not start from a uniform distribution, but was instead released from the coast, scaled according to the population density. Tracer was released in 6 pulses over the course of the first year, after which it was advected for 1100 years. After 1 year, almost all the tracer had already

been transported into the open ocean, which after 10 years led to the formation of garbage patches in all the subtropical gyres. Like Lebreton et al. [30] and Maximenko et al. [18] before, van Sebille et al. [31] found that the garbage patches are not necessarily permanent, with tracer being able to escape the garbage patches over time. After 1100 years the patches in the South Atlantic and Indian oceans had completely dissipated, with the North Pacific garbage patch continuing to grow. Additionally, van Sebille et al. [31] found that debris also accumulates in the Barents Sea, and observations have since confirmed elevated microplastic concentrations in this region [5].

All in all, the various 2012 modeling studies agree that floating marine debris tends to accumulate in the subtropical gyres. In order to obtain an estimate of the number and mass of microplastic in the oceans, the modeled global distributions were combined with microplastic measurements [9], with the modeled distributions shown in figure 1. For each ocean basins the modeled debris concentrations from the three models were fit to standardized sample measurements of microplastic mass and count concentrations. By summing over all basins, it was estimated that there are 93,300 tons (Maximenko et al. [18] model) to 236,000 tons (van Sebille et al. [31] model) of microplastic at the ocean surface. While the different models predicted different amounts of total microplastic, all of the estimates have the same order of magnitude. Furthermore despite regional differences, the overarching patterns from each of the model outputs are roughly the same with relatively low concentrations in the equatorial and polar regions and elevated concentrations in the subtropical gyres. It was then also possible to see to what extent the predicted concentrations from the models agreed with observations. It must be noted only a limited part of the ocean has been sampled for microplastic, of which 90% of all considered measurements have been taken in the northern hemisphere. Van Sebille et al. [9] showed that models performed best in the North Pacific, with all performing poorly in the North Atlantic. Model performance in the other basins was hard to evaluate given the limited sampling that has taken place here. No explanation was given for these differing levels of model performance in the different basins.

Contributions of surface current components on garbage patch locations

While modeling attempts have succeeded in reproducing locations of garbage patches that match those observed in the ocean, few focus on the physical mechanisms that are behind these accumulation distributions. Generally, the accumulation is attributed to either Ekman convergence or the convergence of Ekman surface currents [18, 31], but the isolated effects of the different current mechanisms are often not considered. Kubota [32] (with a follow up study by Kubota et al. [33]) studied the contributions of the geostrophic and Ekman currents and the Stokes drift to the locations of garbage patches in the North Pacific basin with Lagrangian simulations. Since the initial study was conducted before the availability of instantaneous surface current measurements, virtual particles were advected using flow fields derived from climatological means of ocean temperature, salinity and surface wind data. Geostrophic currents are due the balance between the Coriolis force and surface pressure gradients and were computed by Kubota [32] using the temperature and salinity gradients. Meanwhile, surface Ekman currents are the result of wind stress acting upon the ocean surface boundary layer, and according to Ekman theory [46], Kubota [32] computed these currents from mean surface wind data to be at a 45° angle to the right of the wind velocity. Finally, Kubota [32] included Stokes drift, which is defined as the difference between the average Lagrangian velocity of a fluid parcel and the average Eulerian flow velocity of the fluid at a given position. The Stokes drift is in the direction of wave propagation and can be computed from wavenumber-direction spectrum of a wavefield [47].

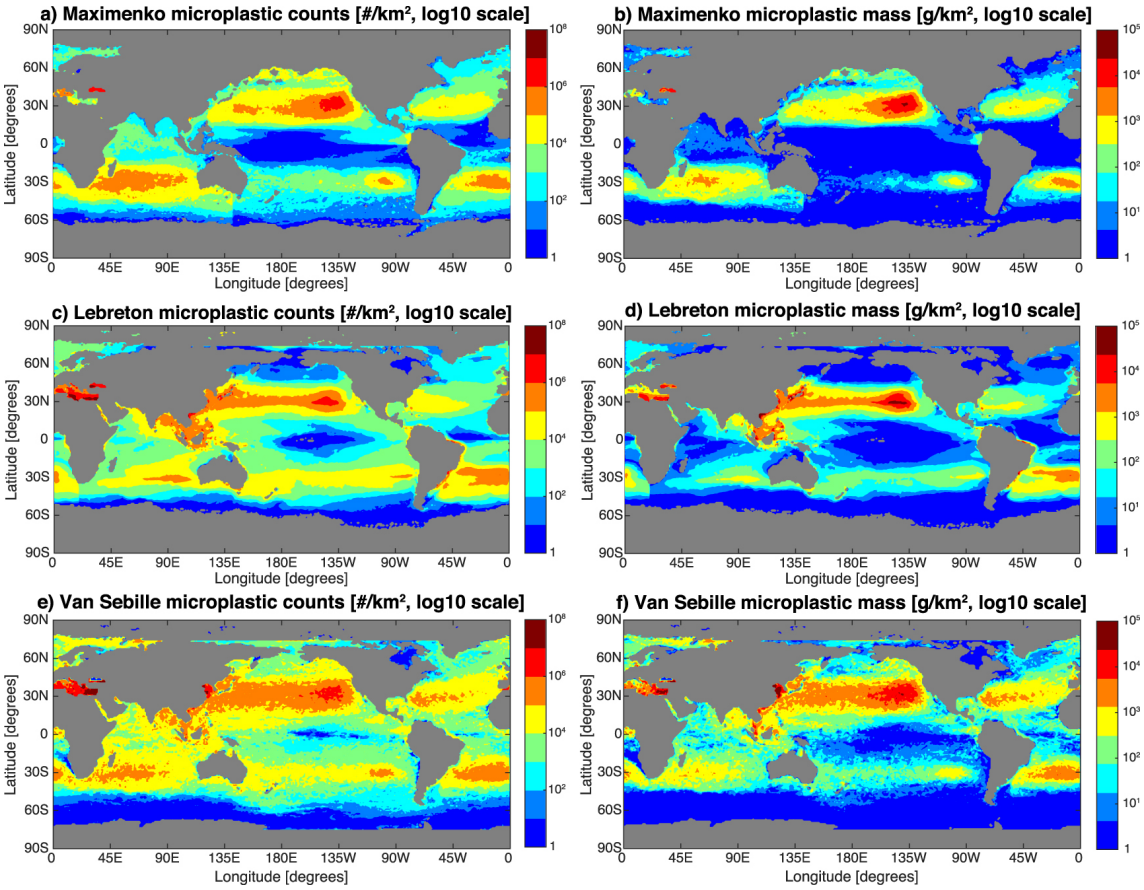

Figure 1: Microplastic count and mass distributions derived using the Maximenko et al. [18], Lebreton et al. [30] and van Sebille et al. [31] models. Adapted from figure 3 from van Sebille et al. [9]

However Kubota [32] parametrized the Stokes drift to be in direction of the surface wind with a magnitude equal to 1% of the surface wind, as Stokes drift data obtained from wave field spectra were not available at the time.

Starting from an initial uniform distribution of virtual particles (50 particles in total for the entire North Pacific), Kubota [32] found that the Ekman currents are responsible for the transport of the particles towards the subtropics. Meanwhile, advection with just geostrophic currents resulted in almost all particles beaching near Seattle and in the Philippines due to unresolved boundary currents, with no accumulation regions in the open ocean. Finally, Kubota [32] found that the Stokes drift led to an accumulation of particles in the western North Pacific, probably due to the low average winds in this region. Combining all the current fields as a linear sum led to the formation of several garbage patches, with one of these being between Hawaii and California where elevated debris and microplastic concentrations are now known to be found [39, 40]. However, at the time no measurements of debris concentrations were available, and thus Kubota [32] was limited to stating that the modeled garbage patch matched the region where marine debris was commonly spotted by shipping.

Based on his findings, Kubota [32] suggested a three part mechanism for the accumulation of debris in the North Pacific. Debris is first transported by the subtropics by the Ekman currents after which geostrophic currents transport it towards the eastern end of the basin. It is then concentrated north of Hawaii by Ekman convergence due to the pres-

ence of the atmospheric subtropical high. Stokes drift was not found significant for the transport of debris. However, there are many limitations to consider for this study, from the use of climatological mean fields with low spatial resolution, to the simple formulations of the various currents components from the climatological mean fields. Additionally, Kubota [32] used only 50 particles for the simulations. Most of these issues were due to the unavailability of better data and a lack of computing powerat the time, and a follow-up study was published 11 years later. Kubota et al. [33] repeated the study of the contributions of the different current components to the position of the North Pacific garbage patch, but the flow fields were now obtained using satellite observations for the geostrophic currents and wind data to calculate the Ekman currents [33]. Furthermore, the simulations were then done with 5,954 particles. The results of Kubota et al. [33] supported the mechanism proposed by Kubota [32]. The Ekman currents were found to be crucial for microplastic accumulation, as the geostrophic currents on their own did not lead to debris accumulation in any particular region. Kubota et al. [33] also did global simulations, with the Ekman currents also being responsible for garbage patch formation in the other basins. Kubota et al. [33] noted that for the Atlantic basins the accumulation tended to be more to the center of the basin rather than towards the eastern end like in the Pacific, but this was deemed to possibly be due to the smaller scale of the basin. Despite more than 10 years having passed since the initial study, Kubota et al. [33] still did not have many debris concentration measurements to compare with the modeled distribution, and so the conclusions regarding model performance were the same as for Kubota [32].

While Kubota [32] provided a mechanism for debris transport for the North Pacific, accumulation in other ocean basins was only briefly covered in Kubota et al. [33] and a separate study of the South Pacific debris accumulation mechanism was published by Martinez et al. [34]. Martinez et al. [34] used geostrophic currents derived from satellite observations between 1993 and 2001 and Ekman currents derived based on 10m-high wind fields measured by ERS-1/2 scatterometers to obtain flow fields for the geostrophic, Ekman and total (sum of geostrophic and Ekman) currents. These flow fields had a spatial resolution of $1/3° \times 1/3°$ and a temporal resolution of 7 days and was to referred to as high resolution data by Martinez et al. [34]. Martinez et al. [34] obtained mesoscale filtered current data by carrying out a 200 km moving average filter over all the flow fields in order to remove the effect of mesoscale current structures. Martinez et al. [34] showed that the high resolution total currents advected almost all debris to between $20° - 40°$S within 2 years, after which it was gradually transported towards the east. Simulations with separate Ekman and geostrophic flow fields indicated that the Ekman currents were responsible for transporting the debris to and keeping it within the subtropics, while the geostrophic currents contribute to the eastward transport of debris. Using the mean sea level anomalies over 1993-2001, Martinez et al. [34] computed geostrophic currents anomalies which in turn were used to compute the eddy kinetic energy (EKE), which is the square of the geostrophic current anomaly divided by two. This measure indicates how energetic the currents within a given region are and Martinez et al. [34] found that high debris densities were generally found within regions with a low mean EKE. Overall, Martinez et al. [34] reports the same mechanism for basin-scale transport as Kubota [32] reported for the North Pacific: transport towards the subtropics by the Ekman currents, followed by eastward transport due to the geostrophic currents. The debris was kept in the east by the Ekman currents. Meanwhile, the mesoscale filtered currents showed similar behavior as the high resolution currents, but since the impact of the mesoscale geostrophic eddies are weakened, Martinez et al. [34] showed that the debris was transported more slowly towards the east. Since the zonal dispersion of the debris in the subtropics was already reported to decrease, mesoscale eddies were deemed by Martinez et al. [34] to be critical for the strength of the

effect of the geostrophic currents. Like Kubota [32] and Kubota et al. [33], Martinez et al. [34] did not compare the modeled debris distribution with observations, for very few measurements have been carried out the South Pacific.

In summary, various studies focused on modeling the global distribution of marine debris have shown that debris tends to accumulate in the subtropical gyres in each of the ocean basins, which corresponds with findings from observational studies. In the Pacific basins, the mechanism that leads to this accumulation consists of a combination of Ekman and geostrophic currents, with Stokes drift appearing to have little effect on the distribution (although the effect of Stokes drift has received no little attention outside of Kubota [32]). Comparing the garbage patch location modeled with the different current components was not possible for the North and South Pacific due to the lack of measurements that were available at the time. With more recent studies, models tend to perform more poorly in the Atlantic basins than in the Pacific when compared to available measured microplastic concentrations. Kubota et al. [33] noted differing accumulation behavior of debris in the Atlantic basins in comparison to the Pacific ones, but as of yet no study has been done to identify the accumulation behavior for the Atlantic basins.

3 Regression analysis

Regression analysis is used as a preliminary approach to investigate which physical processes are important for setting the location of the garbage patches to be in the subtropical ocean gyres. For individual processes, this can be studied by computing the Pearson R correlation coefficient between microplastic concentration data and a time averaged physical field that represent a physical process. The Pearson R correlation coefficient indicates the linear correlation between two variables X and Y according to:

$$r_{X,Y} = \frac{\mathrm{cov}(X,Y)}{\sigma_X \sigma_Y} \tag{1}$$

where $\mathrm{cov}(X,Y)$ is the covariance between X and Y and σ_X and σ_Y are the respective standard deviations of X and Y. The correlation coefficient has a value between +1 and -1, with the extremes indicating either total positive or negative linear correlation between the two variables. A stronger Pearson R correlation coefficient indicates a close correspondence between peak microplastic concentrations and either a maximum or minimum in the physical field values, which implies that the physical process represented by the physical field likely contributes to the locations of the garbage patches.

3.1 Theory

Surface current components

As was explained in section 2, several mechanisms have been identified as being critical in explaining the formation of garbage patches in the subtropical gyres. The most crucial are the surface ocean currents, as the majority of microplastic is found in the top few meters of the ocean surface [41, 42]. The surface currents consist of various components, which are governed by different physical processes. The first is the 2D geostrophic surface current component $\vec{u_g}$, which is due to the balance of the Coriolis force and surface pressure gradients:

$$\begin{aligned} u_g &= -\frac{1}{f\rho}\frac{\partial p}{\partial y} \\ v_g &= \frac{1}{f\rho}\frac{\partial p}{\partial x} \end{aligned} \tag{2}$$

where u_g and v_g are the respective zonal and meridional components of geostrophic velocity, $f = 2\Omega\cos(\phi)$ is the Coriolis parameter dependent on the latitude ϕ and the rotation rate of the Earth Ω and ρ is the water density. However, the pressure can be expressed as $p = p_0 + \rho g \zeta$, where p_0 is the mean atmospheric pressure at $z = 0$, g is the acceleration due to gravity and ζ is the sea surface height. Making this substitution into equation 2, under the assumption that p_0 and ρ are independent of x and y,the geostrophic current components become:

$$\begin{aligned} u_g &= -\frac{g}{f}\frac{\partial \zeta}{\partial y} \\ v_g &= \frac{g}{f}\frac{\partial \zeta}{\partial x} \end{aligned} \tag{3}$$

By measuring the sea surface slope using satellite altimetry (where the sea surface height relative to a geiod is measured, with the geoid being the geopotential surface of the ocean if the ocean would be at rest), direct measurements of the surface geostrophic currents can be made. With u_g and v_g known, the 2D convergence of the geostrophic currents at the ocean surface is shown to be:

$$\nabla \cdot \vec{u_g} = \frac{\partial}{\partial x}\left(-\frac{g}{f}\frac{\partial \zeta}{\partial y}\right) + \frac{\partial}{\partial y}\left(\frac{g}{f}\frac{\partial \zeta}{\partial x}\right) = -\frac{g}{f}\frac{\partial^2 \zeta}{\partial y \partial x} + \frac{g}{f}\frac{\partial^2 \zeta}{\partial y \partial x} = 0 \tag{4}$$

The geostrophic currents thus by definition not convergent, and if debris is considered as a passive tracer that accumulates where surface currents converge, I expect that geostrophic currents do not contribute significantly to location of the garbage patches, and thus that the Pearson R coefficient will be close to zero. This matches what Kubota [32], Kubota et al. [33] and Martinez et al. [34] found with regards to the geostrophic currents. Instead, it was the Ekman currents that were found to be responsible for debris accumulation. The Ekman currents are the response of the ocean currents to a wind stress at the surface in a rotating frame [46], and under the assumptions that one is considering a ocean of infinite depth with no boundaries, where the vertical eddy viscosity A_z is constant with depth, the wind forcing $\vec{\tau}$ is steady and the Coriolis parameter is constant, the balance between the Coriolis force and the induced two dimensional surface current $\vec{u_{ek}}$ is:

$$\begin{aligned} \frac{1}{\rho}\frac{\partial \tau_x}{\partial z} &= -f v_{ek} \\ \frac{1}{\rho}\frac{\partial \tau_y}{\partial z} &= f u_{ek} \end{aligned} \tag{5}$$

where u_{ek} and v_{ek} are the zonal and meridional Ekman velocities. Rewriting the vertical structure of the wind stress can be expressed in terms of the vertical eddy viscosity:

$$\begin{aligned} \frac{\partial \tau_x}{\partial z} &= \rho A_z \frac{\partial^2 u_{ek}}{\partial z^2} \\ \frac{\partial \tau_y}{\partial z} &= \rho A_z \frac{\partial^2 v_{ek}}{\partial z^2} \end{aligned} \tag{6}$$

Substituting this into equation (5) yields:

$$\begin{aligned} A_z \frac{\partial^2 u_{ek}}{\partial z} &= -f v_{ek} \\ A_z \frac{\partial^2 v_{ek}}{\partial z} &= f u_{ek} \end{aligned} \tag{7}$$

Applying the boundary conditions that $\vec{u_{ek}} \to 0$ as $z \to -\infty$ and that the wind stress is equal to friction at the free surface (z=0), along with the simplification that the wind is

blowing northward along the y-axis, yields:

$$\begin{aligned} u_{ek} &= \pm V_0 \cos\left(\frac{\pi}{4} + \delta_E z\right) e^{\delta_E z} \\ v_{ek} &= V_0 \sin\left(\frac{\pi}{4} + \delta_E z\right) e^{\delta_E z} \\ V_0 &= \frac{\tau_y}{\sqrt{\rho^2 |f| A_z}}, \delta_E = \sqrt{\frac{|f|}{2A_z}} \end{aligned} \tag{8}$$

where V_0 is the induced surface current magnitude and δ_E is the Ekman depth, which is the depth of the surface mixing layer. A positive sign of the $\pm$ term in u_{ek} indicates that the northern hemisphere is being considered, while a negative sign corresponds to the Southern Hemisphere. At the surface, the Ekman current is at a 45° angle to the wind stress, and going down the water column the current decreases in magnitude and has its direction spiral. Furthermore, unlike the geostrophic currents, it is possible for the surface Ekman currents to converge, since they are dependent on the wind-stress. With floating plastic as a tracer, the plastic would be carried by the currents and accumulate in these regions of surface Ekman current convergence. Therefore I hypothesize that there will be a correlation between the convergence of the mean Ekman currents and microplastic concentration. Since the convergence is computed mathematically as $\nabla \cdot \vec{u}$, with regions of converging currents having a negative value, I expect a negative Pearson R coefficient between the Ekman surface current convergence and microplastic concentration.

A final component of the surface currents is the Stokes drift, which is induced by the presence of a waves and is defined as the difference between the Lagrangian and Eulerian averages of a flow field [48]. Physically, if one considers a particle below the surface of a surface gravity wave, then to linear order of the wave steepness the particle follows a closed, elliptical orbit. However, since the particle spends more time within the forward moving crest than in the backwards moving though, the particle has a net velocity in the direction of wave propagation over the course of one wave cycle, with this net velocity being the Stokes drift. The effect of the Stokes drift on marine debris transport is uncertain. Kubota [32] found it to be insignificant to microplastic accumulation, but a very simple parametrization for the Stokes drift was used with it just being a fraction of the local wind speed (similar to how windage effects are generally modeled). While this can give an indication of the waves that are induced locally by the wind, they do not take into account swell waves that travel over long distances. Methods are available to determine the Stokes drift from the energy spectrum of a wavefield, with Kenyon [49] deriving that for a wavefield consisting of waves with arbitrary direction and wavenumber, Stokes drift is equal to:

$$\vec{u_s} = g \int \int_{-\infty}^{\infty} F(\vec{k}) \frac{\vec{k}}{\omega} \frac{2k \cosh(2k(z+h))}{\sinh(2kh)} d\vec{k} \tag{9}$$

where $k = |\vec{k}|$ is the magnitude of the 2D wavenumber vector, ω is the angular frequency of the wave, h is the water depth and $F(\vec{k})$ is the wave variance spectrum in wavenumber coordinates. Reanalysis products of Stokes drift derived with such a spectrum-based approach are now available, but have not been widely applied to marine debris modeling research. Stokes drift has been shown to be important for debris transport on small scales, such as the drift of oil from an oil spill [50, 51]. However, on ocean-wide scales the role of Stokes drift for debris accumulation is unclear. In the case of modeling wreckage from the MH370 flight, including Stokes drift had a significant impact on the modeled wreckage trajectories [19], while Lebreton et al. [8] did include Stokes drift in the modeling of floating plastic debris in the North Pacific garbage patch, but did not report the effect that its inclusion had on the observed accumulation patterns. When modeling the transport of

rafting keystone kelp in the Southern Ocean, Fraser et al. [52] found that including Stokes drift in the flow fields resulted in the kelp reaching the Antarctic coasts. Given that this study only focused on the Southern Ocean, its not possible to say what the effect of Stokes drift will be in the subtropics in the ocean gyres. As such, it is not possible to hypothesize in advance the strength nor sign of the Pearson R correlation coefficient between Stokes drift convergence and plastic accumulation.

While the logic between the link of current convergence and plastic accumulation is sound, it must be noted that the mathematical definition of the convergence yields a very local description of the flow field, since it only calculates the convergence of that specific point. However, it might be the case that considering the mean current convergence over a larger area is a better predictor of the locations of garbage patches. I considered the flux F of the flow fields. The flux can be interpreted as the amount of fluid flow through a closed loop C around a given area. According to the Gauss divergence theorem, this can also be expressed as the integral of the divergence of the volume V enclosed by the surface C. Given that we are dealing with two dimensional flow fields with the surface currents, the flux for a region R thus equal to:

$$F = \int_C \vec{u} \cdot \mathrm{d}\vec{n} = \int\int_R \nabla \cdot \vec{u} \mathrm{d}A \tag{10}$$

The hypothesis is that the sign of the Pearson R correlation coefficient between the mean flow fields of the surface currents remains the same, but that the correlation is stronger due to the flux considering effects of over a larger area. The strength of the correlation can also be dependent on the size of the area over which the flux is computed.

Vertical Ekman pumping velocity

Aside from the convergence of surface currents, there are various other variables that I consider. The first of these is the vertical Ekman pumping velocity. In regions where currents converge, it is necessary that there is a downward pumping velocity in order to conserve mass. It has already been shown that geostrophic currents are by definition not convergent, so a pumping velocity would be due to the convergence of Ekman currents. To see this, consider an incompressible fluid, such that the continuity equation (when integrated over the entire vertical water column) is given by:

$$\int_{-\infty}^{0} \Big(\frac{\partial u}{\partial x} + \frac{\partial v}{\partial y} + \frac{\partial w}{\partial z}\Big) dz = 0 \tag{11}$$

$$w_{ek} = w(z=0) - w(z=-\infty) = w(z=0) = -\int_{-\infty}^{0} \Big(\frac{\partial u}{\partial x} + \frac{\partial v}{\partial y}\Big) dz \tag{12}$$

The vertical velocity at $z \to \infty$ is taken to be zero, since this would correspond to the vertical pumping velocity at the ocean bottom. If this bottom is taken to be impervious, then the pumping velocity would need to be equal to zero. Now, taking the x-derivative of u_{ek} and the y-derivative of v_{ek} from Equation 5 and substituting this into Equation 12 yields:

$$w_{ek} = -\frac{1}{\rho f} \int_{-\infty}^{0} \frac{\partial}{\partial z} \Big(\frac{\partial \tau_y}{\partial x} - \frac{\partial \tau_x}{\partial y}\Big) dz = -\frac{1}{\rho f} \nabla \times \vec{\tau} \tag{13}$$

Thus, regions where the Ekman currents converge and there is thus a downward pumping velocity are regions where $(\rho f)^{-1} \nabla \times \vec{\tau} > 0$, which in the Northern Hemisphere is where the curl of wind stress is negative. Since buoyant plastic floats, it would remain at the surface in these downward pumping (downwelling) regions and over time plastic concentrations

would build up. Therefore, it is expected that there will be an negative Pearson R correlation coefficient between the Ekman pumping velocity and microplastic concentrations. In comparison to the Pearson R coefficient of the surface current convergence, the coefficient for the Ekman pumping velocity will likely be closer to zero. Instead of only considering the surface Ekman currents, the depth integrated currents are used in the derivation of the pumping velocity. While the surface currents are at a 45° angle to the wind stress, the depth integrated currents are at a 90° angle to wind stress and regions of depth integrated current convergence are not necessarily the same as regions of surface current convergence. Given how microplastic is located at the ocean surface, the correlation coefficient for the Ekman pumping velocity will be closer to zero than the correlation coefficient for surface current convergence.

Eddy kinetic energy and mixing layer depth

Martinez et al. [34] reported a tendency for microplastic to accumulate in regions of relatively low EKE, where the EKE was computed from geostrophic current anomalies $\vec{u_g}'$ with respect to mean geostrophic currents for 1993-2001 according to:

$$EKE = \frac{(u_g')^2 + (v_g')^2}{2} \tag{14}$$

The EKE is an indication in the amount of variability in the currents, with a higher EKE indicating greater variability with respect to the mean flow. This can be seen as an indication of the presence of mesoscale eddy activity. Mesoscale eddies have been shown to be important in the trapping of microplastic within the garbage patches, with models that are eddy resolving showing more particles escaping the garbage patches than models that are eddy permitting or models that use solely mean currents [23]. Non-linear eddies (where the rotation speed of the eddy is greater than the propagation speed of the eddy) are mass-transporting [53], and eddies passing through would be able to transport some of the microplastic out of a garbage patch. This would reducing the amount of microplastic left behind, and the hypothesis is that there will thus be an negative Pearson R correlation coefficient between the EKE and microplastic concentration.

The EKE is seen as an indicator of mixing in the horizontal plane, but vertical mixing is also known to affect surface microplastic concentrations. Studies have shown that most of the microplastic is within the top few meters of the ocean surface [41, 42], with the concentration dropping off exponentially with depth. The decay constant for this drop-off in concentration is dependent on local wind conditions, with higher winds leading to more mixing and microplastic deeper in the water column. The mixing layer depth (MLD) is a measure of the degree of mixing in a given area, indicating the depth to which turbulence has homogenized the surface layer. The goal is to see whether there is a strong Pearson R correlation coefficient between the EKE and the MLD so that the two can be combined into a total mixing parameter. If this is possible, then it will be seen if there is any strong Pearson R correlation coefficient between the total mixing parameter and microplastic concentrations.

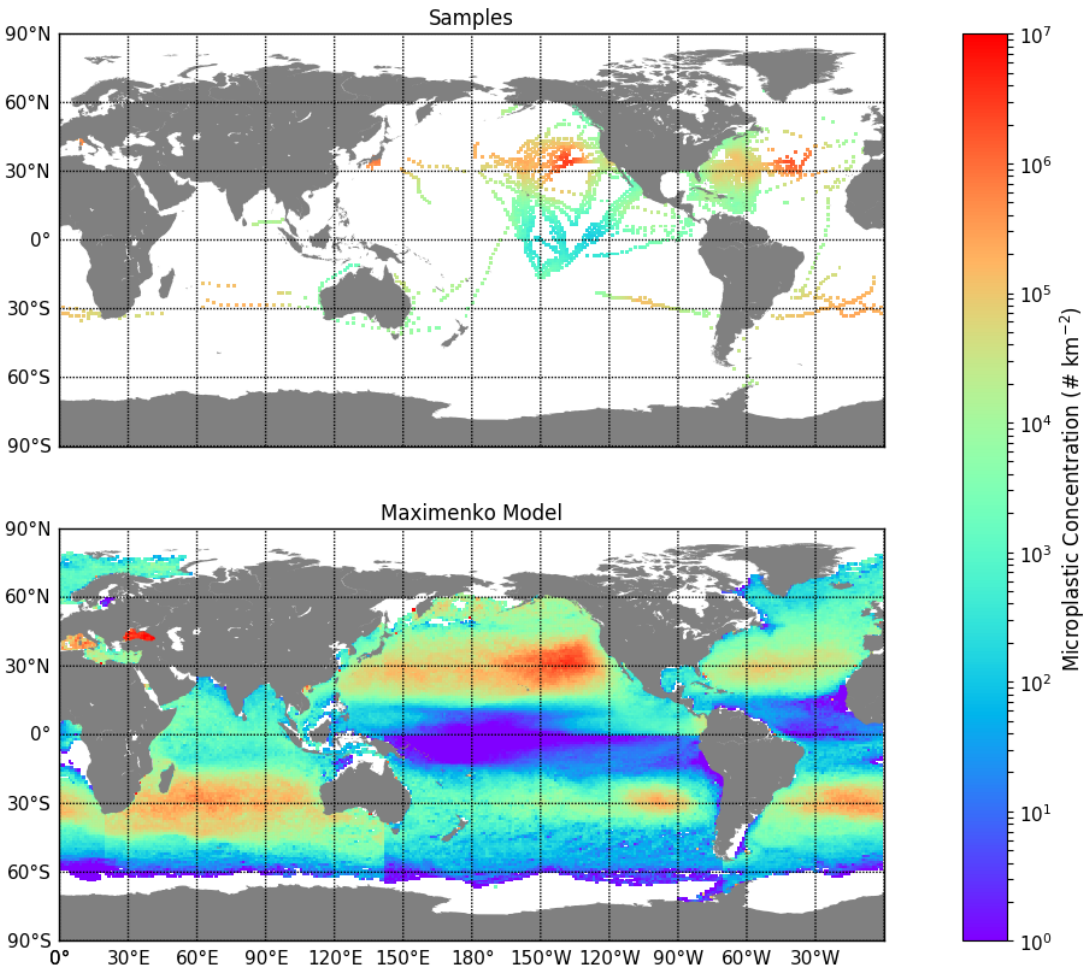

Figure 2: Microplastic distributions from standardized samples and generated using the Maximenko model [9, 18]

3.2 Methods

Computation of the Pearson R correlation coefficients between microplastic concentrations and time averaged physical fields representing physical processes yields a first indication of which processes are important for the determination of the location of the garbage patches. The physical fields that are considered are those of the various variables outlined in section 3.1: the convergence and fluxes of surface geostrophic, Ekman and total currents and Stokes drift, the EKE, the vertical Ekman pumping velocity, and the MLD. Based on the processes that showed strong Pearson R correlation coefficients with the microplastic concentrations, linear regression models were created that predicted microplastic concentrations in the basins based on linear regression. All the code that was written for this and for all other parts of this thesis can be found on Github.

Microplastic data

Microplastic data was taken from van Sebille et al., 2015 [9] and came in the form of both observational data and model output. The sample data was based on microplastic measurements taken with plankton net trawls and included all samples taken between 1979 and 2013. With plankton net trawls, a net with a mesh size of typically around 0.33 mm is dragged behind a ship, outside of the ship's wake, for 15-60 minutes [7]. Then, the net is

brought back onboard and the amount of plastic in the net is cataloged, depending on the study, according to size, number count and where possible plastic type and origin [4, 7, 8]. 11,632 observations were taken as part of the dataset, which were then standardized to account for differences in the sampling year and wind conditions at the time of sampling. A discontinuity at the Americas between the Pacific and Atlantic basins was also included (for full details see van Sebille et al., 2015 [9]). Samples were binned onto a $1^\circ \times 1^\circ$ spatial grid, where the average was taken of all concentrations in each bin to get the final sample distribution. Modeled plastic distribution data was used which was generated using the Maximenko et al. [18] model, which is described in section 2. The modeled plastic distribution will henceforth be referred to as the Maximenko distribution. The microplastic distributions are shown in figure 2.

Mean surface current convergence and flux

Datasets from the GlobCurrent project [35] were used for the total, Ekman and geostrophic surface currents, which GlobCurrent [35] derived using a combination of satellite observations and in situ measurements as described in Rio et al. [54]. First, a geodetic mean dynamic tomography (MDT) was calculated by subtracting a geoid model (in this case the EGM-DIR R4 model [55]) from an altimeter mean sea surface. Since the raw difference between the two surfaces has various commission and omission errors from the geoid model, an optimal filter is applied to smooth out the geodetic MDT, as explained in Rio et al. [56]. In order to improve the resolution of the geodetic MDT, estimates of mean heights and mean geostrophic currents are obtained from in situ ocean measurements, with the measurements being processed to be consistent with the physical signal as was measured by altimetry. The measurements for the geostrophic currents were obtained using drifter velocities from 15 m drogued and undrogued drifters from the Surface Velocity Program (SVP). A 15 m and surface Ekman velocity model (to be described shortly) was used to provide estimates of Ekman velocities, which were subtracted from the SVP drifter velocities to obtain an estimate of the geostrophic current (the undrogued drifters were also corrected for wind slippage according to Rio [57]). Once these corrections had been made, a 3 day low-pass filter was applied to drifter trajectories to remove other ageostrophic currents (such as tides, Stokes drift, and inertial oscillations), although it was noted that the cut-off of the filter might not be sufficient to remove inertial oscillations within 10° of the equator. The mean velocities and surface heights were used to improve the geodetic MDT by means of a remove-restore technique, in which the first guess estimate from the geodetic MDT is removed from the mean observations. Afterwards objective analysis is carried out on the residual surface heights and velocities according to Rio et al. [56]. This is added back to the estimated field to improve the geodetic MDT. The final CNES-CLS13 MDT was obtained by using the mean heights with all available mean velocity data from drogued and undrogued SVP-drifters and Argo floats. Using sea level anomaly data and the CNES-CLS13 MDT, GlobCurrent [35] obtained the geostrophic current fields.

GlobCurrent [35] computed the surface Ekman currents $\vec{u}_{ek}$ as a response to the wind stress forcing $\vec{\tau}$ with a two-parameter $(\beta(z), \theta(z))$ formulation:

$$\vec{u}_{ek}(z) = \beta(z)\vec{\tau}e^{i\theta(z)}$$

The values for $\beta(z = 0)$ and $\theta(z = 0)$ were estimated by applying a least squares fit between estimates of $\vec{u}_{ek}$ and simultaneous wind stress $\vec{\tau}$ values from ERA-Interim [58]. GlobCurrent [35] obtained estimates of $\vec{u}_{ek}$ from subtracting the geostrophic velocities which were obtained from altimeter maps obtained by adding the geodetic MDT and surface level anomaly maps from drifter velocities. The Argo floats were used for the estimates of the surface velocities since they proved less affected by windage than the SVP-drifters. At the

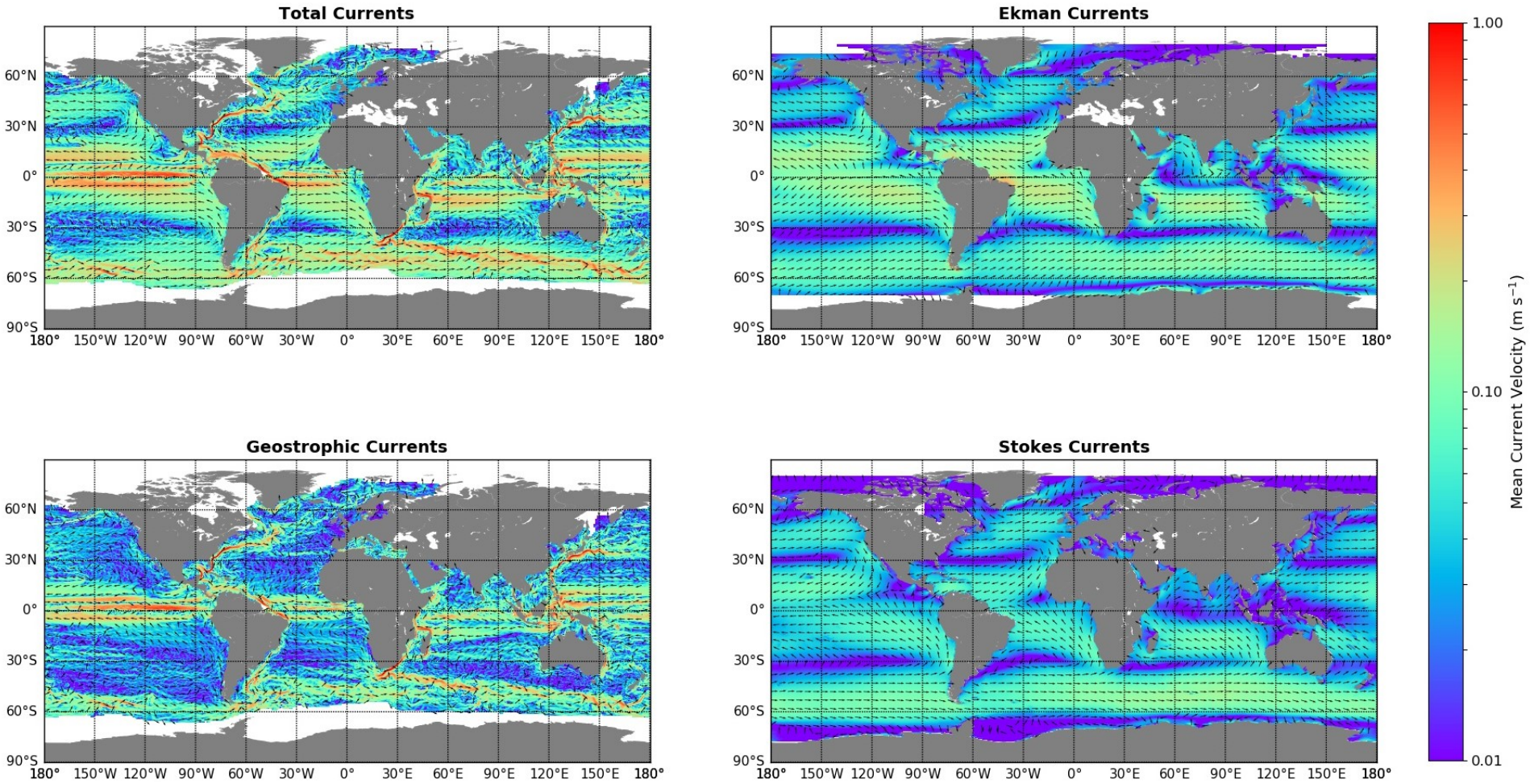

Figure 3: Mean flow fields for the total, Ekman and geostrophic surface currents and the surface Stokes drift. Averages are taken for 2002-2014, with the normalized vectors indicating the mean direction and the colormap indicating the current magnitude. Note that the velocity scale is logarithmic.

surface (based on 841,746 Argo float velocities), the Ekman currents are at an angle of $\theta(0) = 30.75°$ to the wind stress (to the right in the northern hemisphere, to the left in the southern hemisphere), with an amplification factor of $\beta(0) = 0.61\text{m}^2$ s/kg. At 15 m depth (based on 7,537,441 drogued SVP-drifter velocities), these factors are $\theta(15\text{m}) = 48.18°$ and $\beta(15m) = 0.25\text{m}^2$ s/kg. This matches Ekman's theory [46] by exhibiting a spiral-like structure of the Ekman current direction and a reduction in the magnitude of the Ekman currents with depth. The total currents are the linear sum of the computed geostrophic and Ekman surface velocities. The geostrophic current data has a temporal resolution of 1 day, while the total and Ekman currents have temporal resolutions of 3 hours. All the datasets have a spatial resolution of $0.25° \times 0.25°$, but GlobCurrent [35] notes that the effective resolutions of the datasets are 5-10 days/50-100 kilometers .

I obtained the current convergence fields for the total, Ekman and geostrophic currents by calculating the two dimensional current divergence $\nabla \cdot \vec{u}$ for each spatial position according to:

$$\nabla \cdot \vec{u} = \frac{\partial u}{\partial x} + \frac{\partial v}{\partial y} \tag{15}$$

A negative divergence value corresponds to convergence of the surface currents. To obtain the time averaged current convergence field, the current convergence was averaged in time from 00:00 01/01/2002 to 21:00 31/12/2014. For regression analysis, the mean current divergence field is averaged onto a $1° \times 1°$ spatial grid. The surface current flux is calculated according to:

$$\int \nabla \cdot \vec{u} \mathrm{d}A = \int \Big(\frac{\partial u}{\partial x} + \frac{\partial v}{\partial y}\Big) \mathrm{d}A \tag{16}$$

where $\mathrm{d}A$ id the surface area of one $0.25° \times 0.25°$ grid box. The flux was either integrated over $1° \times 1°$ or $2° \times 2°$ areas to obtain surface current flux fields with spatial resolutions of $1° \times 1°$ or $2° \times 2°$. Time averaged surface current flux fields are obtained by averaging the fields in time from 00:00 01/01/2002 to 21:00 31/12/2014.

The Stokes drift flow fields are from the WaveWatch III hindcast dataset [59, 60]. The magnitude and the direction of the Stokes drift is computed from the wavenumber-direction spectrum [47] and yields the Stokes drift with a $0.5° \times 0.5°$ spatial resolution and a temporal resolution of 3 hours. The Stokes drift current convergence and flux fields are computed in an identical fashion to the total, Ekman and geostrophic current convergence and fluxes and the mean convergence and flux fields are obtained by averaging in time from 00:00 01/01/2002 to 21:00 31/12/2014. The mean fields are averaged onto a $1° \times 1°$ spatial grid for the regression analysis. The mean flow fields for the total, Ekman, and geostrophic surface current components are shown in Figure 3.

Eddy kinetic energy, Ekman pumping velocity and mixing layer depth

I computed the EKE using the mean total currents calculated from the GlobCurrent [35] dataset. With 3 hour time steps, the meridional and zonal total velocity anomalies (u', v') were computed by subtracting the mean zonal and meridional total velocities $(\bar{u}, \bar{v})$ from the zonal and meridional total velocities. The EKE is computed according to equation (14). The time averaged EKE field is computed by averaging the EKE in time from 00:00 01/01/2002 to 21:00 31/12/2014. The resultant mean EKE field has a spatial resolution of $0.25° \times 0.25°$, which for the regression analysis was averaged onto a $1° \times 1°$ spatial grid.

I computed the Ekman pumping velocity using monthly mean 10m zonal and meridional wind speeds on a $1° \times 1°$ spatial grid which were obtained from the EMCWF ERA-Interim

global atmospheric reanalysis [58]. The wind stress is computed according to:

$$\tau_x = C_D \rho_a |U_{10}| U_{10}, \tag{17}$$

$$\tau_y = C_D \rho_a |V_{10}| V_{10} \tag{18}$$

where τ_x and τ_y are the zonal and meridional wind stress, $C_D = 0.0013$ is a drag coefficient and U_{10} and V_{10} are the zonal and meridional wind velocities [61]. The mean Ekman pumping velocity is calculated by taking the curl of the windstress according to equation (13), after which the mean Ekman pumping velocity field is obtained by averaging the Ekman pumping velocity field from 00:00 01/01/2002 to 21:00 31/12/2014.

The mean MLD field was obtained from monthly mean mixing layer depths climatologies from an Argo mixed layer climatology database [62]. The monthly mean fields in the database have been computed based on over 1.5×10^6 Argo float profiles measured up to February 2017 and were provided on a $1° \times 1°$ spatial grid with a monthly time resolution. For all other mean fields care was taken to take the mean data from the same time period of 01/01/2002 to 31/12/2014, but this was not possible for the mean MLD field since the dataset consists of monthly mean fields that have already been computed. To get an annual mean field, which was used for the linear regression, I took a time average of the monthly mean MLD fields.

Regression analysis and linear regression models

The Pearson R correlation coefficients are calculated between binned sample and Maximenko distribution concentrations with the physical field values according to equation (1) on a point by point basis. One of the assumptions of regression analysis is that the values being considered are statistically independent, but this is not necessarily the case since the spatial correlation between neighboring points is generally not zero. Therefore, the calculation of the significance of the Pearson R correlation coefficient assumes a number of degrees of freedom that is greater than the actual number of degrees of freedom. The reported significance p of each regression coefficient is therefore higher than what it is in reality and many of the weaker correlation coefficients are likely in reality insignificant. Since the microplastic concentrations cover multiple orders of magnitude, all Pearson R correlation coefficients for the time averaged physical fields were computed with the natural logarithm of the microplastic concentrations to prevent overfitting to high concentrations.

The linear regression models predict the amount of microplastic based on linear regressions of several of the time averaged physical fields with observed or modeled microplastic concentrations. As with the computation of the Pearson R correlation coefficients, the linear regression models are computed based on the natural logarithm of the microplastic concentrations. The linear regression models is predicts the microplastic concentration C_i at a point i according to:

$$\ln(C_i) = c_i + \sum_j \alpha_j g(F_j) \tag{19}$$

where c_i is a constant and a sum is carried out over the contributions of j time averaged physical fields F_j. For each field F_j, the strength of the contribution is determined by α_j. These coefficients are computed to minimize the least square difference between the predicted natural logarithm of the microplastic concentration and the natural logarithm of the concentration from either observations or the Maximenko distribution. Since it not necessarily the case that the fit between a time averaged physical field and the microplastic concentrations is linear, various fitfunction $g(F_j)$ are considered, which yield the square of F_j or the square, cubed or 4th root of F_j. For negative values of the current convergence

and fluxes and the Ekman pumping velocity, the fitfunction is applied to the absolute value of the variable, after which the result is multiplied by -1. For example, consider the fitfunction square(F_j) that yields the square of F_j. This fitfunction is described according to:

$$\text{square}(F_j) = \begin{cases} F_j^2, F_j \geq 0 \\ -|F_j|^2, F_j < 0 \end{cases} \tag{20}$$

If F_j is the Ekman pumping velocity with a value of -2 m s^{-1}, then square(F_j) would be -4 m^2 s^{-2}. This way, the signs of the values of the fields are preserved. The same approach was taken for the square, cubed or 4th root of F_j. Since the EKE is by definition always positive, a fitfunction that returns the natural logarithm of F_j is used. All the fitfunction definitions can be found in Table 4 in Appendix A. Since the current fluxes and convergences are not independent variables, a linear regression model only uses one of the mean geostrophic, Ekman and total current convergence and flux. This this prevents fitting with both the surface current flux and convergence of the same current component, which reflect the same process, and fitting using for example both geostrophic and total fluxes (since the geostrophic currents are part of the total currents).

In order to determine the best linear regression model in describing the garbage patch, two approaches are taken. The first is to determine the relative performance of models based on the Akaike Information Criterion (AIC) [63]. The AIC is defined as:

$$AIC = n * \ln\left(\frac{RSS}{n}\right) + 2k \tag{21}$$

$$RSS = \sum_i \left(y_i - f(x_i)\right)^2 \tag{22}$$

where n is the number of samples considered in the fit, RSS is the residual sum of squares, k is the number of parameters being fit in the model, y_i is the i-th observation and $f(x_i)$ is the model prediction at the x_i position. While the AIC does not offer an absolute measure of how well a model fits to data, it does allow the comparison between numerous models. The model with the lowest AIC is the one that is deemed 'best', for it is generally the one with the lowest RSS and so the closest agreement between observations and the model prediction. In order to prevent overfitting by using a large number of variables, there is a penalty for each additional parameter being fitted with $+2k$ term in equation (21).

For the North Pacific, another approach is taken to see which linear regression model best predicts the garbage patch location. The North Pacific garbage patch is known to be in the Eastern North Pacific [8]. Therefore, the best model is selected according to which has the highest average top 10% of predicted concentrations in the region between $10° - 50°$N and $150° - 120°$W. For each model the concentrations within this region were sorted from highest to lowest, and then the average was taken of the top 10% of the highest concentrations. This should pick out the model that best predicts a region of high microplastic concentrations, which indicates a garbage patch in the approximately correct location.

3.3 Results

Correlations between time averaged physical fields and microplastic concentrations

The first stage of the regression analysis consisted of the computation of the Pearson R correlation coefficients between time averaged physical fields and microplastic concentrations obtained both from the measurements and the Maximenko distribution. The benefit

of carrying out regression analysis with the sampled concentrations is that actual measurements are being considered. However, the collected measurements are spread unevenly over the globe (Figure 2 and Table 1), with the vast majority having been taken in the northern hemisphere. Meanwhile, the advantage considering the Maximenko distribution is that there is basin-wide concentration data, which is closely correlated with observed concentrations in the Pacific Basins (Table 1). The Maximenko distribution matches observations in the Atlantic Basins more poorly, but Figure 2 shows that the Maximenko distribution has elevated concentrating the subtropics. The main difference with observations is the absence of clear peak in the middle of the North Atlantic Basin at around 35°N and 40°W. The regression analysis largely relies on the Maximenko distribution due to the full coverage of the basins, but the differences with observations must be kept in mind during the analysis of the results.

Table 1: Pearson R correlation coefficients for the Maximenko distribution with sampled concentrations in each of the ocean basins and the number of samples taken in each of the basins.

Basin	**Pearson R**	**Samples**
North Pacific	0.899	2551
South Pacific	0.718	789
North Atlantic	0.139	6812
South Atlantic	0.525	155

The MLD is included as a possible variable to examine whether it could be combined with the EKE create a 3D mixing parameter. However, no strong, consistent correlations were found between the EKE and the MLD that held in all the ocean basins (see Table 5 in Appendix A), and as such MLD is not considered further. The Pearson R correlation coefficients of the remaining time averaged physical fields with the sample and Maximenko distributions can be seen in Table 2. The presented regressions were all carried out on fields with spatial resolutions of $1° \times 1°$, although spatial grids of $2° \times 2°$ are also considered for the surface current fluxes so that the effect of considering larger areas for the fluxes could be examined (Table 6 in Appendix A). The fluxes over larger areas generally resulted in slightly stronger correlations, but I decided to stay on the $1° \times 1°$ grids since allowed higher spatial resolutions to be used in the linear regression modeling. In general, the strength and direction of the correlation coefficients of a physical field with samples and the Maximenko distribution agree more Pacific basins than in the Atlantic ones, which matches the closer agreement in between observations and the Maximenko distribution in the Pacific. Additionally, since the samples tend to be clustered in only part of the total basin, the significant correlations of the samples tend to be stronger than those of the Maximenko distribution. Also, the largest correlation coefficient has a value of only 0.424, which means that none of the correlations are extremely strong (close to 1) and references to strong correlations implies that the correlations are strong relative to the correlations of the other variables. In the case of the weak correlations, it is likely that many that are considered significant are in fact insignificant since the number of degrees of freedom is overestimated in the computation of the significance level.

For the Pacific basins, the Ekman currents appear to be the most important mechanism for accumulation, with relatively strong negative correlations for both the Ekman convergence and flux on basin-wide scales (with insignificant or weak correlations for the total or geostrophic currents). Considering just the samples, depth integrated Ekman transport

Table 2: Pearson R correlation coefficients for various variables with the natural log of either the sample data or the Maximenko distribution. Bold-faced values indicate that the correlations are significant at the p<0.05 level, but this is computed with an overestimation of the degrees of freedom.

Basin	**Ekman Pumping Velocity**		**EKE**		**Total Convergence**	
	Sample	Model	Sample	Model	Sample	Model
North Pacific	**-0.400**	**-0.0674**	**-0.444**	**-0.309**	**-0.0777**	**-0.0785**
South Pacific	**-0.306**	**-0.134**	**-0.172**	**-0.294**	-0.0850	0.00714
North Atlantic	-0.0415	**-0.152**	-0.0195	**-0.0538**	0.0380	0.00393
South Atlantic	0.101	**-0.113**	-0.0931	**0.0965**	-0.0671	-0.00929
Basin	**Total Flux**		**Geostrophic Convergence**		**Geostrophic Flux**	
	Sample	Model	Sample	Model	Sample	Model
North Pacific	**-0.0803**	**-0.0858**	0.0147	0.0173	0.0155	0.0173
South Pacific	-0.0856	0.00745	-0.0356	**0.0367**	-0.034	**0.0444**
North Atlantic	0.0416	0.00486	0.0400	0.0215	0.0415	0.0242
South Atlantic	-0.0272	-0.0150	-0.0214	0.0329	0.0253	**0.0369**
Basin	**Ekman Convergence**		**Ekman Flux**		**Stokes Convergence**	
	Sample	Model	Sample	Model	Sample	Model
North Pacific	**-0.164**	**-0.264**	**-0.158**	**-0.259**	**0.395**	**0.293**
South Pacific	**-0.323**	**-0.309**	**-0.315**	**-0.294**	0.0671	**0.182**
North Atlantic	-0.0604	**-0.0745**	-0.0295	**-0.0700**	**-0.131**	**0.411**
South Atlantic	**-0.423**	**-0.424**	**-0.417**	**-0.404**	-0.0607	**0.339**
Basin	**Stokes Flux**					
	Sample	Model				
North Pacific	**0.398**	**0.323**				
South Pacific	0.0375	**0.193**				
North Atlantic	**-0.137**	**0.424**				
South Atlantic	-0.0395	**0.331**				

(as indicated by the Ekman pumping velocity) appears a stronger predictor of microplastic accumulation, but on basin-wide scales with the Maximenko distribution, the correlations are much weaker. The large difference is likely due to the fact that the majority of samples have been taken within the subtropical gyre in the Eastern North Pacific, which is indeed a downwelling region. This leads to relatively strong correlations, but over the entire basin the transport due to the surface currents does appear to be of greater importance microplastic transport than depth-integrated transport, matching the made hypothesis.

In the North Atlantic basin, there are no strong correlations with any of the variables with either the samples or the Maximenko distribution. With the Maximenko distribution, this could be due to the poor agreement with the samples and thus the true microplastic distribution. However, the same issue is present with the sample data, and one interpretation is that none of the considered variables are relevant to microplastic concentrations. Another possibility is that the issue arises due to considering solely time averaged physical fields. Also, it must be kept in mind that the linear regression is simple approach and as such might be of only limited use in plastic modeling. For the South Atlantic basin, the correlations are stronger once again, with the Ekman surface current convergence and flux being the strongest. This suggests that microplastic accumulation in the South Atlantic

basin is predominantly driven by the surface Ekman currents.

Martinez et al. [34] reported that microplastic in the South Pacific tends to accumulate in regions of low EKE, and that is supported by the correlations in both the North and South Pacific basins. However, the correlations are most likely all insignificant in the Atlantic basins if one considers overestimation of the degrees of freedom in the regression. With EKE as measure of mesoscale eddy activity, this implies that mesoscale eddies play a smaller role in garbage patch formation in the Atlantic than the Pacific basins.

Finally, the Stokes surface drift convergence and flux have relatively strong positive correlation coefficients, which means that the highest microplastic concentrations are in regions of diverging flow. Therefore, Stokes drift appears not to contribute to microplastic accumulation, instead leading to microplastic being carried away garbage patches. There is a discrepancy between sample and Maximenko distribution correlations for the Atlantic basins, with the correlation with samples indicating that Stokes drift might actually contribute to accumulation. However, the correlations are weaker (in the case of the South Pacific not significant) and so it is not possible to draw firm conclusions regarding to the role of the Stokes drift in the Atlantic basins from examining Pearson R correlation coefficients alone.

Linear regression models

Based on the Pearson R correlation coefficients, I decided not to include Stokes drift convergence and flux for the linear regression modeling of the microplastic distribution since the correlation coefficients with the Maximenko distribution suggest that Stokes drift does not contribute to microplastic accumulation. Furthermore, while the correlation coefficients of the time averaged physical fields are computed with both the samples and the Maximenko distribution, I only use the Maximenko distribution for the linear regression modeling since the data covers the entirety of the ocean basins. Furthermore, the Maximenko distribution has a larger range of concentrations. Linear regression modeling with the sample data led to microplastic distributions that tended to be homogeneous over the entire basin, since the majority of samples have relatively low concentrations as they were collected outside the garbage patches. Linear regression modeling is done by minimizing the residual sum of squares between the model and observations, and thus the fit is predominantly done with the observations outside the garbage patch. Additionally, observed concentrations can not be much lower than 540 # km^{-2}, since this corresponds to just one microplastic fragment found over the course of a trawl of one nautical mile [9]. Since the Maximenko distribution does not have such a lower bound for the possible concentrations, it can have lower non-zero concentrations. Together with the basin-wide coverage of the dataset, there is a smaller tendency for linear regression modeling to return a homogeneous modeled microplastic distribution.

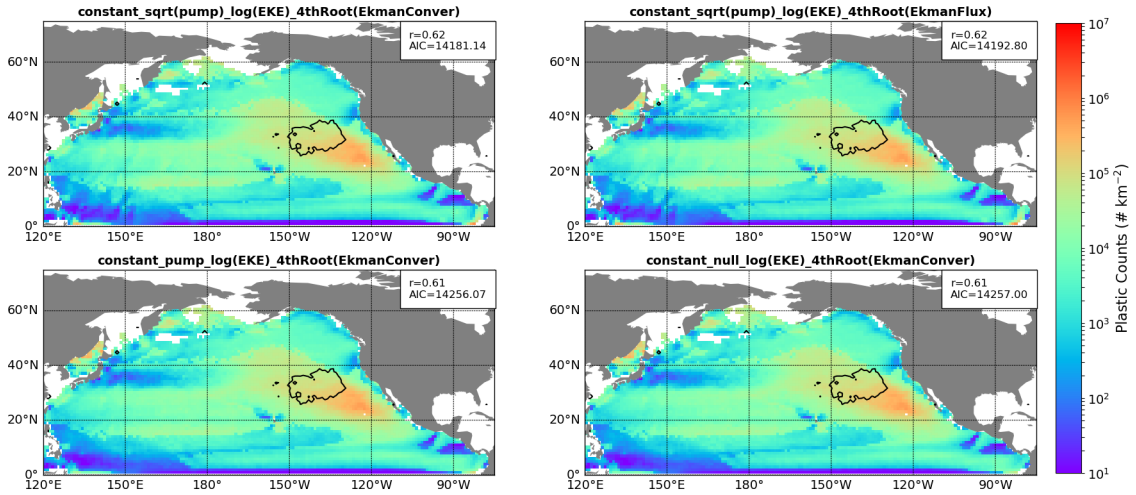

Figure 4: Best performing linear regression models for the North Pacific basin, selected according to the lowest AIC values. Contour shows the 1×10^6 # km^{-2} from the Maximenko distribution. The subplot titles indicate the time averaged physical fields and fitfunctions used in the linear regression model, see Table 4 in Appendix A.

Starting with the North Pacific basin, the best performing linear regression models were selected based either having the lowest AIC value (Figure 4), or on having the highest average concentrations in the region in which the peak concentrations are observed in the Maximenko distribution (Figure 5). In general terms, the modeled distributions selected with the AIC match that of the Maximenko distribution, with low concentrations at the equator and highest concentrations in the subtropics in the Eastern end of the basin (Figure 4). The difference in the garbage patch location is that it is farther south and east compared to the Maximenko distribution, and that the magnitude of the peak concentrations are lower than the Maximenko distribution. All models depend on the Ekman surface currents (either the current convergence or flux) and the EKE, with a smaller dependence on the Ekman pumping velocity (reflected by the fact that a model not including any form of Ekman pumping velocity has only a slightly higher AIC value than those including it). The position of the peak concentrations is determined largely by the EKE, for the peak concentrations are found at the exact point of lowest average EKE (not shown). Meanwhile, the surface Ekman current convergence and flux are highest in the subtropics, leading to highest concentrations here. Regarding the fitfunctions used, it is not possible to attribute much physical meaning to them, since the fitfunctions are relative to the natural logarithm of the Maximenko distribution concentrations. In the case of EKE, since the best fits are done with the natural logarithm of EKE, we can state that there appears to be a power law relationship between the EKE and microplastic concentrations. However, I do not have an physical explanation for why the relation takes this form.

While the AIC considers performance of the model over the entire basin, the main goal of the linear regression modeling is to see which models best predict the location and elevated concentrations of just the garbage patch. This was done by selecting the best performing models by taking those that have the highest average concentrations in the region between $10^\circ - 50^\circ$N and $150^\circ - 120^\circ$W. The resulting distributions are not very different from those selected with the AIC (Figure 5), with the garbage patch still being too far southeast and not reaching the same peak concentrations. Linear regression modeling solely on the subtropics between $20^\circ - 40^\circ$N did not yield improved performance (Figure 20 in Appendix A).

The same linear regression modeling approach was applied to the South Pacific and the

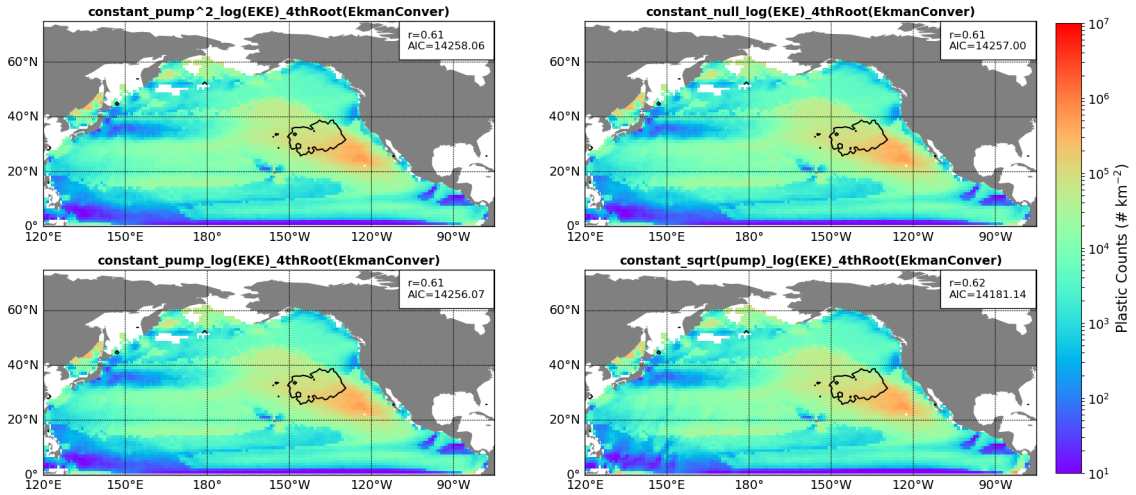

Figure 5: Best performing linear regression models for the North Pacific basin, selected according to the highest average of the top 10% of microplastic concentrations in the region of $10° - 50°$N and $150° - 120°$W. Contour shows the 1×10^6 # km^{-2} contour from the Maximenko distribution. The subplot titles indicate the time averaged physical fields and fitfunctions used in the linear regression model, see Table 4 in Appendix A.

Atlantic basins. While the linear regression models for the North Pacific yielded a clearly defined garbage patch in same approximate location as the Maximenko distribution, such clear patterns were not observed for the other basins (Figures 21, 22 and 23 in Appendix A). While the linear regression models have thus shown that the surface Ekman currents and EKE appear critical to microplastic accumulation in the North Pacific, little insight is gained into accumulation mechanisms in the other ocean basins. For this, we turn to Lagrangian microplastic particle modeling.

4 Lagrangian modeling

4.1 Theory

Section 3.1 has already covered the majority of the theory behind the expected contributions of various physical processes, but the theory was presented largely from a Eulerian perspective. Given the findings of the Pearson R correlation coefficients for the various time averaged physical fields and the linear regression modeling presented in section 3.3, the presented theory is reexamined to provide hypotheses for the Lagrangian modeling.

Surface current components

First, consider the roles of the various current components. Martinez et al., [34], Kubota [32], and Kubota et al. [33] concluded that the geostrophic currents do not contribute to debris accumulation, adding only to the eastward transport of debris in the Pacific basins. Pearson R correlation coefficients of the geostrophic current convergence and flux with microplastic observations are weak and likely insignificant (if one accounts for the overestimation of degrees of freedom) for all the ocean basins. Therefore, it is likely that Lagrangian runs with particles advected just by geostrophic currents will also not show microplastic accumulation in any particular region. The regression analysis does not allow any insight into whether the geostrophic currents contribute to any eastward transport, so the hypothesis is that the contribution of the geostrophic currents, in at least the Pacific basins, will be the same as described by Martinez et al., [34], Kubota [32], and Kubota et

al. [33].

Coming next to the wind-driven Ekman currents, Martinez et al., [34], Kubota [32], and Kubota et al. [33] all found that these currents are responsible for the transport of debris towards the subtropics. This is supported by the regression analysis shown relatively strong anticorrelations between the Ekman current convergence and flux with both the samples and Maximenko distribution. Additionally, surface Ekman current convergence or flux are included in all the best performing lienar regression models. As such, it is expected that, with just the Ekman currents, the Lagrangian simulations will show microplastic accumulation in the subtropics. However, it is possible that the accumulation behavior will differ slightly in comparison to earlier studies due to the different formulations of the Ekman currents. While based on Ekman's theory [46] the surface Ekman currents are directed at a 45° angle to the wind stress (with this formulation being used by both Martinez and Kubota), the GlobCurrent[35] surface Ekman currents are at a 30.75° angle to the wind stress. With regards to the North Atlantic basin, regression analysis showed an insignificant correlation between surface Ekman current convergence and flux and microplastic concentrations, which suggests that the plastic accumulation in this basin might not be wind-driven. However, it must be kept in mind that the Maximenko distribution correlates poorly with observations in the North Atlantic and that regression is carried out solely with time averaged fields of the current convergence and flux, while the Lagrangian simulations include temporal variations in the flow fields.

While studying the isolated current components yields insight into the contributions of individual processes to the accumulation of floating plastic debris, it is ultimately the total ocean currents which are responsible for the transport and accumulation of plastic debris in the subtropics. The regression analysis showed largely insignificant correlations between the total (Ekman + geostrophic) surface current convergence and flux and microplastic concentrations, which can imply that solely looking at where surface current converge is not sufficient to determine the locations of garbage patches. In order to see whether looking at separate components of the total currents can be justified, Lagrangian simulations of with total currents need to be examined first to see whether the modeled plastic debris distributions correspond to observations.

The final surface current component the surface Stokes drift. The effect of Stokes drift on ocean-wide marine debris transport has not received much prior attention, and as such there is little literature to compare results with. Based solely on the regression analysis, it is appears that Stokes drift does not contribute to microplastic accumulation, since there is a positive correlation in all basins between the Maximenko distribution and the Stokes drift convergence and flux. This suggests that Stokes drift acts disperse microplastic. Lagrangian simulations will be able to show if this is indeed the case, and based on the results from the regression analysis and the mean Stokes drift flow field in Figure 3, the microplastic will likely be carried towards the polar and equatorial regions.

Eddy kinetic energy

Martinez et al. [34] noted that debris in the South Pacific tends to accumulate in regions of relatively low EKE. The EKE indicates the deviation of currents from the mean currents at a given location, and is considered in this thesis as a proxy for mesoscale eddy activity. The regression analysis showed a relatively strong anticorrelation between microplastic concentrations and EKE in both Pacific basins, which matches the finding of et al. [34]. However, the correlations for the Atlantic basins are much weaker and most likely all insignificant, which indicates that mesoscale eddies play a less significant role in

floating plastic accumulation in the Atlantic than in the Pacific. The advantage of using Lagrangian simulations is that trajectories for individual particles are obtained along with the evolution of the EKE along the particle trajectory. If it is indeed the case the plastic debris accumulates in regions that are a local minimum in the EKE, then it is expected that the EKE decreases along the trajectory of a particle. Given the findings from the regression analysis, this is expected to be more pronounced in the North Pacific than in the North Atlantic basin.

4.2 Methods

In Lagrangian microplastic modeling, the microplastic is represented by virtual particles which are advected by oceanflow fields. This is done using Parcels (Probably A Really Computationally Efficient Lagrangian Simulator), which is being developed as part of the OceanParcels project. The exact details of how Parcels works can be found in Lange & van Sebille [64], but the basic principles will be outlined here. Parcels is used to advect virtual particles using ocean flow field data and prescribed particle 'behaviors'. A change in the position $\vec{x}$ of a particle can thus be computed from:

$$\vec{x}(t+\Delta t) = \vec{x}(t) + \int_{t}^{t+\Delta t} \vec{v}(\vec{x}(t), \tau)\mathrm{d}\tau + \Delta\vec{x}_b \tag{23}$$

where $\vec{v}(t)$ is the velocity at $\vec{x}(t)$ and $\Delta\vec{x}_b$ is a change in position due to the particle behavior. This behavior can be decided by the user and is completely customizable through the use of 'kernels'. The flow velocity $\vec{v}(\vec{x}(t), t)$ at the particle location is obtained through linear interpolation of the flow field data. It is also possible for the particles to sample other fields that are used in the simulation, such as the local EKE, so that one can track the EKE of the particle along its trajectory.

The Lagrangian simulations were run using the GlobCurrent [35] and Stokes drift [59, 60] flow field datasets described earlier in section 3.2, with varying spatial domains, particle amounts and current components. For all simulations, the initial distribution of particles was a uniform grid, with particles initially spaced at 0.5° intervals for the North Pacific (30,091 particles) and North Atlantic (18,632 particles) simulations and at 1° intervals for the global simulations (34,515 particles). The initial uniform distribution was chosen to allow easy comparison with the Maximenko model results used for the regression analysis. Furthermore, like Maximenko et al. [18], I hoped that the final locations of the garbage patches would not be affected by the initial distribution, even if the number of particles within the garbage patches is undoubtedly dependent on the initial distribution. All simulations are run with an integration time step of 30 minutes where the particles are advected with a 4th order Runge-Kutta scheme. Each simulation started on 01/01/2002 and ended on 31/12/2014, since the GlobCurrent [35] data is available for this time.

Simulations are run with particles being advected with the total currents, the Ekman currents, the geostrophic currents, the Stokes drift and a linear sum of the total currents and Stokes drift. Effects of windage were not considered, for two main reasons: firstly, microplastic is small enough that windage effects are thought not to have a very pronounced effect [27], while secondly, it is not possible to say that windage is not already partially included in the computation of the Ekman currents. As was described in section 3.2, the Ekman currents of the GlobCurrent [35] dataset were derived by applying a fit between wind stress data and non-geostrophic velocities of Argo floats. Part of the Ekman currents might be windage, and as such it was decided to include windage effects as a transport mechanism on its own. Given that the geostrophic current dataset has a spatial resolution of 24 hours, with the timestamp of the data always being set 00:00, it was decided to run

all the simulations using just the datasets with a 00:00 timestamp. This is to maintain consistency and since the temporal resolution of the flow fields, according to GlobCurrent [35], is on the order of days instead of 3 hours. This means that the 3-hourly data does not provide additional information beyond having been interpolated from measured currents to a smaller time resolution than one day. The effect of using the 3-hourly flow fields is studied and is expanded upon in section 4.3. Finally, the main aim of this thesis is to identify the location of the garbage patches and how this shifts depending on the various current components. While important, the beaching behavior of microplastic goes beyond the scope of this thesis. As such, a coastal anti-beaching current is introduced that prevented the beaching of particles. The reason for this is that without this current, the majority of particles tended to beach. This yields less information about the trajectories and it was found that the locations of the garbage patches are not affected by the anti-beaching current. With more particles remaining afloat, more useable trajectories are available for statistical analysis. The anti-beaching current was implemented by first identifying the coastlines in the GlobCurrent [35] datasets, which is done by identifying where both the zonal and meridional surface current components are exactly equal to zero. This allowed a land mask to be created and at each point along the edge of the landmask the landward direction was identified in both the latitudinal and longitudinal directions. The anti-beaching current was then defined to be in the opposite direction, so that a particle that has beached would be pushed off the coast so that it would be carried away by the off-shore currents. At all other points in the ocean, the anti-beaching current is set to be zero to not alter particle trajectories further. The strength of the current is set to approximately 10 m s^{-1}, as this is sufficient to overcome any on-shore current and will propel the particle a sufficient distance off the coast so that it will not immediately beach again at the some location.

For each of simulations, the positions of the virtual particles were binned into 1° bins to obtain particle concentrations. The final microplastic distribution for each run was then taken to be the time averaged density distribution over the final year of the simulation (01/01/2014 to 31/12/2014). Since the garbage patches are not static, the average over the final year serves to give an indication over the average position of the peak concentrations.

4.3 Results

Global

To have an initial overview of the microplastic accumulation on a global scale, global runs were carried out where virtual microplastic particles were advected for 14 years with flow fields as described 4.2. In the total current simulation, garbage patches form in each of the subtropical ocean gyres (Figure 6), which matches observations of increased microplastic concentrations in these regions (Figure 2). As with van Sebille et al., 2012 [31], there is also a garbage patch in the Arctic around Nova Zembla. In terms of the number of particles, the South Pacific garbage patch is found to be the largest, but as Maximenko et al. [18] noted, this is an artifact of the homogeneous initial distribution, as the Southern Pacific basin is the largest and has the most particles initially. Similar to Kubota et al. [33], microplastic in the Atlantic basins tends to accumulate in the center of the basin, in contrast to the Pacific basins when microplastic tends to accumulate closer to the eastern boundary. Given that the total currents lead to a microplastic distribution that generally agrees with observations, it is justifiable to consider the effects of the individual current components.

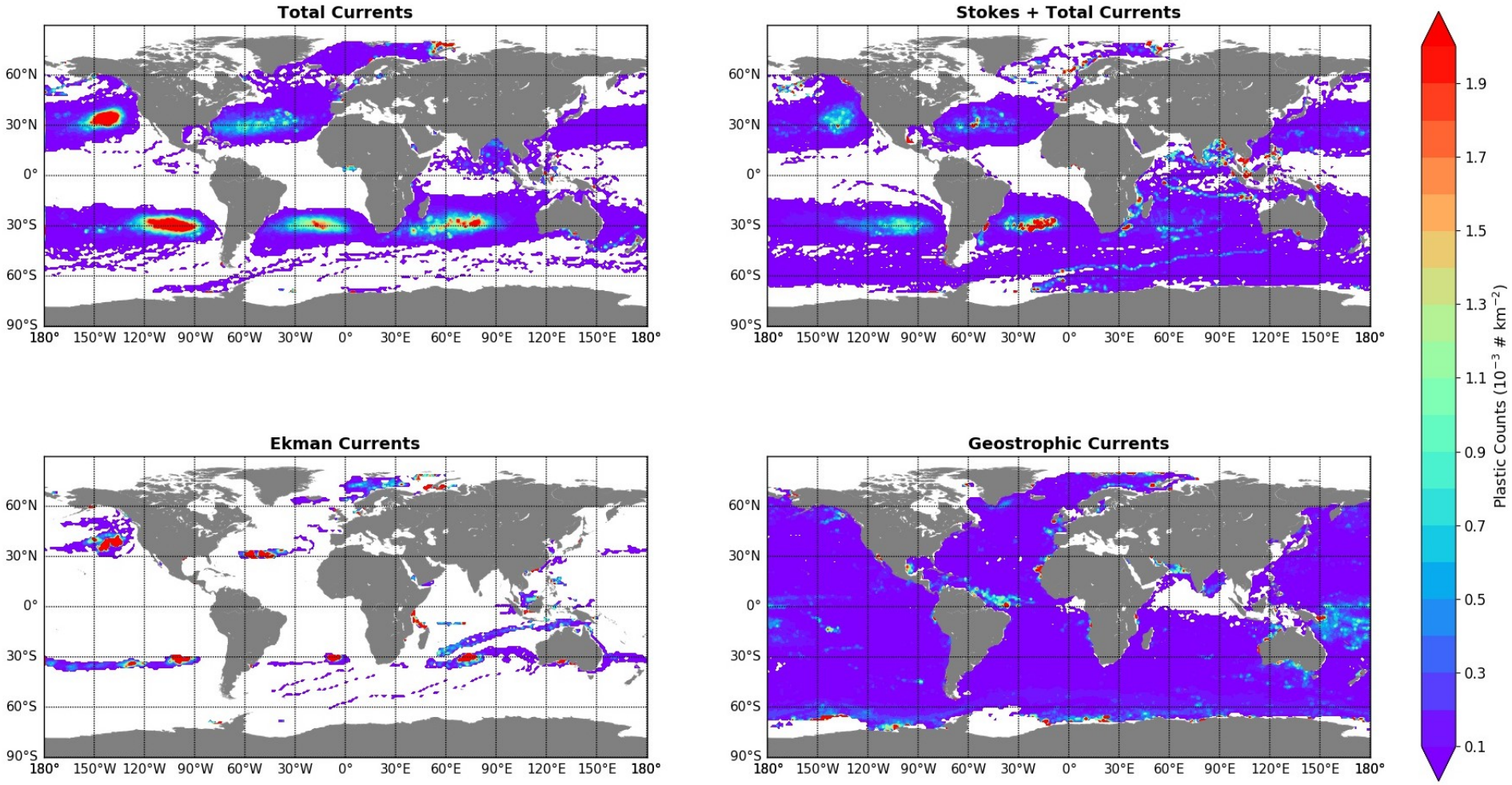

Figure 6: The average particle density of the final year of the global Lagrangian runs with the virtual particles advected by total currents, total + Stokes currents, Ekman currents and geostrophic currents. Simulations are from 01-01-2002 to 31-12-2014 from an initial uniform $1^\circ \times 1^\circ$ distribution of particles.

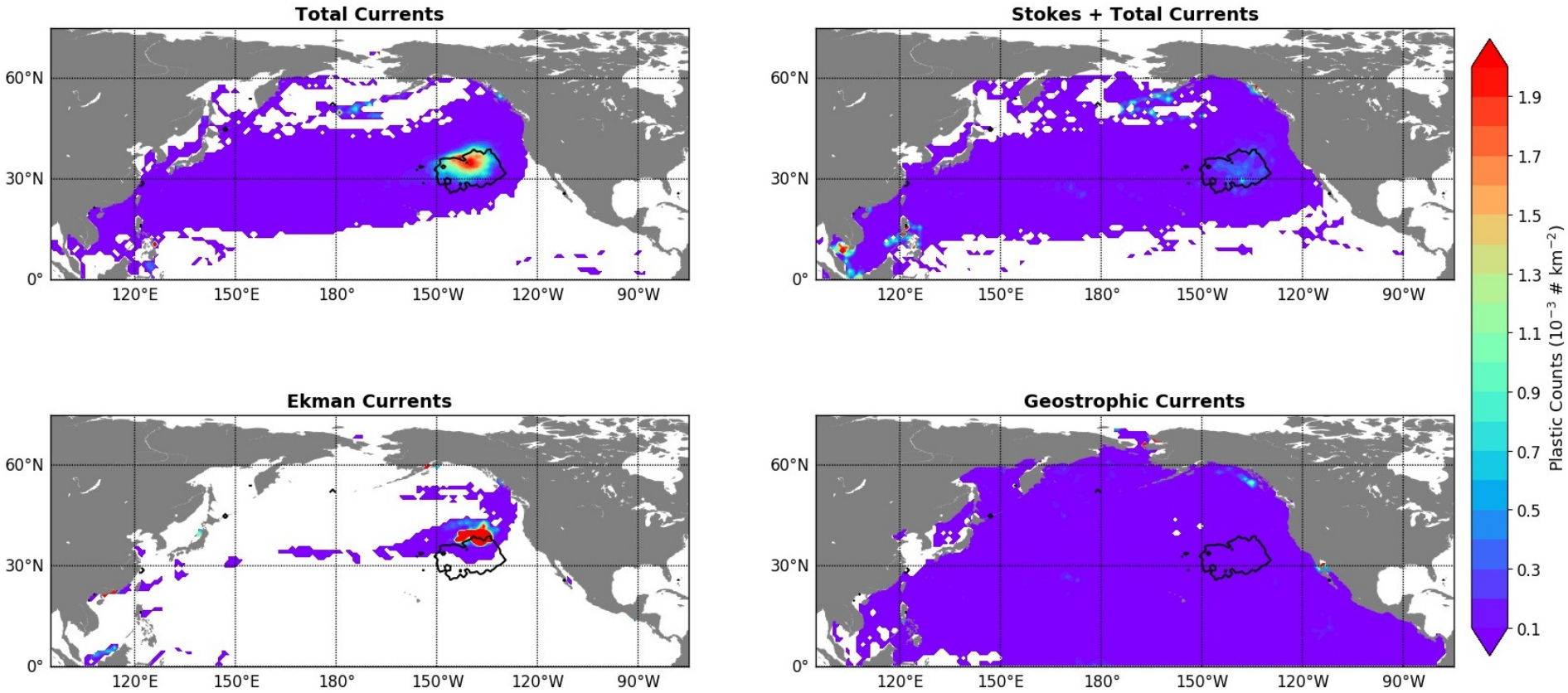

Figure 7: The average particle density of the final year of the North Pacific Lagrangian runs with the virtual particles advected by total currents, total + Stokes currents, Ekman currents and geostrophic currents. Simulations are from 01-01-2002 to 31-12-2014 from an initial uniform $0.5° \times 0.5°$ distribution of particles. Contour shows the 1×10^6 # km^{-2} contour from the Maximenko distribution.

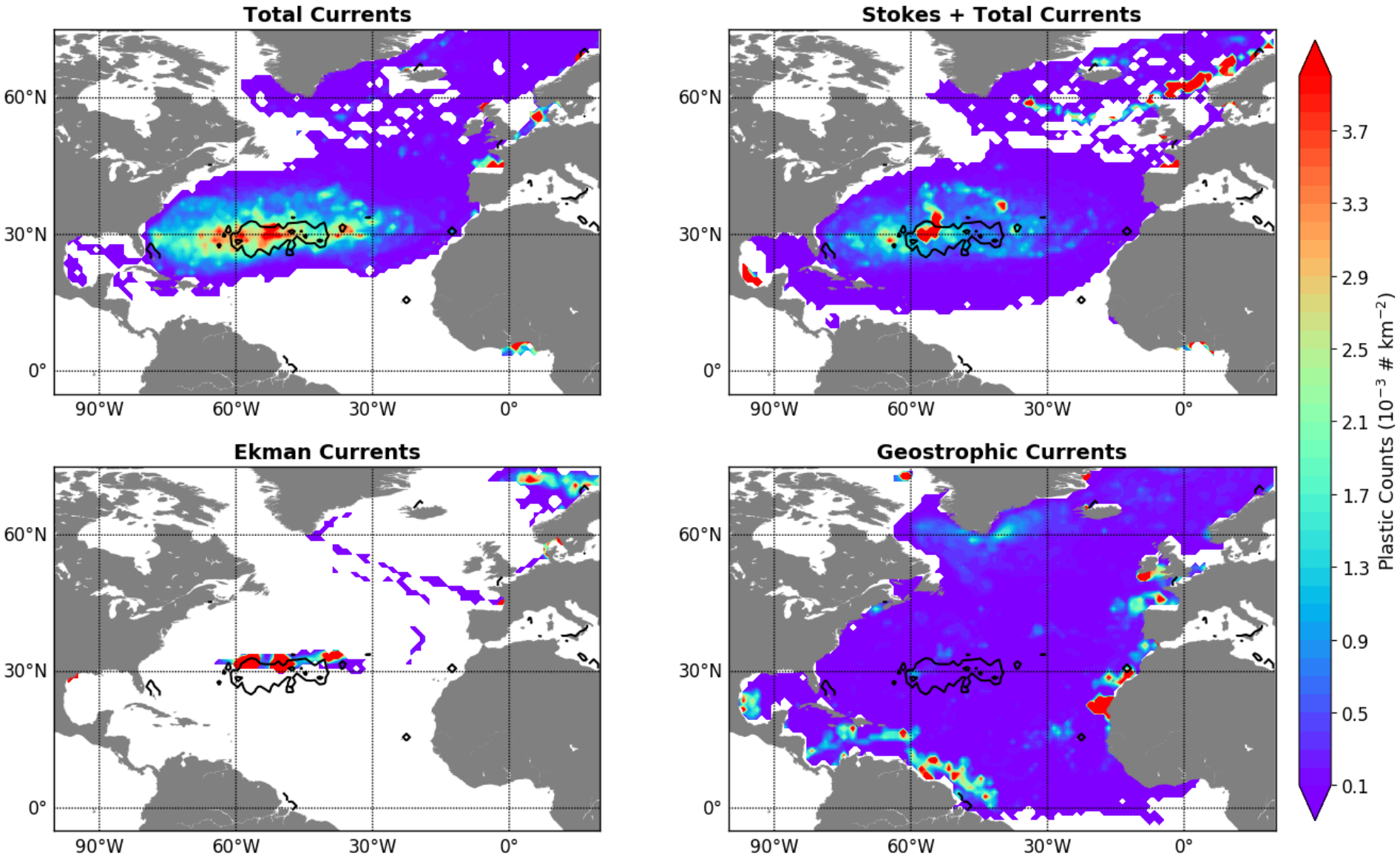

Figure 8: The average particle density of the final year of the North Pacific Lagrangian runs with the virtual particles advected by total currents, total + Stokes currents, Ekman currents and geostrophic currents. Simulations are from 01-01-2002 to 31-12-2014 from an initial uniform $0.5° \times 0.5°$ distribution of particles. Contour shows the 5×10^4 # km^{-2} contour from the Maximenko distribution.

The formation and locations of garbage patches are due to the Ekman currents, matching the conclusions of Kubota [32], Kubota et. al [33] and Martinez et al. [34]. Ekman currents alone are sufficient to accumulate microplastic in the subtropical gyres, but in contrast to the earlier studies, geostrophic currents do not appear necessary for eastward transport. Only in the South Atlantic is the position of the garbage patch strongly affected by the inclusion of geostrophic currents (Figure 6). The Ekman current simulation also shows the polar garbage patch, which indicates that the Ekman currents do not always lead to plastic transport towards the subtropics. Particles whose initial position is in the region of the westerlies or anti-trade winds in the North Atlantic are generally being transported to the polar garbage patch, instead of to the North Atlantic subtropical garbage patch (Figure 16a).

With the exception of the South Atlantic basin, the geostrophic currents play a larger role in microplastic dispersion than in transport or accumulation. Advection with geostrophic currents doesn't result in accumulation in the subtropical gyres, but comparing the surface area of the garbage patches with the Ekman currents and the total currents makes it is clear that the geostrophic currents prevent all the microplastic from being concentrated at a single point (Figure 6). Instead the microplastic is spread out over a larger region in the subtropics. Near the coasts, the geostrophic currents can lead to microplastic accumulation. While the models are set up so that beached particles are kicked off the coast and back into the oceans, coastal plastic buildup can still occur if geostrophic currents are generally directed towards the coast. In the open ocean, the microplastic distributions from the geostrophic current simulations are largely homogeneous, with the exception of the equator (Figure 6). In the Indian ocean, the equatorial regions are completely cleared of microplastic while elevated concentrations are observed off the northern coast of Brasil and east of Borneo. It is possible that this is a product of the computation of the geostrophic currents, which rely on there being a balance between the Coriolis force and surface pressure gradients. However, at the equator the Coriolis force is zero and thus such a balance is physically not possible. Additionally, while the observed geostrophic currents that were assimilated into the geostrophic flowfield dataset were filtered to remove non-geostrophic components, Rio et al. [54] acknowledged that the chosen cut-off time for the filter might not be sufficient to remove inertial oscillations within 10° latitude of the equator. Estimates in the estimated mean error of the geostrophic currents (Figure 24 in Appendix A) indicate the greatest estimated errors in the equatorial regions, supporting the hypothesis that the observed non-homogeneity is a product of the dataset.

The role of Stokes drift is dependent on the basin. In the Pacific basins, Stokes drift leads to the transport of microplastic towards either the equator or the poles, with no garbage patch forming in the subtropics (Figure 25 in Appendix A). In the South Atlantic there continues to be microplastic in the subtropical ocean gyre at the end of the Stokes simulation, but the concentrations are not comparable to those attained with either the total or Ekman current simulations. In the North Atlantic, the Stokes drift leads to microplastic accumulation in the Caribbean and north of Norway. Comparing the run with total currents to that with the linear combinations of the total currents and Stokes drift shows a decrease in peak concentrations in the Pacific basins along with a greater spread of microplastic over the basin (Figure 6). This matches findings from the regression analysis, where regions of peak microplastic concentration were generally found to correspond to regions of the peak Stokes dirft divergence. It also matches how the Stokes drift on its own clears the subtropics of most microplastic (Figure 25 in Appendix A). The North Atlantic basin will be discussed shortly, but it is clear that the Stokes drift increases accumulation in the South Atlantic compared with the total currents on their own, with the garbage

patch there showing much higher concentrations. Related to this, the garbage patch in the Indian ocean has all but disappeared following the inclusion of Stokes drift. Part of this ends up the Northern Indian Ocean, particularly in the Bay of Bengal, but much of the microplastic from the Indian ocean garbage patch ends up in the South Atlantic garbage patch.

The effect of Stokes drift on the fate of microplastic is made clearer by considering the

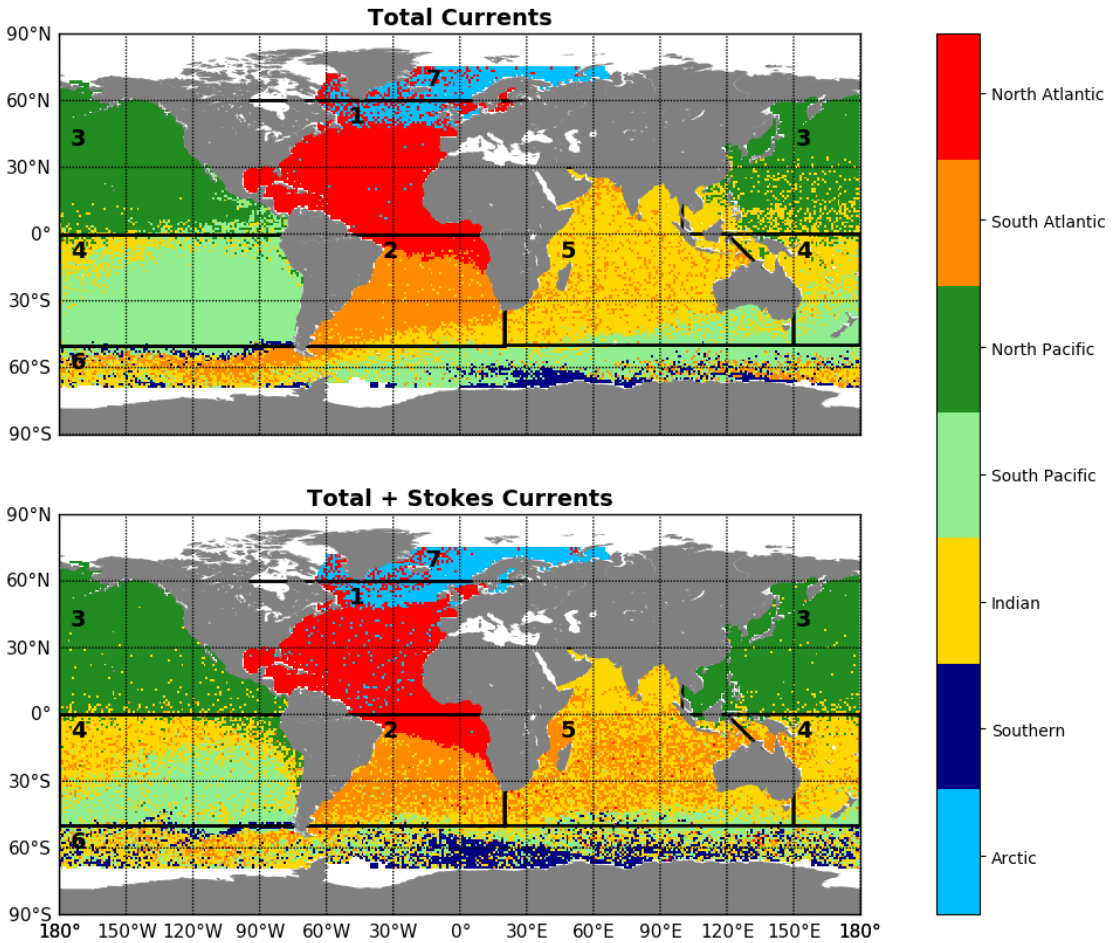

Figure 9: Connectivity of the ocean basins based on virtual particles advected with total and total + Stokes currents. Basins are defined according to: 1 = North Atlantic, 2 = South Atlantic, 3 = North Pacific, 4 = South Pacific, 5 = Indian, 6 = Southern, 7 = Arctic

connectivity of the ocean basins. The ocean basins are defined according to cartographic boundaries, but Figure 9 shows that the ocean does not necessarily adhere to this. Each $1^\circ \times 1^\circ$ grid box is colored according to the basin within which the particle that is initially released there is found at the end of the 14 year total or total + Stokes current simulation. The North Pacific and North Atlantic basins largely stick to their respective defined basins in the total current simulation (as shown in Table 3, 96.1% and 81.8% of particles within the basins at the end of the simulation originating from within these respective basin). However the boundaries between the Indian, South Atlantic and South Pacific basins take on a different shape, matching earlier findings based on eigenvalues of transition matrices [65]. With just the total currents, the southern basins stretch out westward in bands, and for each of the southern basins only around half of the particles had their initial position within the same basin as their end position.

Introducing Stokes drift has a strong effect on these southern hemisphere connections. The connections of the North Pacific and North Atlantic with the other basins are affected much, with the number of particles in the North Pacific increasing only slightly due to increased transport from the South Pacific to the north (Table 3). Meanwhile, the number of particles in the North Atlantic remains approximately constant, for while more particles from the South Atlantic travel to the North Atlantic, there is a also slight increase in the amount of microplastic that go to the Arctic ocean. In the southern hemisphere, Stokes drift leads to an increased number of particles in the South Atlantic, Indian and Southern basins (Table3), which explains the increase in size of the garbage patch in the South Atlantic and the increased concentrations of the coasts of Antarctica (Figure 6). The increase in the number of particles in the South Atlantic is largely due to particles from the Indian basin, with the fraction of particles originating from the Indian basin increasing from 17.6% to 42.0% through the addition of the Stokes drift. Despite this increased particle leakage to South Atlantic basin, the number of particles in the Indian basin is increased due to a more particle leakage from the South Pacific, which is the sole southern basin to undergo a decrease in the total number of particles. These South Pacific particles do not end up in the subtropical ocean gyre, instead accumulation in the coastal regions of the Indian subcontinent (Figure 6). Similar to the Arctic basin, the Southern basin experiences an increase in the total number of particles within the basin at the end of the total + Stokes simulation and neglecting Stokes can thus lead to an underestimation of the amount of microplastic reaching the Antarctic regions.

Table 3: The total number of particles within each basin (according to the definitions in Figure 9), at the end of the global simulations, with particles advected by either total or total + Stokes currents. Particle origins are given as percentages of the total number of particles within the basin at the end of the simulation.

Basin of Origin	**North Pacific**		**South Pacific**		**North Atlantic**		**South Atlantic**	
	Total	Total + Stokes	Total	Total + Stokes	Total	Total + Stokes	Total	Total + Stokes
North Pacific	96.1%	93.2%	2.4%	0.0%	0.0%	0.0%	0.0%	0.3%
South Pacific	3.1%	5.6%	55.9%	52.2%	0.0%	0.0%	0.5%	9.3%
North Atlantic	0.0%	0.0%	0.0%	0.0%	81.8%	16.4%	0.0%	0.0%
South Atlantic	0.0%	0.0%	0.1%	1.3%	13.0%	77.9%	54.1%	36.4%
Indian	0.8%	1.0%	8.0%	8.2%	0.0%	0.8%	17.6%	42.0%
Southern	0.0%	0.2%	33.6%	38.3%	0.0%	0.9%	27.8%	12.0%
Arctic	0.0%	0.0%	0.0%	0.0%	5.2%	4.0%	0.0%	0.0%
Total Particles	6688	7862	8997	4706	4169	4145	4011	5008

Basin of Origin	**Indian**		**Southern**		**Arctic**	
	Total	Total + Stokes	Total	Total + Stokes	Total	Total + Stokes
North Pacific	9.2%	2.7%	0.0%	0.0%	0.0%	0.0%
South Pacific	16.3%	34.3%	1.4%	2.0%	0.0%	0.0%
North Atlantic	0.0%	0.0%	0.0%	0.0%	37.6%	44.4%
South Atlantic	5.2%	6.2%	0.0%	0.3%	0.0%	0.1%
Indian	50.7%	33.3%	0.1%	1.7%	0.0%	0.0%
Southern	18.6%	23.5%	98.5%	96.0%	0.0%	0.0%
Arctic	0.0%	0.0%	0.0%	0.0%	62.4%	55.5%
Total Particles	8521	9521	934	2202	1167	1403

North Pacific

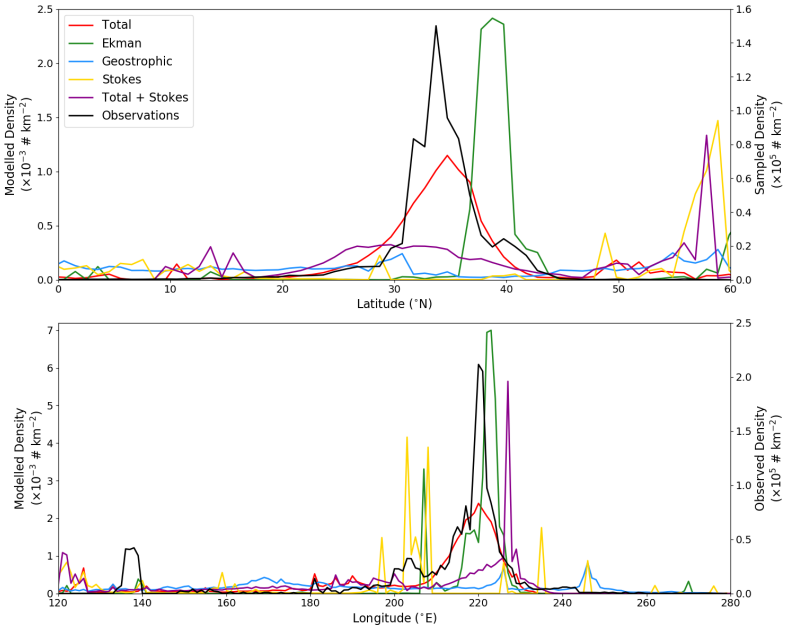

Figure 10: The zonal and meridional means for the modeled microplastic distributions (averaged over the final year of model run) with the various surface current components for the North Pacific. The left y-axis indicates the modeled concentrations, while the right y-axis indicates the sampled microplastic concentrations (as shown in Figure 2), with the black line indicating the respective zonal and meridional means of the sampled concentrations. The zonal and meriodional means are computed for the region of $0° - 60°$N and $120° - 280°$E.

The global runs have 34,515 particles initially uniformly spread with a spacing of 1°, but only several thousand of those particles are within the North Pacific. Separate simulations with the current components were conducted with 30,091 particles that are initially uniformly spread with a spacing of 0.5° in the North Pacific. With the total current simulations, the position of the garbage patch closely matches both the Maximenko distribution (Figure 7) and observations, with the locations of the peaks in the zonal and meridional mean concentrations from the total current simulation matching those of the zonal and meridional mean of the sampled microplastic concentrations (Figure 10). As with the global simulations, the average location of the garbage patch is determined almost solely by the Ekman currents, with the peak with the Ekman currents in the meridional direction matching exactly with observations, while the peak in the zonal direction is approximately 5° farther north than observations. The peak with the Ekman currents is much narrower than that of the total currents, indicating that the geostrophic currents are responsible for microplastic dispersion and while also shifting the garbage patch to the south.

Inclusion of Stokes drift causes homogenization of the microplastic distribution, with only slightly higher concentrations in the garbage patch in comparison to the surroundings. While concentrations in the garbage patch region are indeed lower with Stokes drift included than without, the decrease in the average peak concentrations is largely due to increased movement of the garbage patch smearing the concentrations out over a larger area (Figure 11). The magnitude of these movements might be overestimated, since if the Ekman (and thus also the total) currents already includes a Stokes drift component due to its parametrization, then adding the Stokes drift to the total currents might be

an overestimation of the total current strength. With Stokes drift included there are also more regional increases in plastic concentrations near coasts (Figures 7 and 10), especially in the Gulf of Thailand (seen in the slight increase in the meridional average at around 120°E) and by Alaska (responsible for the sharp peak at 57°N and 225°E in Figure 10). Stokes drift might thus play a critical role in microplastic beaching by directing microplastic towards the coasts. However, further studies with higher resolution flow fields would be necessary to determine if this is indeed the case.

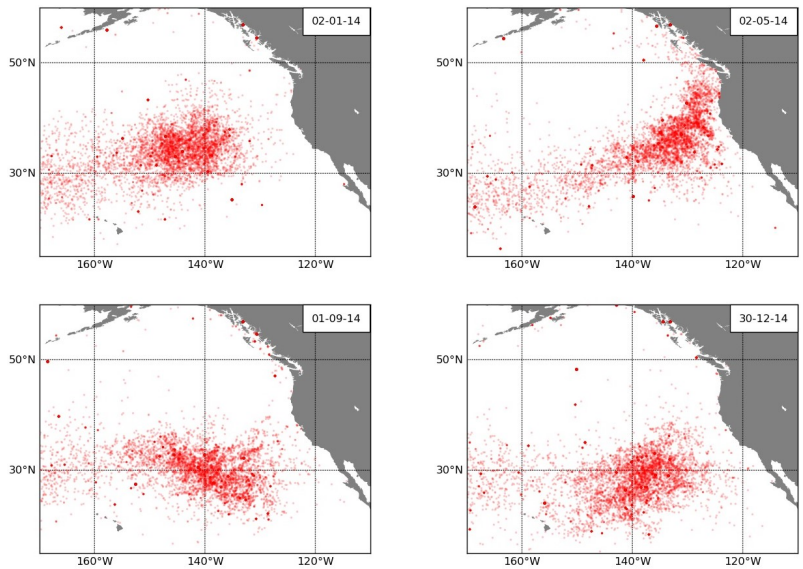

Figure 11: Frames of the microplastic distribution in the eastern North Pacific over the last year of the 12 year Lagrangian simulation simulation with the microplastic advected by total + Stokes currents. Darker shades of red indicate higher microplastic particles densities.

Kubota [32] and Kubota et al. [33] proposed a mechanism for marine debris transport where the Ekman currents are responsible for transport to the subtropics and the trapping of debris in the garbage patch, while the geostrophic currents are responsible for eastward transport of the debris. Based on the simulations, the Ekman currents do first transport the microplastic towards the subtropics, where it forms a line of particles where the southward and northward Ekman currents meet. This accumulation behavior can be seen in Figure 12a, for accumulation of particles results in a decrease in the standard deviation of the particle latitudes and longitudes. By comparing the rates at which the standard deviations decrease, it is clear the accumulation in the meridional direction occurs much more rapidly than in the zonal direction. Meanwhile, the rate with which the microplastic is accumulated in the garbage patch is the same when advected by total or Ekman currents. This shows that the eastward transport of the microplastic is almost entirely due to the Ekman currents. If the geostrophic currents played a role in the eastward transport, then the total currents would show a faster decrease in the standard deviation of the longitudes. However, this is not the case. The role of the geostrophic of counteracting microplastic accumulation is visible, for the standard deviation of the particle longitudes and latitudes when advected by the total currents is constantly higher than when advected by the Ekman currents. The higher initial standard deviation with the total currents is the result of that the particles that are within the North Pacific subtropics at the end of the simulation are initially spread over a larger area with the total currents than with the

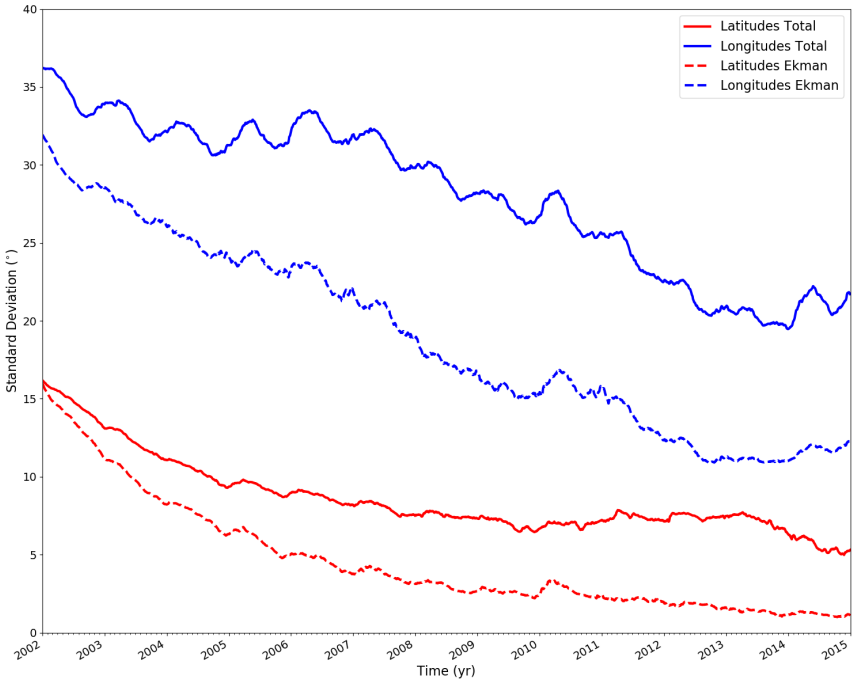

(a) Standard deviation the latitude and longitude

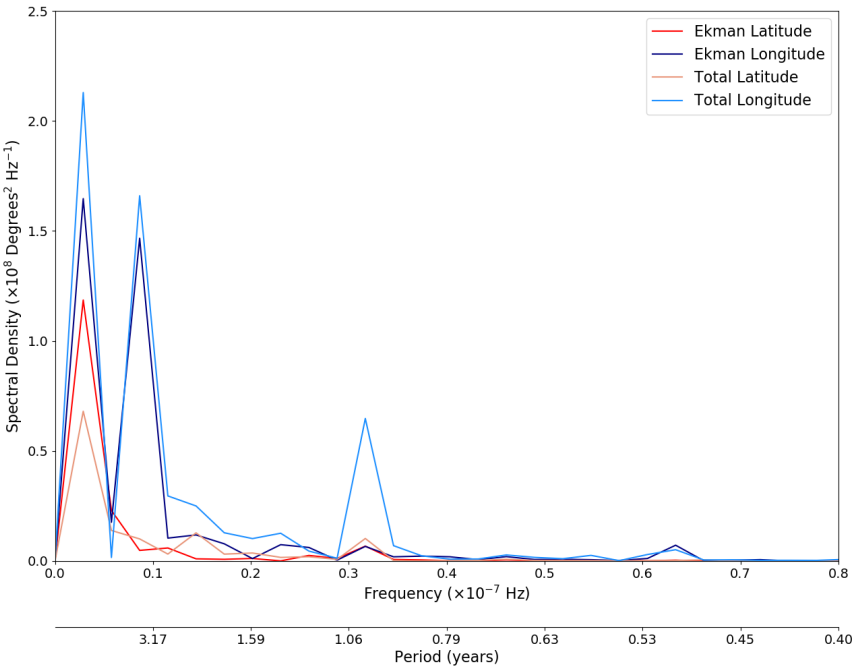

(b) Power Spectrum

Figure 12: The time evolution of the standard deviation of the latitude and longitude (Figure 13a) and its power spectra (Figure 13b) for all particles in the North Pacific whose final position is in the North Pacific subtropics (10° − 50°N,130°E-120°W). The power spectrum is computed from the detrended time series from 01-01-2004 to 31-12-2014.

Ekman currents. However, the slower reduction in the standard deviation and the higher final standard deviation of both the particle latitudes and longitudes is due to the presence of the geostrophic currents.

The time series of the standard deviations of the latitudes and longitudes of the particles which are within the North Pacific subtropics at the end of the model runs show a consistent decrease towards some final limit. Variations in the decrease are visible on multiple time scales, and the variations tend to match between the total and Ekman current simulations. This suggests that the temporal variability in the accumulation of microplastic is largely wind-driven. Power spectra of the detrended time series (with the time series starting from 01-01-2004) showed that the majority of the variability of the standard deviation has a period of 11 years (Figure 12b). While the first two years of the time series were not included in the Fourier analysis so that the majority of the particles would be in the subtropics, the particles are still in the process of being transported towards the garbage patch, which in turn leads to these low frequencies dominating the signal. Meanwhile, the standard deviation time series of the longitudes also exhibit a strong peak corresponding to a period of 3.67 years. One possible mechanism behind this periodicity is be the El Niño-Southern Oscillation (ENSO), which has a frequency of around 3-5 years [66] and which causes shifts in the wind fields. This can potentially lead to variability in the transport of microplastic, since this is largely the result of the Ekman currents. Finally, there is also a peak corresponding to a periodicity of one year for the standard deviation of the longitude with the total currents, which suggests a seasonal cycle. However, the peak is only prominently visible with the total currents, which suggests that this periodicity could be the result of a seasonal cycle in the geostrophic currents rather than the Ekman currents.

While studying the periodicities in the standard deviation of the particle coordinates yields insight into the accumulation behavior of the microplastic, it does not reflect the dynamics of the location of the garbage patch. For this, time series of the mean longitude and latitude of the particles are more appropriate, since as a large fraction of the total particles in the North Pacific subtropics are within the garbage patch, the average of the coordinates will approximately match the location of the garbage patch. Figure 13a shows that the mean latitudes approximately match the latitude of peak microplastic concentrations (Figure 10), while the mean longitude approaches the longitude of peak concentrations at the end of the simulation. The spectrum, computed from the detrended time series starting from 01-01-2004, shows peaks at 11 and 5.5 years, which are likely again the result of the microplastic still being transported towards the garbage patch. This is supported by the peaks being more pronounced for the mean longitudes, which have not yet reached a stationary value by the end of the simulation. The peaks of the mean longitudes corresponding to a periodicity of 1 year, indicating a seasonal cycle, are much stronger than for the mean latitude. The garbage patch therefore appears to oscillate in the zonal direction with a periodicity of 1 year, but not in the meridional direction. There is no prominent peak at 3.67 years for any of the coordinate means, so if the signal with the longitude standard deviations is indeed due to ENSO, then ENSO appears to affect only microplastic transport, and not the average location of the garbage patch.

The regression analysis showed that there is a relatively strong anticorrelation between EKE and microplastic concentrations in the North Pacific, and the expectation with the Lagrangian simulations is that the particles that end up accumulating in the garbage patch have a decrease in EKE over time. This trend is observed (Figure 14), and while initially the mean EKE of all particles (including those whose final position is outside the garbage patch) shows a similar decrease in mean EKE, at the end of the simulation the mean EKE

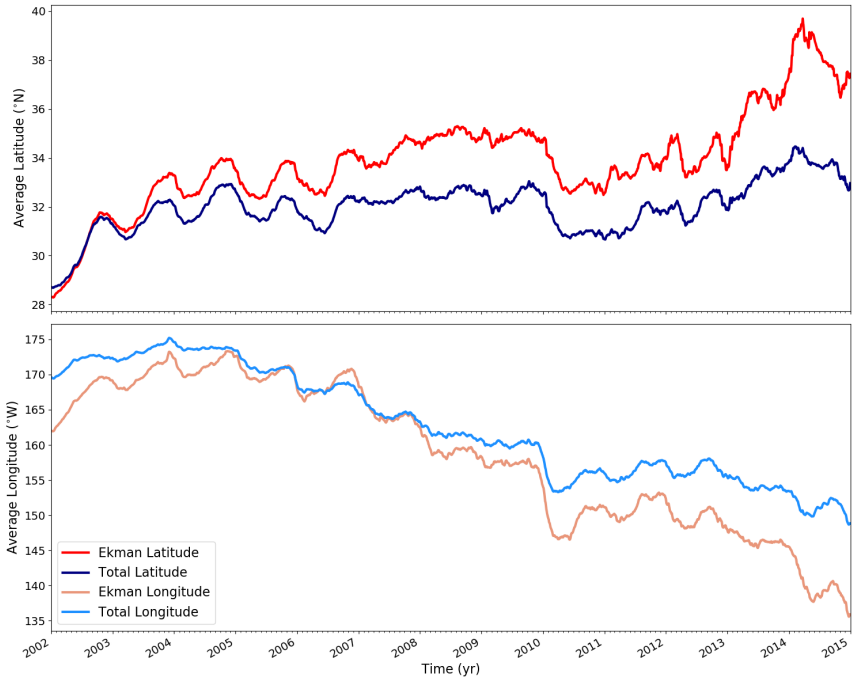

(a) Mean latitude and longitude

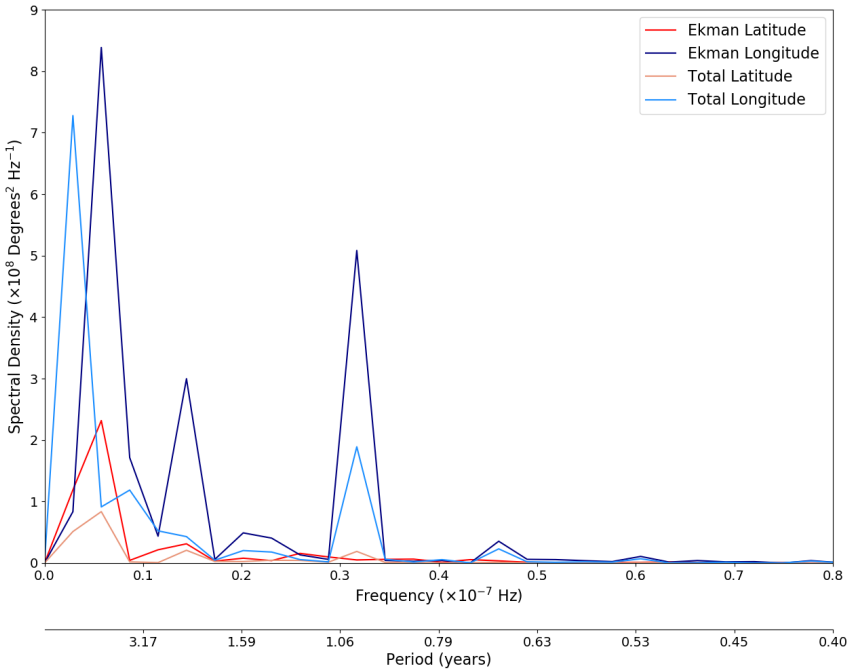

(b) Power Spectrum

Figure 13: The time evolution of the mean latitude and longitude (Figure 13a)and its power spectra (Figure 13b) for all particles in the North Pacific whose final position is in the North Pacific subtropics ($10° - 50°$N,130°E-120°W). The power spectrum is computed from the detrended time series from 01-01-2004 to 31-12-2014.

of all particles rises, while that of the garbage patch-bound particles continues to fall. This indicates that particles move to an area of low EKE, rather than the basin-averaged EKE decreasing.

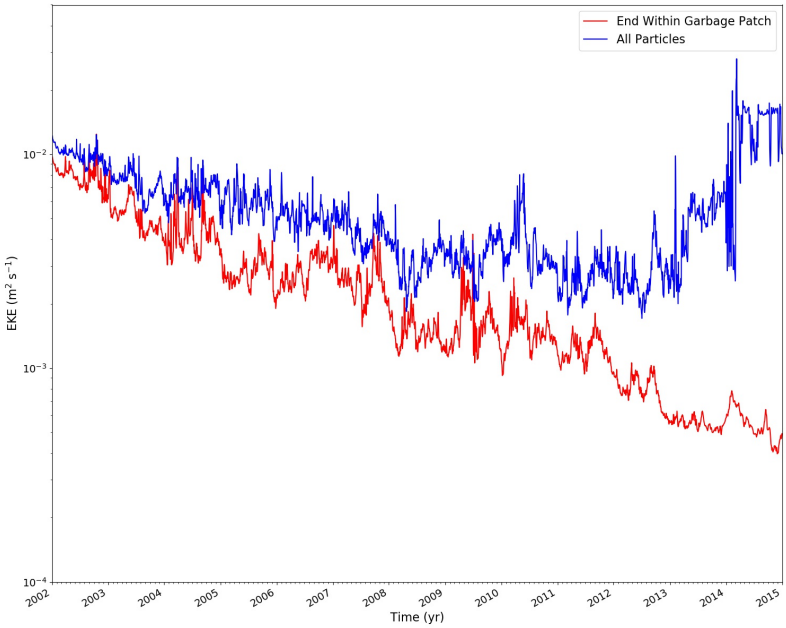

Figure 14: Mean EKE for particles that have their final position within the garbage patch (25° − 45°N,130° − 150°W) in the North Pacific (red line) and the mean EKE for all particles in the North Pacific (blue line) over the course of the North Pacific Lagrangian run with particles advected by total currents.

North Atlantic

The North Pacific simulations show that using the total currents, the formation of garbage patch can be modeled at a average location that matches observations and the Maximenko distribution. Now, the same approach is applied to the North Atlantic, which has proven more challenging to model in the past [9] in terms of matching observations. Advecting the microplastic with the total currents leads to the formation of a garbage patch in the subtropics, with the peak concentrations at 30°N and spread out over a wide meriodional range (Figure 15). The position of these peak concentrations matches the Maximenko distribution (Figure 7), but unlike the Maximenko distribution, there is now a clearer central peak (Figure 2). In comparison with observations, the modeled garbage patch is 5° too far south, while the peak concentrations in the meridional direction are around 10°-25° too far west.

Like with the North Pacific, the position of the garbage patch is determined by the Ekman currents, with the geostrophic currents showing no accumulation of microplastic (except near coastal regions and off the coast of Brazil, as was discussed for the Global simulations). The peak concentrations in the meridional direction are shifted several degrees to the North in comparison to the total currents and thus do approximately match observations. In the meridional means the Ekman currents have two peaks in the microplastic concentrations which are 7° apart and which are both at least 10° too far west in comparison to observations. The role of the geostrophic currents is to disperse the microplastic, so that the microplastic is spread out over a larger area instead of all accumulating at these two points. However, aside from the slight southward shift of the garbage patch with the

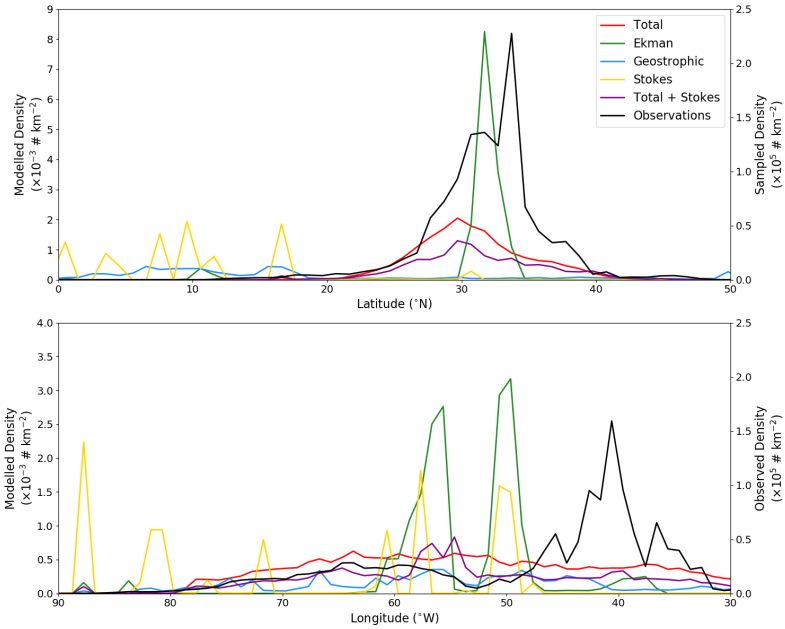

Figure 15: The zonal and meridional means for the modeled microplastic distributions (averaged over the final year of model run) with the various surface current components for the North Atlantic. The left y-axis indicates the modeled concentrations, while the right y-axis indicates the sampled microplastic concentrations (as shown in Figure 2), with the black line indicating the respective zonal and meridional means of the sampled concentrations. The zonal and meridional means are computed for the area between $0° - 50°$N and $30° - 90°$W.

total currents relative to the garbage patch with just the Ekman currents, the geostrophic currents do not strongly affect the location of the garbage patch. As such, the discrepancy between the microplastic distribution from the total currents simulation and observations is likely due to the modeling of the Ekman currents.

With the Lagrangian simulations the contribution of Stokes drift microplastic accumulation and dispersal in the North Atlantic is visible. On its own, Stokes drift leads to increased transport towards the pole and the Caribbean (Figure 27 in Appendix A). When combined with the total currents, the simulation shows that the resultant garbage patch is smaller than that modeled with just total currents, but that the microplastic is more concentrated towards a single point. However, the location of this peak does not match more closely with observations, as it is too far south at 30°N and too far west at 55°W. The effect of Stokes drift is dependent on the section of the basin, which explains the mismatch in the time averaged Stokes drift flux and convergence Pearson R correlation coefficients in Table 2. With the samples, there is a weak negative correlation, which means that in the subtropics (where almost all samples have been taken), Stokes drift contributes to microplastic accumulation. Meanwhile, on a basin-wide scale Stokes drift acts to disperse microplastic, as indicated by the positive Pearson R correlation coefficient with the Maximenko distribution.

Similar to the North Pacific, the Ekman currents first lead to convergence of microplastic in the subtropics, forming a zonal line at 33°N (Figure 16a) which slowly converges to 52°W. The end position of the microplastic within the final Ekman current distribution is highly dependent on the starting location, with clear zonal bands where a southerly initial position generally leads to a more western final position. The convergence of particles to the

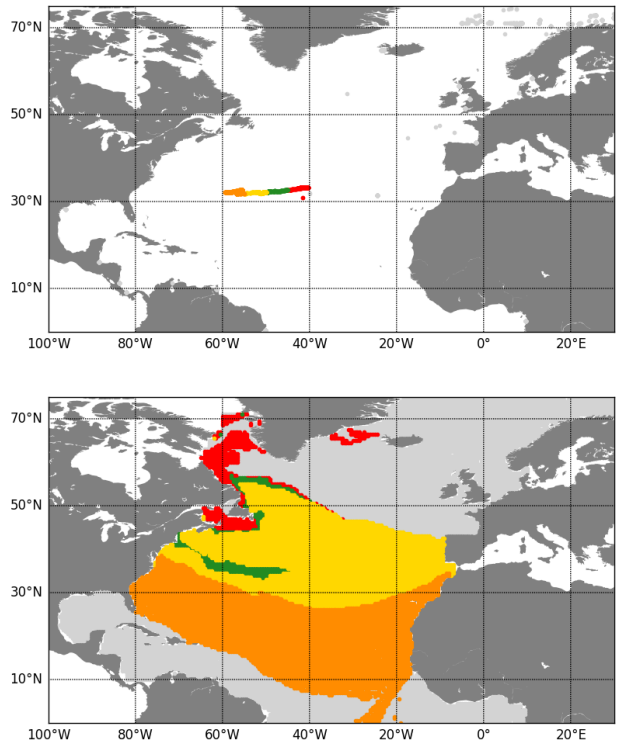

(a) Regions of Attraction

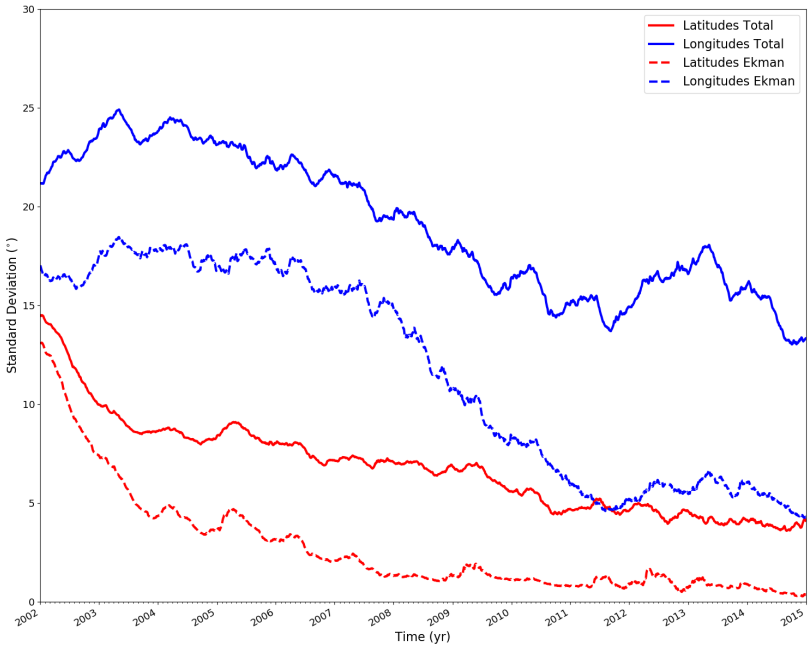

(b) Ekman Particle Accumulation

Figure 16: Convergence behavior of the total and Ekman currents in the North Atlantic. Subfigure 16a shows the origin regions (bottom subplot) of particles in various regions of the final Ekman particle line (top subplot). Subfigure 16b shows the standard deviation of the latitudes and longitudes of particles advected by total and Ekman currents that have final positions within the North Atlantic subtropics ($10° - 40°$N,$0° - 80°$W) as a function of time.

subtropics happens on a much faster timescale than convergence to 52°W (Figure 16b). After 6 years of simulation, the particles whose final position is within the Ekman line shown in Figure 16a have already reached their final approximate latitude in the subtropics, as reflected by the low standard deviation of the particle latitudes at $1 - 2°$. Convergence towards a central longitude of 52°W occurs more slowly, with a minimum of of the latitude standard deviation not occurring until 10 years into the simulation and with the standard deviation of the longitudes from both Ekman and total current runs continuing to decrease over the final year of simulation (Figure 16b). Since there is only flow data for 12 years, it is not possible to extend the simulation to see whether the zonal convergence continues, but it is noteworthy that this convergence occurs at a slower rate than in the North Pacific despite the North Pacific basin being larger. One possibility is that the larger stretches of ocean in the North Pacific allow for stronger winds and thus stronger Ekman currents than in the North Atlantic, but comparing the mean surface wind stress for the two basins does not indicate that the wind stress in the North Pacific is indeed stronger (Figure 28 in Appendix A), nor are the mean Ekman currents in the North Atlantic significantly stronger or weaker than in the North Pacific (Figure 3). Further research is therefore required to investigate the differing convergence rates. Comparing the convergence behavior of the particles advected by the total currents and those advected by the Ekman currents shows that convergence happens more quickly without the inclusion of the geostrophic currents, which supports that geostrophic act mainly to disperse plastic.

Like with the North Pacific, the time series of the standard deviations of the coordinates show variations on various time scales, but Fourier analysis of the time series indicate that almost all the variance of the detrended time series is at frequencies of either 11 years or 5.5 years (Figure 29 in Appendix A). The time series were analyzed from 2004-01-01 onwards to assure that the majority of particles are already within the subtropics when the analysis starts, but since the longitudinal time series do not converge to a single steady value by the end of the time series, the signal remains dominated by the slow transport of the particles to the garbage patch. Analyzing the mean latitudes and longitudes provides better understanding of the variability of the garbage patch, with the spectrum of the mean coordinate time series showing a clear peak for both mean latitude and mean longitude corresponding to a period of 1 year This indicates that there is a seasonal cycle in both the mean latitude and longitude of the North Atlantic garbage patch. All the time series also show periodicities on longer timescales such as 2.2 and 3.67 years, but there is no single time scale present in the longitudes or latitudes of both the Ekman and total current simulations. Therefore, it is difficult to attribute these periodicities to a single phenomenon.

Regression analysis has already shown weak or insignificant correlation between the EKE and microplastic concentrations in the North Atlantic, and the North Atlantic total currents simulation further shows that microplastic does not tend to accumulate in regions of low EKE in the North Atlantic (Figure 18). While in the North Pacific there is a clear trend of the mean EKE of particles that end up in the North Pacific garbage patch decreasing as they move towards the garbage patch, the North Atlantic showed no clear difference between the mean EKE of particles which end up in the garbage patch and the mean EKE of all particles over time. Over the last year of the simulation there is a decrease in the EKE for the garbage patch particles, but its emergence at the end of the simulation suggests it might be a product of the selected garbage patch boundaries.

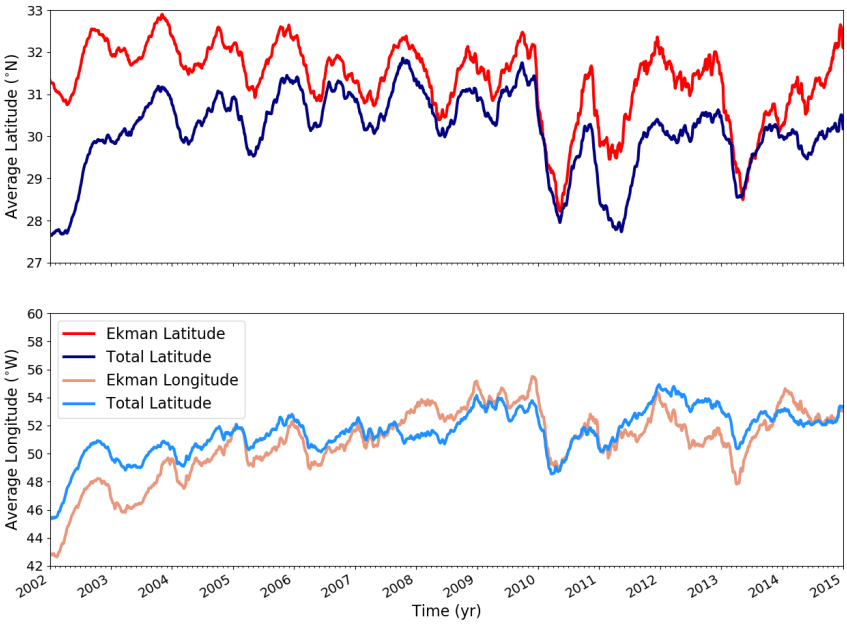

(a) Mean latitude and longitude

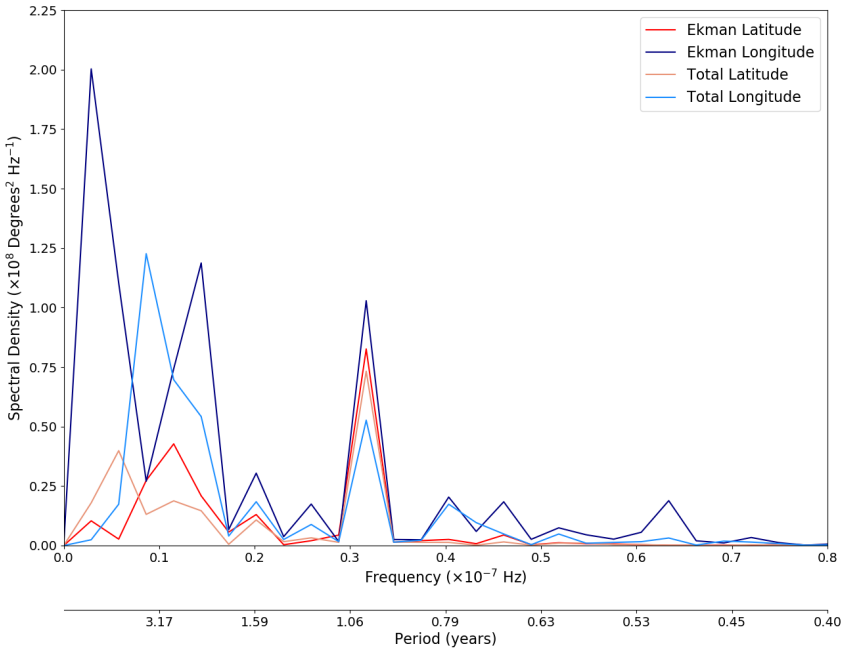

(b) Power Spectrum

Figure 17: The time evolution of the mean latitude and longitude (Figure 17a)and its power spectra (Figure 17b) for all particles in the North Atlantic whose final position is in the North Atlantic subtropics ($10° - 40°$N,$0° - 80°$W). The power spectrum is computed from the detrended time series from 01-01-2004 to 31-12-2014.

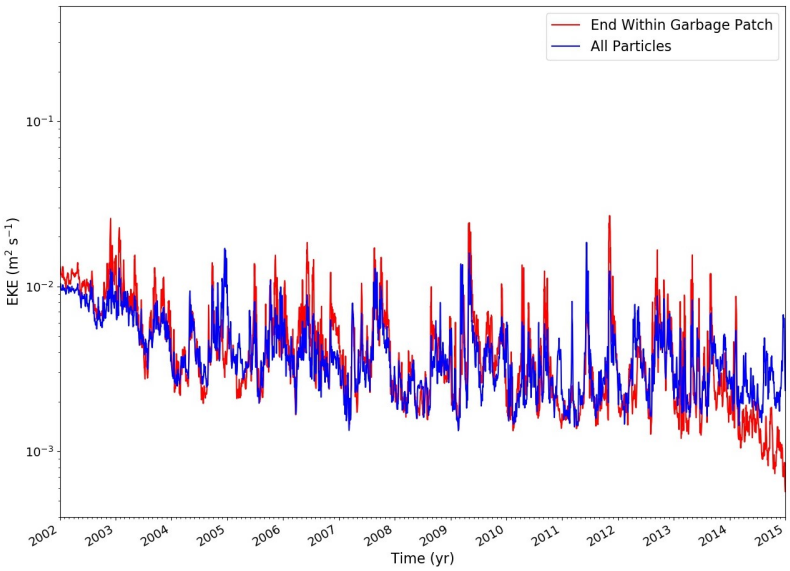

Figure 18: Mean EKE for particles that have their final position within the garbage patch ($25° - 35°$N,$40° - 70°$W) in the North Atlantic (red line) and the mean EKE for all particles in the North Atlantic (blue line) over the course of the North Atlantic Lagrangian run with particles advected by total currents.

Influence of the temporal resolution of flow fields

Given that the geostrophic flow field data was available with a temporal resolution of 1 day and that the GlobCurrent [35] project states that the actual temporal resolution of their flow data is on the order of 3-5 days, I decided to only use the 00:00 UTC hour data for all of the total, Ekman and geostrophic runs. This way the temporal resolution of the Ekman and total current flow fields would be consistent with that of the geostrophic current flow fields. The North Atlantic total currents simulation is repeated using the 3 hourly current data to see the effect of the higher temporal resolution (Figure 19). The higher resolution caused a shift in the peak microplastic accumulation towards the east, so that the location of the peak concentration is closer to the peak concentration in from observations (Figure 2). The reason for this is unclear, but it is likely related to that the wind stress (and thus by extension the Ekman currents) are variable over a range of different time scales and that taking the wind stress at one point in time is not representative of the winds over the entire day.

Modeling of microplastic in the North Atlantic is highly sensitive to the temporal resolution of the flow fields being used. For the North Pacific the particles are advected using mean fields of the total, Ekman and geostrophic currents, which led to microplastic accumulation at exactly the same location as using the time-variable flow fields, albeit with the microplastic being more concentrated to a single point (Figure 30 in Appendix A). However, in the North Atlantic similar use of the mean currents causes a shift in the location of the garbage patch with the Ekman currents to the northeast, while with the mean total currents the peak accumulation experienced a shift to the east (Figure 31 in Appendix A). Future modeling efforts of the North Atlantic must take great care with the selection of the temporal resolution of the flow fields being used, for it affects the final distribution of microplastic.

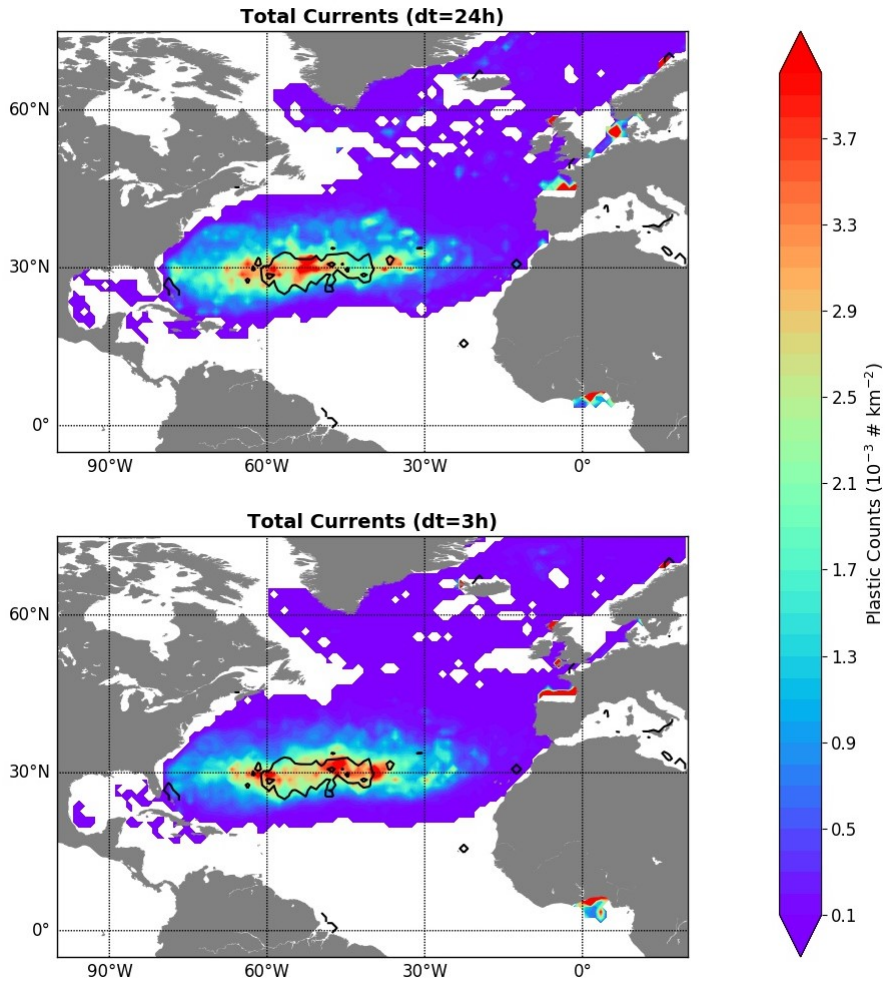

Figure 19: Mean particle density of the final year of the North Atlantic Lagrangian simulations with the virtual particles advected by total currents using data with a time resolution of 24 hours or 3 hours. Simulations are from 01-01-2002 to 31-12-2014 from an initial uniform $0.5° \times 0.5°$ distribution of particles. Contour shows the 5×10^4 # km^{-2} contour from the Maximenko distribution.

5 Discussion

Confidence in the regression analysis approach

In this thesis two modeling approaches were described, and from the results the linear regression modeling, at least the form used here, performs more poorly when it comes both to describing the position of the garbage patches in comparison to the Lagrangian modeling approach. Part of the reason for poor performance could lie in the physical processes that were considered. The chosen physical processes and the corresponding time averaged physical fields are selected based on reading of the literature on debris transport in the oceans. It is possible that critical variables were left out of the analysis. For example, it is assumed that windage effects can be neglected based on Monroy et al. [27], which indicated that windage effects are negligible in comparison with passive transport of the particle with the flow field. If this is not the case, wind effects would have to be directly taken into account, and their omission here could be one possible reason for the poor performance of the linear regression modeling. It is also possible that the issue lies not with the variables, but with the use of time averaged physical fields. The Lagrangian simulations demonstrate that

the positions of the garbage patches are sensitive to the temporal variability of the flow fields, and so mean fields might not be the optimal choice. A further issue can lie with the use of linear regression itself. One critical assumption required for the use of linear regression is that all samples in the analysis are independent from one another. However, in this case this assumption is not met, since two values of a physical field in adjacent grid cells are linked. The autocorrelation most likely stretching over several degrees of latitude and longitude at the very least. With lack of better approach, I decided to stick with linear regression and take a conservative view of the probabilities listed as statistical significance of the regression coefficients (with the actual significance being much lower due to a smaller number of degrees of freedom). However, I am aware that this is not a solution to the described issue.

One final issue that I have identified with the linear regression modeling is that it is dependent on the Maximenko distribution instead of on sampled concentrations. The Maximenko distribution is itself a modeled distribution of microplastic and is thus dependent on the assumptions taken by Maximenko et al. [18] in terms of how the microplastic was released and advected. The focus of my research was to determine the locations of the garbage patches and not there relative sizes, which is dependent on the global distribution of microplastic input sources. As such, I do not see Maximenko's use of an initial uniform microplastic distribution as an issue for identifying the positions of the garbage patches, since these ought to stay the same if the physical processes are adequately modeled. This is supported by that the approximate debris distribution found by Maximenko et al. [18] matches those modeled by Lebron et al. [30] and van Sebille et al. [31] despite the different input distributions used. In the case of the Maximenko distribution, issues are more likely to arise with the debris advection. Firstly, Maximenko et al. [18] does not take into account any time dependence, for the transition matrix was calculated using all drifters irregardless of the time of the trajectory. Furthermore, Maximenko et al. [18] used drogued drifters which follow the currents at 15 m depth, while the microplastic is transported at the surface. The currents are depth dependent and so this can lead to differences between garbage patches in the Maximenko distribution and observed garbage patch locations.

Being aware with all these issues with the Maximenko distribution, I still decided to use it for the linear regression modeling over the sample distribution since it provides a microplastic distribution that is both basin-wide and consistently generated. Given the sizes of the oceans and the expenses involved in organizing research cruises to take microplastic measurements, only small regions of the oceans have been sampled, with almost all the samples that were used for the regression analysis having been taken in the North Pacific and the North Atlantic. Basing the linear regression modeling on such limited datasets works poorly, with the obtained distributions being largely homogeneous since only a small fraction of the total measurements show highly elevated concentrations. Since the linear regression modeling is done by minimizing the total difference between model and observations, the models are fit to match these lower concentrations. This is in part an issue with the regression approach, but it is also dependent on the limited number of samples. Especially in the Southern Hemisphere, basing linear regression modeling on only a couple of measurements for the entire southern basins would not be justifiable, and the limited sampling in the Southern Hemisphere is part of the reason why I focused largely on the Northern Hemisphere for my modeling efforts. Even there, only 6812 microplastic measurements have been taken in the North Atlantic basin since 1979, which is very little for a basin that has an area of more than 1×10^6 km^2. Furthermore, most of these samples were taken close to the North American coast, and so the amount and distribution of microplastic in the eastern North Atlantic is highly incomplete. Finally, consider that the samples

have been collected in all sorts of weather conditions with differing sampling methodologies. In an attempt to compensate for these differences, all the sample data from van Sebille et al., 2015 [9] has been statistically processed based on various assumptions and parametrizations, which bring their own set of limitations. Given all the issues with the linear regression modeling, I give more weight to the findings of the Lagrangian modeling.

The role of Ekman and geostrophic currents

To explain the formation of garbage patches in the subtropical gyres, literature has turned to the convergence of surface ocean currents [18] and Ekman pumping [9]. However, these are slightly different processes, since the standard definition of the vertical Ekman pumping velocity involves on the convergence of mass integrated over the entire surface layer, while microplastic is generally found only at the very upper reaches of this surface layer. The Ekman pumping velocity explanation provides a schematic model for describing how microplastic accumulates at the surface, with buildup due to buoyant microplastic remaining at the surface while the water mass with which it was transported is pumped downwards to conserve mass. However, the Lagrangian simulations for the North Pacific have shown that using the surface currents is sufficient to obtain a very close correspondence between modeled and observed distributions, which would indicate that it is indeed the surface and not the depth-integrated mass transport that best describes the transport of microplastic. This is also supported by the Pearson R correlation coefficients for the Ekman pumping velocity generally being weaker than those for the Ekman current convergence and flux when looking at basin-wide scales with the Maximenko distribution.

While the accumulation of microplastic is due to the surface Ekman currents, the other current components do contribute to the observed final distributions. The geostrophic currents largely result in microplastic dispersion, counteracting the accumulation behavior of the Ekman currents and spreading out the microplastic over a larger area than would be observed with Ekman currents alone. The geostrophic currents also led to slight shifts in the average position of the garbage patches, although for both the North Pacific and North Atlantic these shifts in either the zonal or meridional direction is only on the order of several degrees.

Meanwhile, the geostrophic currents do not appear to contribute to the eastward transport of microplastic as was reported by Kubota [32], Kubota et al. [33] and Martinez et al. [34]. Global, North Pacific and North Atlantic simulations all show that the Ekman currents on their own are sufficient to transport the microplastic towards the east, with the geostrophic currents appearing to have no contribution to the speed at which occurs. A possible reason for this discrepancy with literature is the different formulation of the surface Ekman currents. Kubota [32], Kubota et al. [33] and Martinez et al. [34] all used Ekman currents computed based on Ekman's theory for steady wind [46], which has the Ekman currents at a 45° angle to the windstress. Meanwhile, the GlobCurrent [35] Ekman currents were computed with a parametrization based on the non-geostrophic surface velocities of ARGO drifters, which has the Ekman current at a 30.75° angle to the wind stress. The smaller angle implies that the Ekman currents have a stronger along-wind component. Given that the predominant wind stress direction in the Pacific subtropics is easterly, it is clear why the Ekman currents demonstrate stronger eastern transport on their own than in previous studies using the Ekman's theory formulation. Furthermore, since the computed Ekman currents were used to compute the geostrophic velocities of surface drifters that are incorporated into the computation of the final geostrophic flow fields, the strengthened zonal component of the Ekman currents in the subtropics would lead to a reduction in the zonal component of the geostrophic currents in this region. Therefore, the geostrophic contribu-

tion to zonal transport in the subtropics would be weakened.

The different formulation of the Ekman currents and its effect on the strength of the geostrophic currents can explain the differences in the contributions of the Ekman and geostrophic current components with earlier studies. It does bring to question whether Ekman current is an appropriate label. It is assumed in the parametrization that the non-geostrophic current component of the drifter is wind driven. However, there are other processes at work such as Stokes drift from the surface waves and windage on the section of the ARGO-float that is above the surface. This is indicated by the different surface current angle in comparison to theoretical Ekman currents. However, it must be kept in mind that Ekman's theory [46] is in itself based on a number of assumptions, with several, such as assuming the wind forcing is steady and that there are no basin boundaries, not always being met in the ocean. Discrepancies between theory and actual wind-induced surface currents are to be expected, and while the parametrization used by GlobCurrent [35] is not ideal in isolating the wind-driven surface currents, basing the Ekman currents on observed surface drifters means that the flow fields used in this study show closer correspondence to actual ocean circulation than those used by Kubota [32], Kubota et al. [33] and Martinez et al. [34].

The role of Stokes drift

The formulation of the Ekman currents leads to difficulties in deciding upon the exact role of the Stokes drift. It is clear from the Lagrangian simulations that, in contrast to the conclusion of Kubota [32], Stokes drift influences the basin-wide microplastic distribution. The nature of this effect depends on the basin. In the Pacific and Indian basins, the Stokes drift acts to disperse the microplastic away from the subtropical gyres towards the coasts. In the Pacific basins there are still garbage patches, albeit smaller in size and with less microplastic particles contained within them, while in the Indian basin the garbage patch in the subtropical gyre has almost completely disappeared. Most of the microplastic ends up either by the coast at the northern end of the Indian basin and in the South Atlantic garbage patch. In the Atlantic basins the role of the Stokes drift is more complex, leading both to higher peak concentrations in the subtropical gyres, but less particles in the North Atlantic garbage patch and increased microplastic concentrations in the polar and Caribbean regions.

Considering that the Ekman currents might have a Stokes component included in the parametrization, it is possible that the effects of the Stokes drift are overestimated when combined with the total currents. In order to better differentiate these current components, it is critical to be able to directly measure the Stokes drift, which would be possible with the potential Sea surface KInematics Multiscale (SKIM) satellite [67]. Using doppler radar techniques, the SKIM satellite would be able to directly measure surface currents, ice drift and ocean waves, and by having two incidence angles, it would be possible to directly measure the directional wave spectrum. From this spectrum the Stokes drift could be directly computed. With the Ekman current parametrization as described in Section 3.2, both Stokes drift and geostrophic currents could be subtracted from the ARGO drifter velocities. This would leave behind a drifter velocity that is more purely wind based and there would be no problem in including the Stokes drift in the simulations as was done in this thesis, since the Stokes drift would be independent of the Ekman currents.

Including Stokes drift results in a lot more microplastic reaching the polar regions (Figures 6 and 9), which matches the findings of Fraser et al. [52] that including Stokes drift in ocean transport modeling led to rafting keystone kelp being able to reach Antarctica from

subtropical sources. This means that the ecological impact of microplastic on polar ecosystems might be more severe than currently thought. Furthermore, the inclusion of Stokes drift resulted in increased connectivity between the basins of the southern hemisphere, which implies that regional pollution can spread over larger areas than expected based on considering just the total currents. However, they do not to result in much stronger mixing between hemispheres, which means that microplastic from the more abundant sources in the northern hemisphere are still probably not a major source of microplastic contamination in the southern hemisphere. Better understanding of the role of Stokes drift is thus essential in future to be able to further model the global transport of microplastic and other floating debris.

Differences with eddy kinetic energy in the Pacific and Atlantic basins

The EKE is taken in this thesis to be an indication of the amount of mesoscale eddy activity by considering the deviation of the currents away from the mean currents. In practice there will always be some measure of EKE since currents aren't static even without the presence of mesoscale eddies. Given that the EKE has peaks in regions that are known to have a large amount of eddy activity such as in the regions of the western boundary currents, I do consider mesoscale eddy activity to be a justifiable interpretation of the EKE. Since the flow fields have spatial resolutions of $0.25° \times 0.25°$, it can be questioned whether mesoscale eddies are properly resolved, since HYCOM, with a spatial resolution of $1/12° \times 1/12°$, is deemed to be only eddy permitting [23]. However, the GlobCurrent [35] flow fields are detected from satellite measurements and mesoscale eddy detection is possible from sea surface height measurements with a $0.25° \times 0.25°$ spatial resolution [68]. Therefore, mesoscale eddies ought to be present in the flow fields.

The role of EKE in microplastic accumulation remains uncertain. In the North Pacific, the particles accumulated in a region of relatively low EKE, which matches the findings of Martinez et al. [34] for the South Pacific. Furthermore, tracking the mean EKE of the particles which at the end of the simulation were within the North Pacific garbage patch shows a steady decrease over time, indicating transport towards regions of lower EKE. The region of peak accumulation is not the same as the minimum of EKE as is visible with the linear regression modeling of the North Pacific, but the EKE within the gyre is still relatively low. A combination of weak currents in the gyre together with infrequent mesoscale eddies can lead to accumulation in this region. However, this behavior is not seen in the North Atlantic. Tracking the mean EKE of particles that are within the North Atlantic garbage patch at the end of the simulation does not yield a EKE that is significantly lower than the mean EKE of all particles within the basin over time. This suggests that in the North Atlantic, mesoscale eddies do not play a significant role in microplastic accumulation. There have been indications that the size and strength of eddies is dependent on basin size [69], where larger zonal basin lengths lead to larger and stronger eddies in subtropical gyres. Seeing how the zonal extent of the North Atlantic is much smaller than of the North Pacific, this is a possible explanation why the EKE appears to be of lesser importance in the North Atlantic.

Periodicity in the transport and accumulation of microplastic

The Fourier analysis of the time series of the mean and standard deviations of the particle coordinates yields several insights into periodicities of microplastic accumulation and the garbage patch locations. For the North Atlantic, the acccumulation behavior of the microplastic does not show strong periodicities, but the mean coordinates, which are taken to indicate the mean position of the garbage patch, show seasonal variability in both the zonal

and meridional directions. In contrast, in the North Pacific such seasonal variability in the garbage patch location is only visible in the zonal direction, with no clear peak for such a periodicity in the meridional direction. Given the close correlation between the total and Ekman current simulations for all time series of the mean and standard deviation of the particle coordinates, the variability of the garbage patch location and of the microplastic accumulation appears largely wind driven. This matches the dependence of the average locations of the garbage patches on the Ekman currents.

The accumulation mechanism of the microplastic in the zonal direction of the North Pacific shows a periodicity of 3.76 years, which similar to the periodicity of ENSO. Lebreton et al., 2018 [8] reported the average position of the North Pacific garbage patch can be affected by ENSO and the Pacific Decadal Oscillation (PDO) and given that ENSO events affect the mean wind fields, it is plausible that ENSO can have an impact on debris transport and accumulation. Given that the ENSO appears largely driven by anomalies by the equator [66], it is reasonable to question whether this would have an influence on microplastic transport in the subtropics. Wind anomalies due to ENSO are still noticeable up to 30° latitude [70], albeit much weaker than at the equator. Furthermore, the absence of such a pronounced peak in the North Atlantic basin adds to the possibility that the periodicity is due to physical process that is only present in the Pacific, such as ENSO. However, several questions remain. First, no 3.76 year periodicity is present in the mean position of the North Pacific garbage patch, and given that the garbage patch is also located at around 30°N, it raises the question why this region is not affected by ENSO-induced wind anomalies. Furthermore, no periodicity is visible in the standard deviation of the latitudes. This can be partly explained by the fact that the time series for the Fourier analysis is set to start at 01-01-2004 instead of 01-01-2002. This was done so that the majority of particles are already within the subtropics, with only dynamics in the subtropics affecting the time series. Therefore, the majority of the transport captured in the time series takes place in the zonal direction and so variations in the standard deviation of the particle latitudes would be less pronounced. However, it would be expected that there would be some signal, and there is none. To gain a clearer understanding of whether the 3.76 periodicity is the result of ENSO longer time series would be required. The model runs in this thesis are limited to 12 years by the availability of flow field data, so this was not possible for this thesis.

Difficulties in modeling the North Atlantic Basin

Given the importance of Stokes drift and the sensitivity of the North Atlantic simulations to the temporal resolution of the flow fields used to advect the microplastic, it is possible to draw some conclusions on why it has proven difficult to model a microplastic distribution that matches observations in the North Atlantic. First, in the North Atlantic simulation Stokes drift plays an important role in focusing the microplastic to a sharp peak at the center of the basin, which was not visible in any of the earlier global microplastic distribution modeling efforts [9, 18, 30, 31]. This is likely because the effects of Stokes drift were not considered in those studies. Lebreton et al. [30] used flow fields from HYCOM/N-CODA, which do not incorporate Stokes drift. Meanwhile, Maximenko et al. [18] and van Sebille et al. [31] work with transition matrices based on drifters, which in theory would be taking Stokes drift into account. However, all of the drifters used by Maximenko et al. [18] and a large part of the drifters used by van Sebille et al. [31] to compute the transition matrices were drogued to follow the 15 m currents. Since the effect of Stokes drift decrease with increasing depth, the effects of Stokes drift on the transport at the surface is likely underestimated or not noticeable. Secondly, there is the increased sensitivity to the temporal resolution of the flow fields of the North Atlantic in comparison to the North

Pacific. Maximenko et al. [18] had no temporal dependence for the transition matrix, while van Sebille et al. [31] had only a seasonal cycle. For the North Pacific such low temporal resolution appears to not be an issue, but for the North Atlantic it is most likely too coarse. Meanwhile, the HYCOM based model used by Lebreton et al. [30] uses a flow field with a higher temporal resolution of 1 day. However, HYCOM is a data-assimilative model and so the flow fields are not purely based on observations like GlobCurrent [35] and the transition matrix. As such, the poor performance of the Lebreton model might be partially explicable by the flow fields in general, not solely the temporal resolution. Finally, it must be considered that very few microplastic samples have ever been taken in the North Atlantic relative to the size of the basin, and even these few samples are almost all from the western North Atlantic. The sample record of microplastic therefore needs to be expanded in order to make any proper evaluations of microplastic distribution modeling efforts, both in the North Atlantic and in the rest of the oceans.

6 Conclusion

Microplastic has been found to accumulate in the subtropical gyres in each ocean basin, but little research has gone into identifying the physical processes that lead to this accumulation outside of the Pacific basins. Furthermore, little attention had been given to the effects of Stokes drift. This thesis presents a study of the contributions of the Ekman, geostrophic surface current and Stokes drift components on microplastic accumulation through regression analysis and Lagrangian particle modeling. The distributions were modeled globally, with particular emphasis on the North Pacific and North Atlantic basins and exception of the Indian ocean basin. Furthermore, the role of mesoscale eddies in the form of the eddy kinetic energy (EKE) proxy was investigated, along with the vertical Ekman pumping velocity for depth integrated transport and the mixing layer depth (MLD) for vertical microplastic mixing. Linear regression modeling with various time averaged physical fields proved to provide only limited insight into the relative importance of the various components, but did indicate that Ekman currents appeared to dominate accumulation, with the role of EKE and Stokes drift appearing dependent on the basin being considered. Given that there was no significant correlation between the EKE and the MLD, the two fields were not combined to create a 3D mixing parameter and the MLD was not considered further. When compared with the sampled microplastic concentrations in the North Pacific, the Ekman pumping velocity had a stronger correlation than the surface Ekman current convergence and flux. However, on basin-wide scales the surface Ekman current convergence and flux had stronger correlations, indicating that it is the surface transport that is a better indication of microplastic transport than the depth-integrated transport.

Langrangian microplastic modeling supported these findings, with the location of the garbage patches being determined by the Ekman currents. The geostrophic currents do not cause microplastic accumulation in the open ocean, instead counteracting the accumulation of the Ekman currents and spreading the microplastic over a larger area. Comparing the location of the modeled garbage patches in the subtropical ocean gyres with observations shows the location of the modeled North Pacific garbage patch corresponds closely to observations. Meanwhile, in the North Atlantic the modeled garbage patch is found to be at approximately the correct latitude, but $10^\circ - 25^\circ$ too far west. Adding Stokes drift leads to particle dispersal in the Pacific basins, while in the North Atlantic it led to the garbage patch having a clearer peak in concentrations in the subtropical gyre while also increasing transport to the poles and Caribbean. Analyzing the periodicity of the garbage patch locations showed that the North Atlantic garbage patch has a clear seasonal cycle in both the meridional and zonal directions, while the North Pacific garbage patch only has a

seasonal periodicity in the zonal direction. The transport of the microplastic in the North Pacific is possibly dependent on ENSO, showing a periodicity of 3.76 years. However, it is unclear whether ENSO is indeed the cause of this and further research with longer time series is required. Finally, the role of mesoscale eddies appears more critical in the North Pacific, with microplastic tending to accumulate in regions of minimal EKE. However, this is not observed in the North Atlantic, with the smaller zonal extent of the North Atlantic basin being a possible reason.

While breaking down the contributions of the Ekman and geostrophic currents is largely of academic interest, since in the end it will always be the sum of the two that leads to microplastic transport, the determination that Stokes drift plays a critical role in the accumulation pattern and transport of microplastic is of great importance for future modeling efforts. Currently, Stokes drift is often not considered with microplastic modeling, but it has significant influence on both garbage patch formation and the transport of microplastic to coastal and polar regions. Especially the later can be significant, since it means that microplastic contamination of polar ecosystems might be more severe than currently thought. Additionally, if Stokes drift is significant for beaching then excluding them can result in overestimation of the lifetime of plastic at sea. Aside from including all significant contributions to microplastic transport, future modeling efforts also require incorporating microplastic source and sink processes. These include realistic microplastic input scenarios and the fragmentation of macroplastic along with the removal of micro (and macro) plastic through sinking, bio-fouling and beaching. Successful modeling of the effects of such processes on the fate of marine plastic will hopefully lead to an eventual closing of the marine plastic budget, which will allow better directing of clean-up efforts to remove plastic from the oceans.

References

[1] "Plastics | uses, benefits, and chemical safety facts," *ChemicalSafetyFacts.org*, March 2018.

[2] G. Gourmelon, "Global plastic production rises, recycling lags," *Worldwatch Institute*, Jan 2015.

[3] J. R. Jambeck, R. Geyer, C. Wilcox, T. R. Siegler, M. Perryman, A. Andrady, R. Narayan, and K. L. Law, "Plastic waste inputs from land into the ocean," *Science*, vol. 347, no. 6223, pp. 768–771, 2015.

[4] A. Cózar, F. Echevarria, J. I. González-Gordillo, X. Irigoien, B. Ubeda, S. Hernandez-Leon, A. T. Palma, S. Navarro, J. Garcia-De-Lomas, A. Ruiz, M. L. Fernandez-De-Puelles, and C. M. Duarte, "Plastic debris in the open ocean," *Proceedings of the National Academy of Sciences*, vol. 111, no. 28, pp. 10239–10244, 2014.

[5] A. Cózar, E. Martí, C. M. Duarte, J. García-De-Lomas, E. V. Sebille, T. J. Ballatore, V. M. Eguíluz, J. I. González-Gordillo, M. L. Pedrotti, F. Echevarría, R. Troublè, and X. Irigoien, "The arctic ocean as a dead end for floating plastics in the north atlantic branch of the thermohaline circulation," *Science Advances*, vol. 3, no. 4, pp. 1–8, 2017.

[6] M. Eriksen, N. Maximenko, M. Thiel, A. Cummins, G. Lattin, S. Wilson, J. Hafner, A. Zellers, and S. Rifman, "Plastic pollution in the south pacific subtropical gyre," *Marine Pollution Bulletin*, vol. 68, no. 1-2, pp. 71–76, 2013.

[7] M. Eriksen, L. C. M. Lebreton, H. S. Carson, M. Thiel, C. J. Moore, J. C. Borerro, F. Galgani, P. G. Ryan, , and J. Reisser, "Plastic pollution in the world's oceans: More than 5 trillion plastic pieces weighing over 250,000 tons afloat at sea," *PLoS ONE*, vol. 9, no. 12, pp. 1–15, 2014.

[8] L.-M. Lebreton, B. Slat, F. Ferrari, B. Sainte-Rose, J. Aitken, R. Marthouse, S. Hajbane, S. Cunsolo, A. Schwarz, A. Levivier, K. Noble, P. Debeljak, H. Maral, R. Schoeneich-Argent, R. Brambini, and J. Reisser, "Evidence that the great pacific garbage patch is rapidly accumulating plastic," *Scientific Reports*, vol. 8, no. 1, 2018.

[9] E. van Sebille, C. Wilcox, L. Lebreton, N. Maximenko, B. D. Hardesty, J. A. Van Franeker, M. Eriksen, D. Siegel, F. Galgani, and K. L. Law, "A global inventory of small floating plastic debris," *Environmental Research Letters*, vol. 10, no. 12, pp. 1–11, 2015.

[10] "Microplastic particles found in antarctic waters," *volvooceanrace.com*, Jan 2018.

[11] R. C. Thompson, Y. Olsen, R. P. Mitchell, A. Davis, S. J. Rowland, A. W. G. John, D. McGonigle, and A. E. Russell, "Lost at sea: Where is all the plastic?," *Science*, vol. 304, no. 5672, p. 838, 2004.

[12] S. C. Gall and R. C. Thompson, "The impact of debris on marine life," *Marine Pollution Bulletin*, vol. 92, no. 1-2, pp. 170–179, 2015.

[13] B. D. Hardesty, J. Harari, A. Isobe, L. Lebreton, N. Maximenko, J. Potemra, E. Van Sebille, A. D. Vethaak, and C. Wilcox, "Using numerical model simulations to improve the understanding of micro-plastic distribution and pathways in the marine environment," *Frontiers in Marine Science*, vol. 4, no. 30, pp. 1–9, 2017.

[14] C. Lott, A. Eich, N.-C. Pauli, T. Mildenberger, C. Laforsch, J. S. Petermann, M. T. Lasut, and M. Weber, "Marine fate of biodegradable plastic—substitution potential and ecological impacts," in *Proceedings of the International Conference on Microplastic Pollution in the Mediterranean Sea*, pp. 195–197, Springer, 2018.

[15] B. Slat, *How the Oceans Can Clean Themselves: A Feasibility Study.* Delft: The Ocean Cleanup, 2 ed., 2014.

[16] L.-M. Lebreton, J. Van Der Zwet, J.-W. Damsteeg, B. Slat, A. Andrady, and J. Reisser, "River plastic emissions to the world's oceans," *Nature Communications*, vol. 8, p. 15611, 2017.

[17] P. G. Ryan, "Does size and buoyancy affect the long-distance transport of floating debris?," *Environmental Research Letters*, vol. 10, no. 8, pp. 1–6, 2015.

[18] N. Maximenko, J. Hafner, and P. Niiler, "Pathways of marine debris derived from trajectories of lagrangian drifters," *Marine Pollution Bulletin*, vol. 65, no. 1-3, pp. 51–62, 2012.

[19] J. A. Trinanes, J. M. Olascoaga, G. J. Goni, N. A. Maximenko, D. A. Griffin, and J. Hafner, "Analysis of flight mh370 potential debris trajectories using ocean observations and numerical model results," *Journal of Operational Oceanography*, vol. 9, no. 2, pp. 126–138, 2016.

[20] F. Beron-Vera, M. J. Olascoaga, and R. Lumpkin, "Inertia-induced accumulation of flotsam in the subtropical gyres," *Geophysical Research Letters*, vol. 43, no. 12, pp. 12228–12332, 2016.

[21] E. van Sebille, S. Waterman, A. Barthel, R. Lumpkin, S. R. Keating, C. Fogwill, and C. Turney, "Pairwise surface drifter separation in the western pacific sector of the southern ocean," *Journal of Geophysical Research: Oceans*, vol. 120, no. 10, pp. 6769–6781, 2015.

[22] K. L. Law, S. E. Moret-Ferguson, D. S. Goodwin, E. R. Zettler, E. Deforce, T. Kukulka, and G. Proskurowski, "Distribution of surface plastic debris in the eastern pacific ocean from an 11-year data set," *Environmental Science & Technology*, vol. 48, no. 9, pp. 4732–4738, 2014.

[23] C. Maes, B. Blanke, and E. Martinez, "Origin and fate of surface drift in the oceanic convergence zones of the eastern pacific," *Geophysical Research Letters*, vol. 43, no. 7, pp. 3398–3405, 2016.

[24] E. A. D'Asaro, A. Y. Shcherbina, J. M. Klymak, J. Molemaker, G. Novelli, C. M. Guigand, A. C. Haza, B. K. Haus, E. H. Ryan, G. A. Jacobs, H. S. Huntley, N. J. M. Laxague, S. Chen, F. Judt, J. C. McWilliams, R. Barkan, J. A. D. Kirwan, A. C. Poje, and T. M. Özgökmen, "Ocean convergence and the dispersion of flotsam," *PNAS*, pp. 1–6, 2018.

[25] L. Brach, P. Deixonne, M. F. Bernard, E. Durand, M. C. Desjean, E. Perez, E. van Sebille, and A. ter Halle, "Anticyclonic eddies increase accumulation of microplastic in the north atlantic subtropical gyre," *Marine Pollution Bulletin*, vol. 126, pp. 191–96, 2018.

[26] Y. Wakata and Y. Sugimori, "Lagrangian motions and global density distributions of floating matter in the ocean simulated using shipdrift data," *Journal of Physical Oceanography*, vol. 20, no. 1, pp. 125–38, 1990.

[27] P. Monroy, E. Hernández-García, V. Rossi, and C. López, "Modeling the dynamical sinking of biogenic particles in oceanic flow," *Nonlinear Processes in Geophysics*, vol. 24, no. 2, pp. 293–305, 2017.

[28] M. Kooi, E. H. van Nes, M. Scheffer, and A. A. Koelmans, "Ups and downs in the ocean: effects of biofouling on vertical transport of microplastics," *Environmental Science & Technology*, vol. 51, no. 14, pp. 7963–7971, 2017.

[29] P. Sherman and E. van Sebille, "Modeling marine surface microplastic transport to assess optimal removal locations," *Environmental Research Letters*, vol. 11, no. 1, pp. 1–6, 2016.

[30] L.-M. Lebreton, S. Greer, and J. Borrero, "Numerical modelling of floating debris in the world's oceans," *Marine Pollution Bulletin*, vol. 64, no. 3, pp. 653–661, 2012.

[31] E. van Sebille, M. H. England, and G. Froyland, "Origin, dynamics and evolution of ocean garbage patches from observed surface drifters," *Environmental Research Letters*, vol. 7, no. 4, pp. 1–6, 2012.

[32] M. Kubota, "A mechanism for the accumulation of floating marine debris north of hawaii," *Journal of Physical Oceanography*, vol. 24, no. 5, pp. 1059–1064, 1994.

[33] M. Kubota, K. Takayama, and D. Namimoto, "Pleading for the use of biodegradable polymers in favor of marine environments and to avoid an asbestos-like problem for the future," *Applied Microbiology and Biotechnology*, vol. 67, no. 4, pp. 469–476, 2005.

[34] E. Martinez, K. Maamaatuaiahutapu, and V. Taillandier, "Floating marine debris surface drift: Convergence and accumulation toward the south pacific subtropical gyre," *Marine Pollution Bulletin*, vol. 58, no. 9, pp. 1347–1355, 2009.

[35] M.-H. Rio, J. Johannessen, and C. Donlan, "Product data handbook: The combined geostropy+ekman currents," tech. rep., Globcurrent, 2016.

[36] F. A. Schott and J. P. McCreary Jr, "The monsoon circulation of the indian ocean," *Progress in Oceanography*, vol. 51, no. 1, pp. 1–123, 2001.

[37] F. A. Schott, S.-P. Xie, and J. P. McCreary, "Indian ocean circulation and climate variability," *Reviews of Geophysics*, vol. 47, no. 1, 2009.

[38] C. Moore, "Trashed - across the pacific ocean, plastics, plastics, everywhere," Nov 2003.

[39] C. Moore, S. Moore, M. Leecaster, and S. Weisberg, "A comparison of plastic and plankton in the north pacific central gyre," *Marine Pollution Bulletin*, vol. 42, no. 12, pp. 1297–1300, 2001.

[40] K. L. Law, S. Moret-Ferguson, N. A. Maximenko, G. Proskurowski, E. E. Peacock, J. Hafner, and C. M. Reddy, "Plastic accumulation in the north atlantic subtropical gyre," *Science*, vol. 329, no. 5996, pp. 1185–1188, 2010.

[41] T. Kukulka, G. Proskurowski, S. Morét-Ferguson, D. W. Meyer, and K. L. Law, "The effect of wind mixing on the vertical distribution of buoyant plastic debris," *Geophysical Research Letters*, vol. 39, no. 7, pp. 1–6, 2012.

[42] J. Reisser, B. Slat, K. Noble, K. D. Plessis, M. Epp, M. Proietti, J. D. Sonneville, T. Becker, and C. Pattiaratchi, "The vertical distribution of buoyant plastics at sea: An observational study in the north atlantic gyre," *Biogeosciences*, vol. 12, no. 4, pp. 1249–256, 2015.

[43] J. A. Cummings, "Operational multivariate ocean data assimilation," *Quarterly Journal of the Royal Meteorological Society*, vol. 131, no. 613, pp. 3583–604, 2005.

[44] G. Prasetya, K. Black, W. De Lange, J. Borrero, and T. Healy, "Debris dispersal modeling for the great sumatra tsunamis on banda aceh and surrounding waters," *Natural Hazards*, vol. 60, no. 3, pp. 1167–188, 2011.

[45] J. G. B. Derraik, "The pollution of the marine environment by plastic debris: A review," *Marine Pollution Bulletin*, vol. 44, no. 9, pp. 842–52, 2002.

[46] V. W. Ekman, "On the influence of the earth's rotation on ocean-currents.," 1905.

[47] A. Webb and B. Fox-Kemper, "Impacts of wave spreading and multidirectional waves on estimating stokes drift," *Ocean Modelling*, vol. 96, pp. 49–64, 2015.

[48] T. van den Bremer and Ø. Breivik, "Stokes drift," *Phil. Trans. R. Soc. A*, vol. 376, no. 2111, p. 20170104, 2018.

[49] K. E. Kenyon, "Stokes drift for random gravity waves," *Journal of Geophysical Research*, vol. 74, no. 28, pp. 6991–6994, 1969.

[50] M. Drivdal, G. Broström, and K. Christensen, "Wave-induced mixing and transport of buoyant particles: application to the statfjord a oil spill," *Ocean Science*, vol. 10, no. 6, pp. 977–991, 2014.

[51] C. E. Jones, K.-F. Dagestad, Ø. Breivik, B. Holt, J. Röhrs, K. H. Christensen, M. Espeseth, C. Brekke, and S. Skrunes, "Measurement and modeling of oil slick transport," *Journal of Geophysical Research: Oceans*, vol. 121, no. 10, pp. 7759–7775, 2016.

[52] C. I. Fraser, A. K. Morrison, A. M. Hogg, E. C. Macaya, E. van Sebille, P. G. Ryan, A. Padovan, C. Jack, N. Valdivia, and J. M. Waters, "Antarctica's ecological isolation will be broken by storm-driven dispersal and warming," *Nature Climate Change*, Jul 2018.

[53] A. Chaigneau, G. E. M. Le Texier, C. Grados, and O. Pizarro, "Vertical structure of mesoscale eddies in the eastern south pacific ocean: A composite analysis from altimetry and argo profiling floats," *Journal of Geophysical Research*, vol. 116, no. C11, pp. 1–16, 2011.

[54] M.-H. Rio, S. Mulet, and N. Picot, "Beyond goce for the ocean circulation estimate: Synergetic use of altimetry, gravimetry, and in situ data provides new insight into geostrophic and ekman currents," *Geophysical Research Letters*, vol. 41, no. 24, pp. 8918–925, 2014.

[55] S. L. Bruinsma, C. Förste, O. Abrikosov, J.-C. Marty, M.-H. Rio, S. Mulet, and S. Bonvalot, "The new esa satellite-only gravity field model via the direct approach," *Geophysical Research Letters*, vol. 40, no. 14, pp. 3607–3612, 2013.

[56] M.-H. Rio, S. Guinehut, and G. Larnicol, "New cnes-cls09 global mean dynamic topography computed from the combination of grace data, altimetry, and in situ measurements," *Journal of Geophysical Research: Oceans*, vol. 116, no. C7, 2011.

[57] M.-H. Rio, "Use of altimeter and wind data to detect the anomalous loss of svp-type drifter's drogue," *Journal of Atmospheric and Oceanic Technology*, vol. 29, no. 11, pp. 1663–1674, 2012.

[58] D. P. Dee, S. M. Uppala, A. J. Simmons, P. Berrisford, P. Poli, S. Kobayashi, U. Andrae, M. A. Balmaseda, G. Balsamo, P. Bauer, P. Bechtold, A. C. M. V. D. Berg, J. Bidlot, N. Bormann, C. Delsol, R. Dragani, M. Fuentes, A. J. Geer, L. Haimberger, S. B. Healy, H. Hersbach, E. V. Hólm, L. Isaksen, P. Kállberg, M. Köhler, M. Matricardi, A. P. McNally, B. M. Monge-Sanz, J.-J. Morcrette, B.-K. Park, C. Peubey, P. D. Rosnay, C. Tavolato, J.-N. Thépaut, and F. Vitart, "The era-interim reanalysis: Configuration and performance of the data assimilation system," *Quarterly Journal of the Royal Meteorological Society*, vol. 137, no. 656, pp. 553–597, 2011.

[59] H. L. Tolman, *User manual and system documentation of WAVEWATCH-III version 1.15.* US Department of Commerce, National Oceanic and Atmospheric Administration, National Weather Service, National Centers for Environmental Prediction, 1997.

[60] H. L. Tolman, "User manual and system documentation of wavewatch iii tm version 3.14," *Technical note, MMAB Contribution*, vol. 276, p. 220, 2009.

[61] A. Kara Birol, E. J. Metzger, and M. A. Bourassa, "Ocean current and wave effects on wind stress drag coefficient over the global ocean," *Geophysical Research Letters*, vol. 34, no. 1, pp. 1–4, 2007.

[62] J. Holte, L. D. Talley, J. Gilson, and D. Roemmich, "An argo mixed layer climatology and database," *Geophysical Research Letters*, vol. 44, no. 11, pp. 5618–5626, 2017.

[63] S. T. Buckland, D. R. Anderson, K. P. Burnham, and J. L. Laake, *Distance Sampling: Estimating Abundance of Biological Populations.* Dordrecht: Springer Netherlands, 1993.

[64] M. Lange and E. Van Sebille, "Parcels v0.9: Prototyping a lagrangian ocean analysis frameworkfor the petascale age," *Geoscientific Model Development Discussions*, vol. 10, pp. 4175–4186, 2017.

[65] G. Froyland, R. M. Stuart, and E. van Sebille, "How well-connected is the surface of the global ocean?," *Chaos*, vol. 24, p. 3, 2014.

[66] F.-F. Jin, "An equatorial ocean recharge paradigm for enso. part i: Conceptual model," *Journal of the atmospheric sciences*, vol. 54, no. 7, pp. 811–829, 1997.

[67] F. Ardhuin, Y. Aksenov, A. Benetazzo, L. Bertino, P. Brandt, E. Caubet, B. Chapron, F. Collard, S. Cravatte, J.-M. Delouis, F. Dias, G. Dibarboure, L. Gaultier, J. Johannessen, A. Korosov, G. Manucharyan, D. Menemenlis, M. Menendez, G. Monnier, A. Mouche, F. Nouguier, G. Nurser, P. Rampal, A. Reniers, E. Rodriguez, J. Stopa, C. Tison, C. Ubelmann, E. van Sebille, and J. Xie, "Measuring currents, ice drift, and waves from space: the sea surface kinematics multiscale monitoring (skim) concept," *Ocean Science*, vol. 14, no. 3, pp. 337–354, 2018.

[68] M. G. Schlax and D. D. Chelton, "The "growing method" of eddy identification and tracking in two and three dimensions," Jul 2016.

[69] M. A. Spall, "Generation of strong mesoscale eddies by weak ocean gyres," *Journal of marine research*, vol. 58, no. 1, pp. 97–116, 2000.

[70] C. Wang, "A unified oscillator model for the el niño–southern oscillation," *Journal of Climate*, vol. 14, no. 1, pp. 98–115, 2001.

A Additional figures & tables

Table 4: Descriptions of all the fitfunctions used for the linear regression modeling, in terms of their action on a physical field value F_j for position j. Titles of the subplots showing the linear regression model results refer to the fitfunctions and time averaged physical fields used in the linear regression model. E.g. square(pump) indicates the square fitfunction applied on the vertical Ekman pumpin velocity

Fitfunction	**Description**
null	$F_j = 0$
square()	$\text{square}(F_j) = \begin{cases} F_j^2, F_j \geq 0 \\ -\lvert F_j \rvert^2, F_j < 0 \end{cases}$
log()	$\log(F_j) = \ln(F_j)$
sqrt()	$\text{sqrt}(F_j) = \begin{cases} \sqrt{F_j}, F_j \geq 0 \\ -\sqrt{\lvert F_j \rvert}, F_j < 0 \end{cases}$
3rdRoot()	$\text{sqrt}(F_j) = \begin{cases} \sqrt[3]{F_j}, F_j \geq 0 \\ -\sqrt[3]{\lvert F_j \rvert}, F_j < 0 \end{cases}$
4thRoot()	$\text{sqrt}(F_j) = \begin{cases} \sqrt[4]{F_j}, F_j \geq 0 \\ -\sqrt[4]{\lvert F_j \rvert}, F_j < 0 \end{cases}$
Time Averaged Variable Field	**Description**
pump	Vertical Ekman pumping velocity
EkmanFlux	surface Ekman current flux
EkmanConver	surface Ekman current convergence
TotalFlux	surface total current flux
TotalConver	surface total current convergence
GeoFlux	surface geostrophic current flux
GeoConver	surface geostrophic current convergence
EKE	eddy kinetic energy

Table 5: Pearson R correlation coefficients between time averaged EKE and MLD physical fields. Bold-faced values are significant at the $p < 0.05$ level, but do not account for the overestimation of the degrees of freedom of the fields.

Basin	**Pearson R**
North Pacific	**-0.158**
South Pacific	**0.0492**
North Atlantic	-0.0288
South Atlantic	-0.0209

Table 6: Pearson R regression coefficients for the Maximenko distribution and time averaged surface current fluxes, where the current fluxes are either computed over $1° \times 1°$ or $2° \times 2°$ areas. Boldfaced values are significant at a $p < 0.05$ level, but do not account for the overestimation of the degrees of freedom of the fields.

Basin	**Total Flux**		**Ekman Flux**		**Geostrophic Flux**		**Stokes Flux**	
	1x1	2x2	1x1	2x2	1x1	2x2	1x1	2x2
North Pacific	-0.0858	**-0.137**	**-0.259**	**-0.316**	0.0173	0.0309	**0.323**	**0.360**
South Pacific	0.00745	0.00975	**-0.294**	**-0.309**	**0.0444**	**0.0688**	**0.193**	**0.225**
North Atlantic	0.00486	0.0212	**-0.0700**	**-0.0781**	0.0242	0.0474	**0.424**	**0.464**
South Atlantic	-0.0150	-0.0317	**-0.404**	**-0.413**	**0.0369**	0.0474	**0.331**	**0.358**

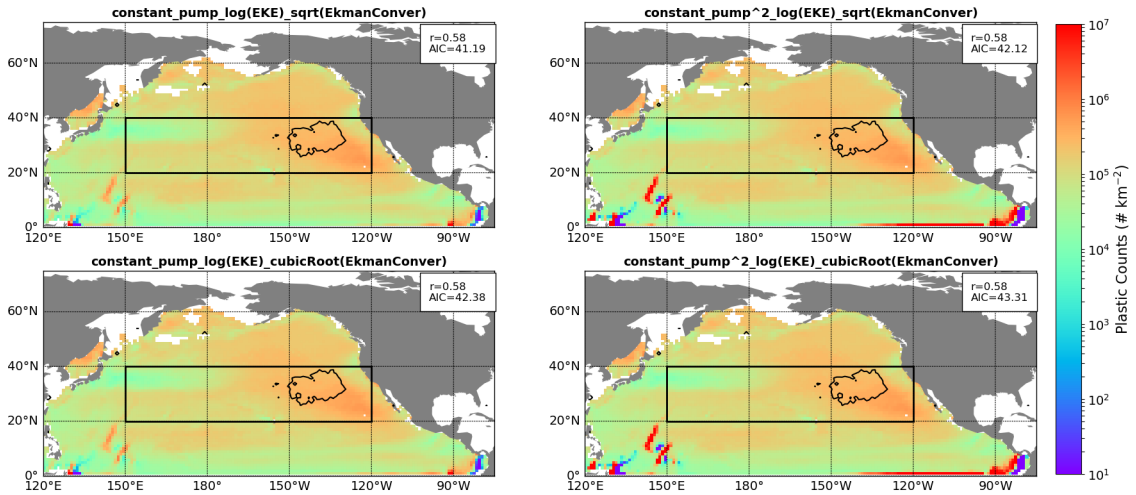

Figure 20: Best performing linear regression models for the North Pacific basin, selected on the basis of the lowest AIC value for fits carried out on the region between $20° - 40°$N and 150°E−120°W. Contour shows the 1×10^6 # km^{-2} contour from the Maximenko distribution. The subplot titles indicate the time averaged physical fields and fitfunctions used in the linear regression model, see Table 4 in Appendix A.

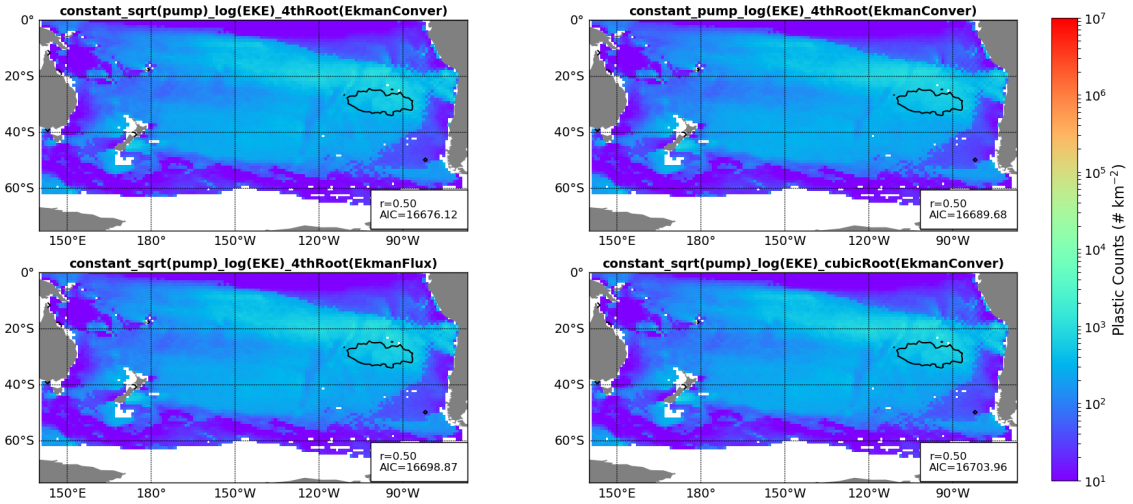

Figure 21: Best performing linear regression models for the South Pacific basin, selected according to the lowest AIC value. Contour shows the 5×10^4 # km^{-2} contour from the Maximenko distribution. The subplot titles indicate the time averaged physical fields and fitfunctions used in the linear regression model, see Table 4 in Appendix A.

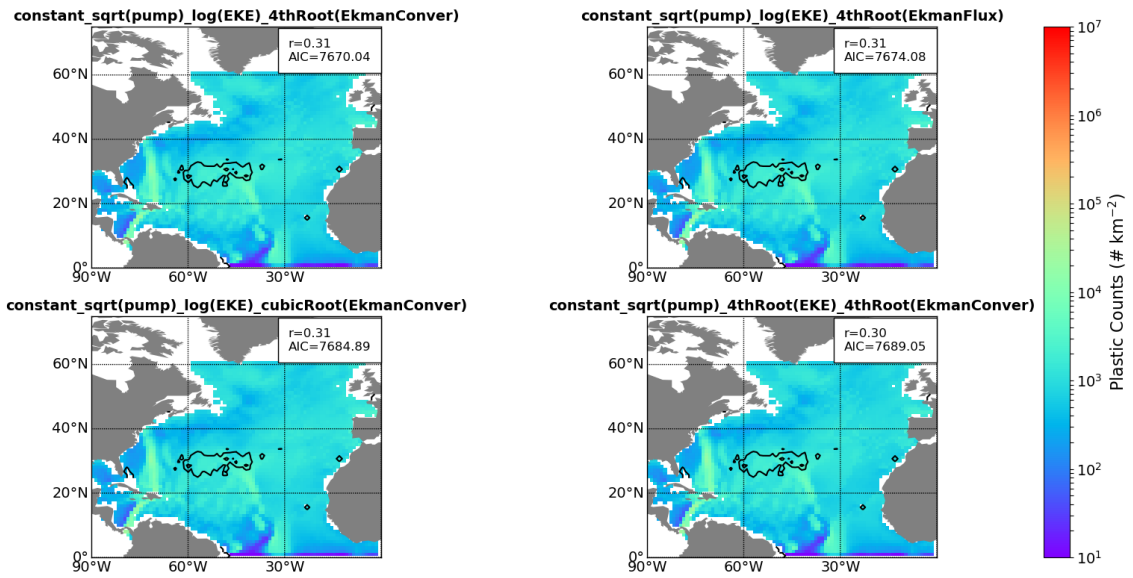

Figure 22: Best performing linear regression models for the North Atlantic basin, selected according to the lowest AIC values. Contour shows the 5×10^4 # km^{-2} contour from the Maximenko distribution. The subplot titles indicate the time averaged physical fields and fitfunctions used in the linear regression model, see Table 4 in Appendix A.

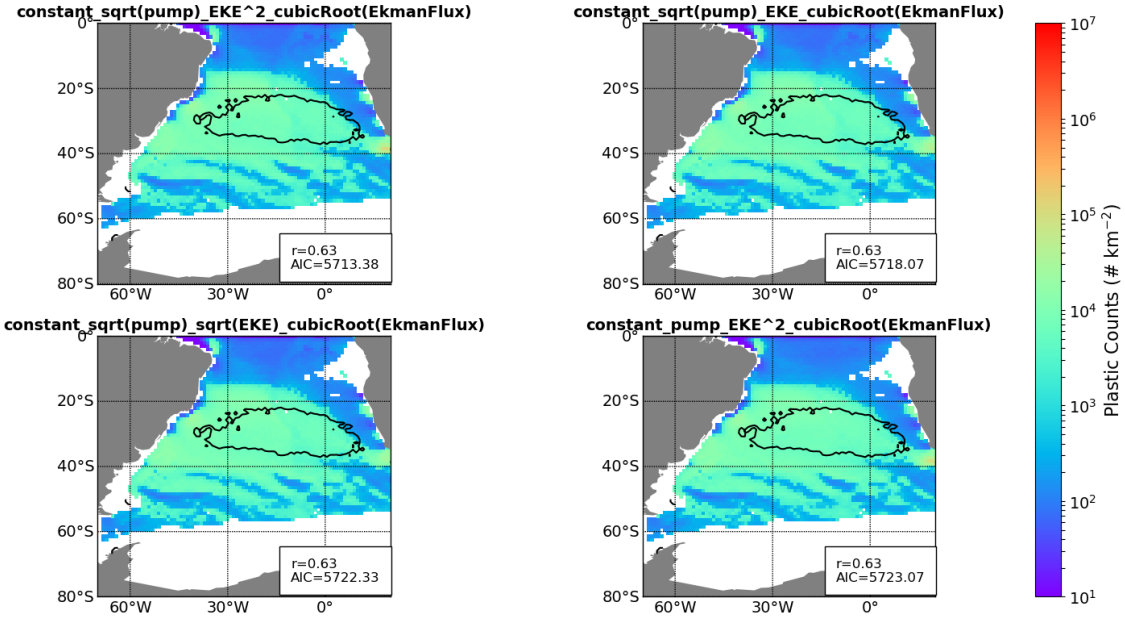

Figure 23: Best performing linear regression models for the South Atlantic basin, selected according to the lowest AIC value. Contour shows the 5×10^4 # km^{-2} contour from the Maximenko distribution. The subplot titles indicate the time averaged physical fields and fitfunctions used in the linear regression model, see Table 4 in Appendix A.

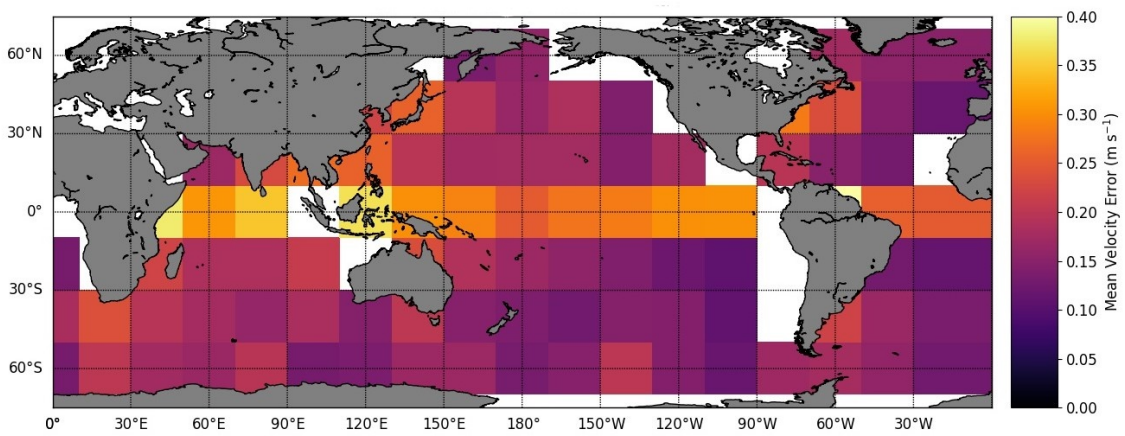

Figure 24: Mean error of the geostrophic currents, as reported by GlobCurrent [35].

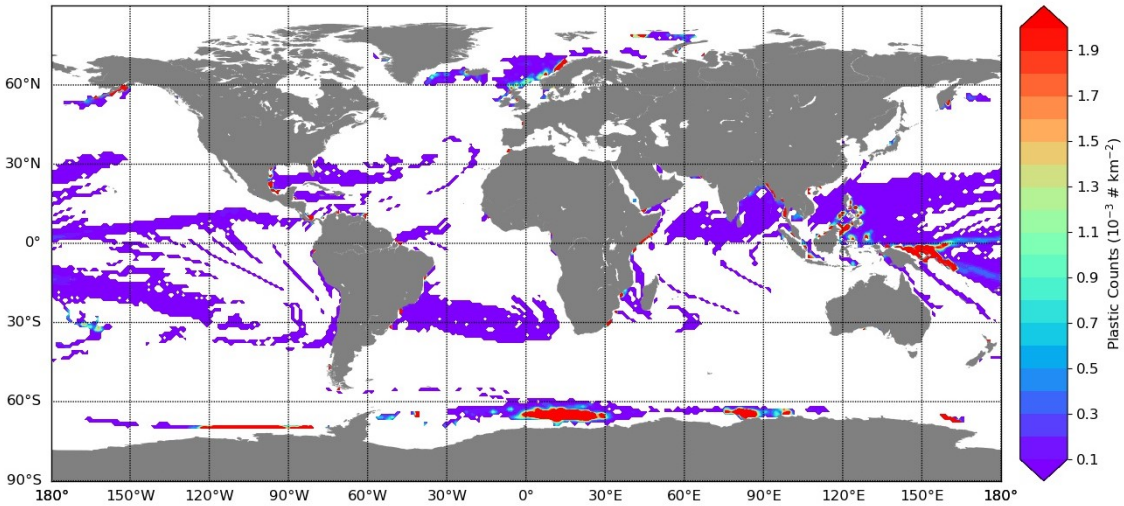

Figure 25: The mean particle density of the final year of the global Lagrangian simulations with the virtual particles advected by Stokes drift. Simulations are from 01-01-2002 to 31-12-2014 from an initial uniform $1^\circ \times 1^\circ$ distribution of particles.

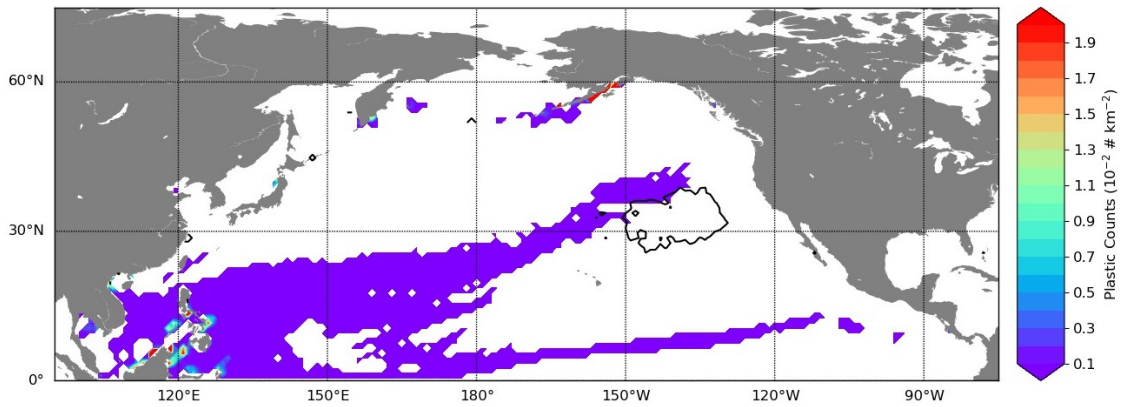

Figure 26: The mean particle density of the final year of the North Pacific Lagrangian simulations with the virtual particles advected by Stokes drift. Simulations are from 01-01-2002 to 31-12-2014 from an initial uniform $0.5^\circ \times 0.5^\circ$ distribution of particles. Contour shows the 1×10^6 # km^{-2} contour from the Maximenko distribution.

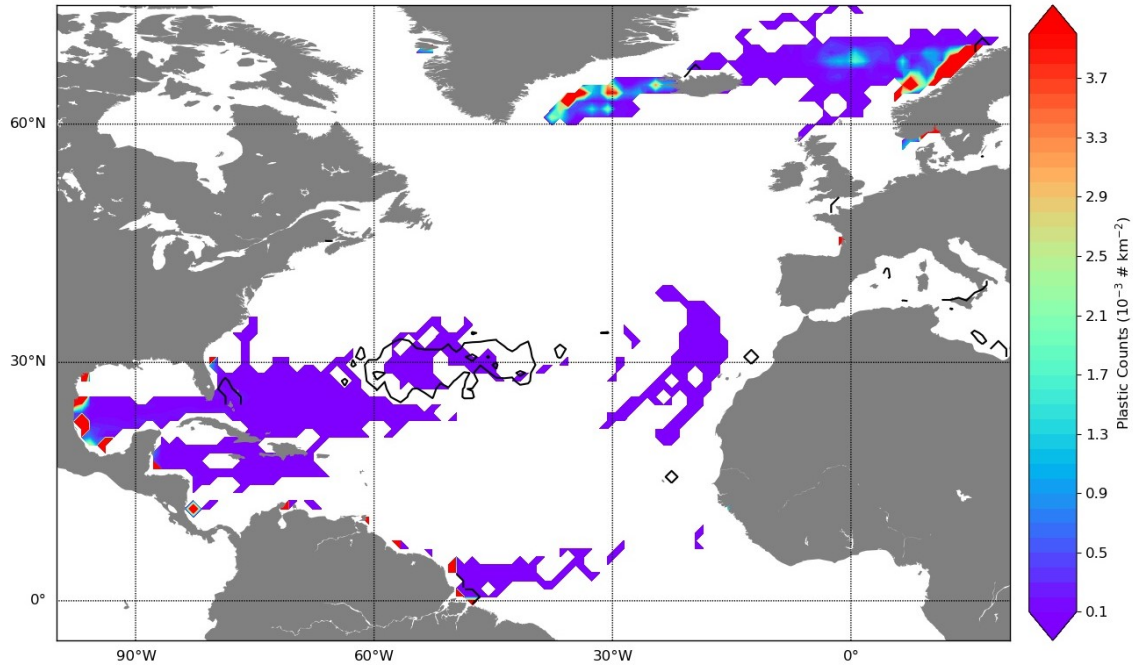

Figure 27: The mean particle density of the final year of the North Atlantic Lagrangian simulations with the virtual particles advected by Stokes drift. Simulations are from 01-01-2002 to 31-12-2014 from an initial uniform $0.5° \times 0.5°$ distribution of particles. Contour shows the 5×10^4 # km^{-2} contour from the Maximenko distribution.

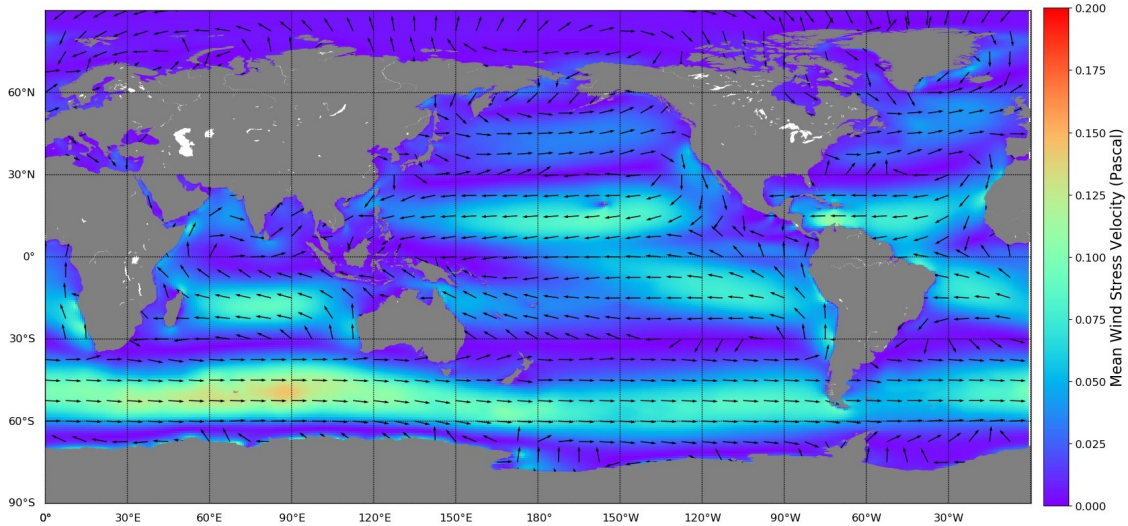

Figure 28: Mean wind stress field for 1979-2017, with the normalized vectors indicating the mean direction and the colormap indicating the wind stress magnitude. The wind stress is computed according to Equation 17.

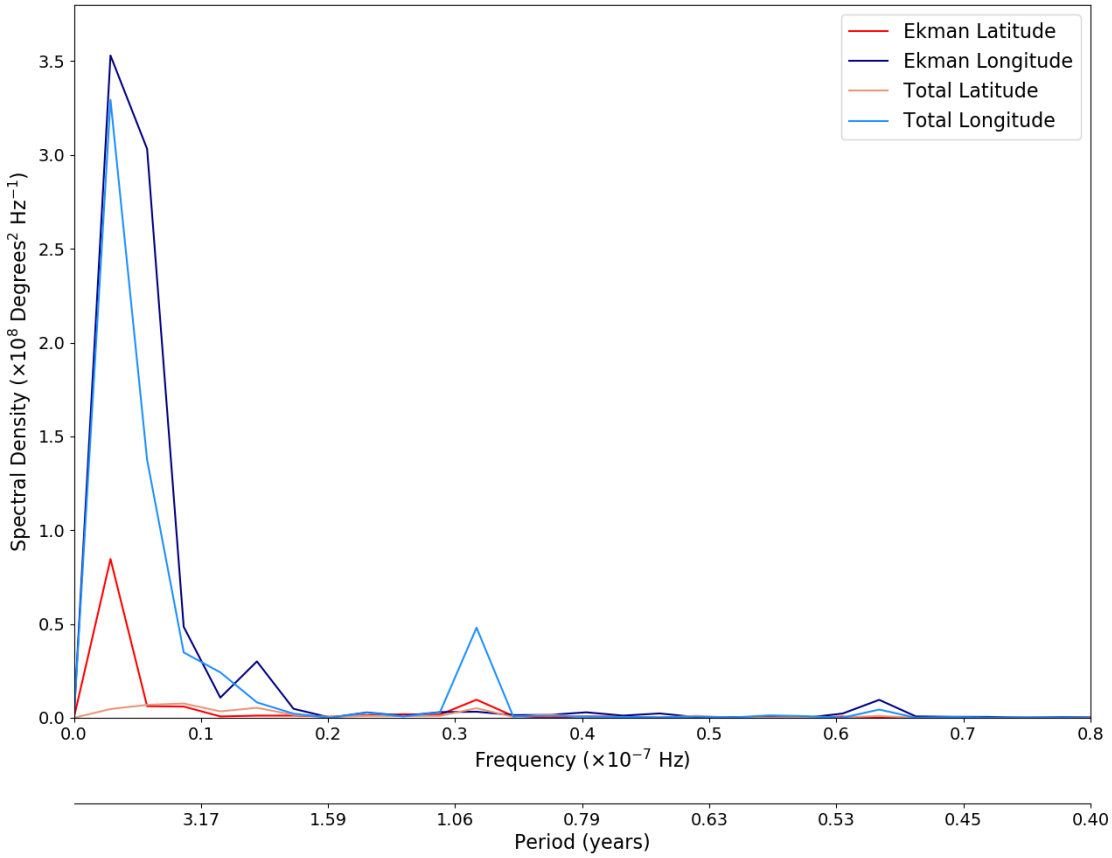

Figure 29: Power spectra of the longitude/latitude standard deviation time series (Figure 16b) for all particles in the North Atlantic whose final position is in the North Atlantic subtropics ($10° - 40°$N,$0° - 80°$W). The power spectrum is computed from the detrended time series from 01-01-2004 to 31-12-2014.

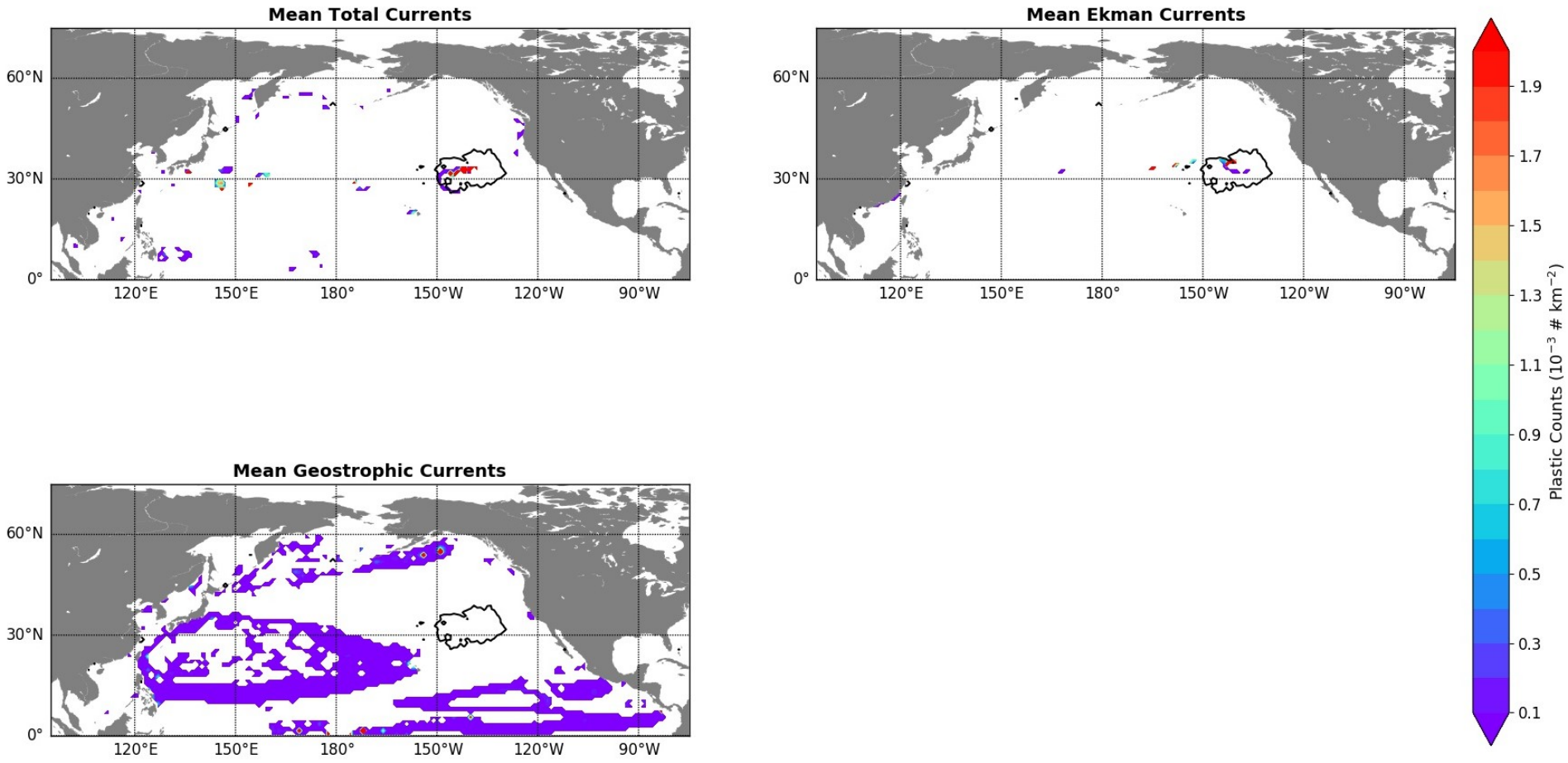

Figure 30: The mean particle density of the final year of the North Pacific Lagrangian simulations with the virtual particles advected by mean total currents, mean Ekman currents and mean geostrophic currents, where the mean currents are calculated for 2002-2014. Simulations are from 01-01-2002 to 31-12-2014 from an initial uniform $0.5° \times 0.5°$ distribution of particles. Contour shows the 1×10^6 # km^{-2} contour from the Maximenko distribution.

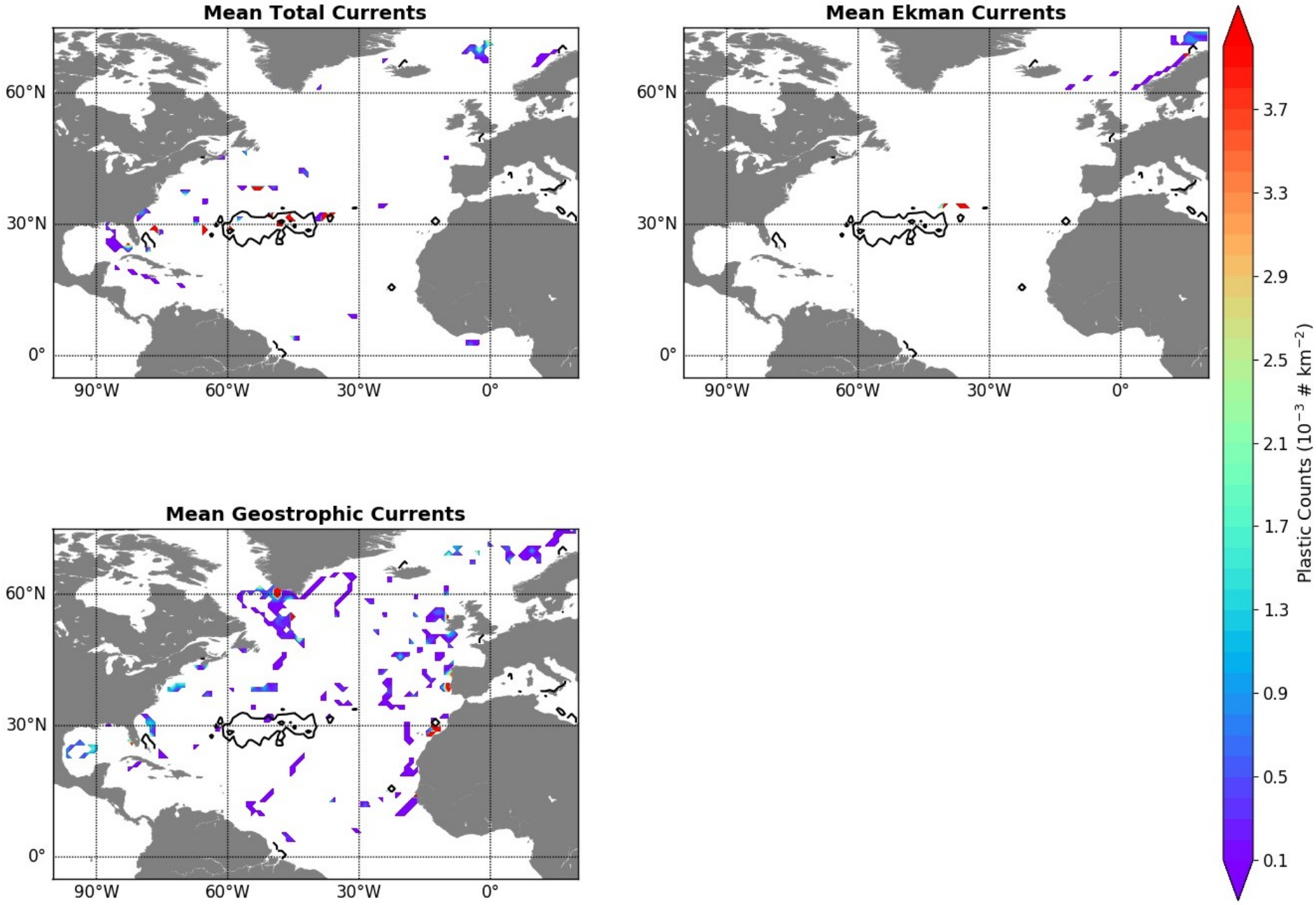

Figure 31: The mean particle density of the final year of the North Atlantic Lagrangian simulations with the virtual particles advected by mean total currents, mean Ekman currents and mean geostrophic currents, where the mean currents are calculated for 2002-2014. Simulations are from 01-01-2002 to 31-12-2014 from an initial uniform $0.5° \times 0.5°$ distribution of particles. Contour shows the 5×10^4 # km^{-2} contour from the Maximenko distribution.